# Laminar flow through Isotropic Granular Porous Media

Sonia Woudberg


Thesis presented in partial fulfilment of the requirements for the degree of Master of Engineering Science at the University of Stellenbosch.

Promoter: Prof. J.P. du Plessis

December 2006

# Declaration

I, the undersigned, hereby declare that the work contained in this thesis is my own original work and that I have not previously in its entirety or in part submitted it at any university for a degree.

Signature: _____ Date: _____

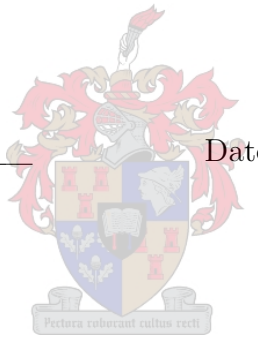

# Abstract

An analytical modelling procedure for predicting the streamwise pressure gradient for steady laminar incompressible flow of a Newtonian fluid through homogeneous isotropic granular porous media is introduced. The modelling strategy involves the spatial volume averaging of a statistical representative portion of the porous domain to obtain measurable macroscopic quantities from which macroscopic transport equations can be derived. A simple pore-scale model is introduced to approximate the actual complex granular porous microstructure through rectangular cubic geometry. The sound physical principles on which the modelling procedure is based avoid the need for redundant empirical coefficients. The model is generalized to predict the rheological flow behaviour of non-Newtonian purely viscous power law fluids by introducing the dependence of the apparent viscosity on the shear rate through the wall shear stress. The field of application of the Newtonian model is extended to predict the flow behaviour in fluidized beds by adjusting the Darcy velocity to incorporate the relative velocity of the solid phase. The Newtonian model is furthermore adjusted to predict fluid flow through Fontainebleau sandstone by taking into account the effect of blocked throats at very low porosities. The analytical model as well as the model generalizations for extended applicability is verified through comparison with other analytical and semi-empirical models and a wide range of experimental data from the literature. The accuracy of the predictive analytical model reveals to be highly acceptable for most engineering designs.

# Opsomming

'n Analitiese modelleringsprosedure is bekend gestel om die stroomsgewyse drukgradiënt vir tydonafhanklike, laminêre, onsaamdrukbare vloei van 'n Newtoniese vloeistof deur homogene, isotrope poreuse media met 'n korrelstruktuur te voorspel. Die modelleringstrategie berus op die ruimtelike volumetriese gemiddelde van 'n statisties-verteenwoordigende gedeelte van die poreuse medium om meetbare makroskopiese groothede te verkry waarvan makroskopiese oordragvergelykings afgelei kan word. 'n Eenvoudige porie-skaal model word voorgestel om die werklike komplekse korrelagtige mikro-struktuur deur 'n reghoekige kubiese geometrie te benader. Die fisiese grondbeginsels waarop die modelleringstrategie gegrond is, vermy die behoefte vir empiriese koëffisiënte. Die model is veralgemeen om die reologiese vloeigedrag van nie-Newtoniese, suiwer viskeuse, magswet-vloeistowwe te voorspel deur die afhanklikheid van die effektiewe viskositeit op die skuifspanningstempo in te voer deur die skuifspanning op die wand. The toepassingsveld van die Newtoniese model is uitgebrei om die vloeigedrag in sweefbeddens te voorspel deur die Darcy snelheid aan te pas om sodoende die relatiewe snelheid van die vastestoffase in berekening te bring. Die Newtoniese model is verder aangepas om die vloei van vloeistowwe deur Fontainebleau sandsteen te voorspel deur die effek van geblokkeerde kanale by baie lae porositeite in ag te neem. Die analitiese model, sowel as die veralgemenings van die model vir uitgebreide toepasbaarheid, is geverifieer deur vergelyking met ander analitiese en semi-empiriese modelle en 'n wye verskeidenheid eksperimentele data vanuit die literatuur. Die akkuraatheid van die voorspelbare analitiese model blyk hoogs aanvaarbaar te wees vir die meeste ingenieursontwerpe.

# Acknowledgements

I wish to express my sincere gratitude to the following people who contributed to this study by inspiring me in their own special way:

- God, for guiding me in life and giving me the potential to follow this path.
- My supervisor, Prof. Prieur du Plessis, for not only guiding me to face the challenges of our competitive world, but also showing me the world and to appreciate the priceless things in life.
- My parents, Johann and Linda Woudberg, for the best moral and financial support one could wish for.
- My sister and bother-in-law, Tania and André Heunis, for their concern and encouragement.
- My family and friends for their wishes of support when I was overseas.
- Our head of division, Dr. Francois Smit, for his moral support at times when it mattered the most and the financial support from BIWUS to attend the conference in India.
- Prof. Mark Knacksteadt for hosting me in Australia, Prof. Britt Halvorsen for hosting me in Norway and Prof. Jack Legrand for financial assistance to visit France.
- The South African National Research Foundation (NRF) for the Prestigious Scholarship and the additional Travel Grant.

# Contents

# Nomenclature

## Standard characters

| | | |
|---|---|---|
| $a$ | $[m^{-1}]$ | specific surface |
| $a_v$ | $[m^{-1}]$ | solid specific surface |
| $A$ | [] | coefficient in the Blake-Kozeny equation |
| $A_p$ | $[m^2]$ | cross-sectional flow area |
| $B$ | [] | coefficient in the Burke-Plummer equation |
| $d$ | $[m]$ | linear dimension of RUC |
| $d_p$ | $[m]$ | grain diameter |
| $d_s$ | $[m]$ | linear dimension of solid cube in RUC |
| $D_h$ | $[m]$ | hydraulic diameter |
| $D_p$ | $[m]$ | spherical particle diameter |
| $f$ | $[m^{-2}]$ | shear factor |
| $f_b$ | $[N.kg^{-1}]$ | external body forces per unit mass |
| $F$ | [ ] | dimensionless shear factor |
| $\mathcal{F}$ | $[N]$ | drag force |
| $g$ | $[N.kg^{-1}]$ | gravitational constant |
| $k$ | $[m^2]$ | hydrodynamic or Darcy permeability |
| $k_{koz}$ | [ ] | Kozeny constant |
| $k_o$ | [ ] | shape factor |
| $K$ | $[N.s.m^{-2}]$ | consistency index of power law fluid |
| $\mathcal{K}$ | [ ] | dimensionless hydrodynamic permeability |
| $l$ | $[m]$ | length scale of microscopic structure |
| $L$ | $[m]$ | length scale of macroscopic structure |
| $n$ | [ ] | behaviour index of power law fluid |
| $\underline{n}$ | [ ] | inwardly directed unit vector normal to surface of solid |

| | | |
|---|---|---|
| $\underline{\widehat{n}}$ | [ ] | unit vector in streamwise direction |
| $p$ | $[Pa]$ | interstitial pressure |
| $\underline{q}$ | $[m.s^{-1}]$ | superficial velocity, Darcy velocity or specific discharge |
| $\underline{q}_{mf}$ | $[m.s^{-1}]$ | minimum fluidization velocity |
| $Q$ | $[m^3.s^{-1}]$ | volumetric flow rate |
| $\underline{r}_o$ | $[m]$ | position vector of REV centroid |
| $R$ | $[m]$ | radius |
| $R_h$ | $[m]$ | hydraulic radius |
| $Re$ | [ ] | pore Reynolds number $(\rho\, q\, (d - d_s)/\mu)$ |
| $Re_c$ | [ ] | critical Reynolds number |
| $Re_p$ | [ ] | particle Reynolds number $(\rho\, q\, d_s/\mu)$ |
| $\mathcal{S}_{ff}$ | $[m^2]$ | fluid-fluid interfaces in REV |
| $S_{fs}$ | $[m^2]$ | fluid-solid interface in RUC |
| $\mathcal{S}_{fs}$ | $[m^2]$ | fluid-solid interfaces in REV |
| $S_g$ | $[m^2]$ | surface area in RUC adjacent to stagnant fluid volume |
| $S_{\|\|}$ | $[m^2]$ | surface area in RUC adjacent to streamwise fluid volume |
| $S_\perp$ | $[m^2]$ | surface area in RUC adjacent to transverse fluid volume |
| $U_f$ | $[m^3]$ | total fluid volume in RUC |
| $\mathcal{U}_f$ | $[m^3]$ | total fluid volume in REV |
| $U_g$ | $[m^3]$ | total stagnant volume in RUC |
| $U_o$ | $[m^3]$ | total (fluid and solid) volume of RUC |
| $\mathcal{U}_o$ | $[m^3]$ | total (fluid and solid) volume of REV |
| $U_s$ | $[m^3]$ | total solid volume in RUC |
| $\mathcal{U}_s$ | $[m^3]$ | total solid volume in REV |
| $U_t$ | $[m^3]$ | total transfer volume in RUC |
| $U_{\|\|}$ | $[m^3]$ | total streamwise volume in RUC |
| $U_\perp$ | $[m^3]$ | total transverse volume in RUC |
| $\underline{u}$ | $[m.s^{-1}]$ | drift velocity |
| $\underline{v}$ | $[m.s^{-1}]$ | interstitial fluid velocity |
| $\underline{w}_{\|\|}$ | $[m.s^{-1}]$ | streamwise average pore velocity |
| $\underline{w}_\perp$ | $[m.s^{-1}]$ | transverse average pore velocity |
| $x, y, z$ | $[m]$ | distance along Cartesian coordinate |

## Greek symbols

| | | |
|---|---|---|
| $\beta$ | [ ] | average pore velocity ratio |
| $\dot{\gamma}$ | $[s^{-1}]$ | shear rate |
| $\delta$ | [ ] | change in transverse property |
| $\Delta$ | [ ] | change in streamwise property |
| $\epsilon$ | [ ] | porosity |
| $\epsilon_B$ | [ ] | backbone porosity |
| $\epsilon_c$ | [ ] | percolation threshold porosity |
| $\epsilon_{mf}$ | [ ] | minimum fluidization porosity |
| $\eta$ | $[N.s.m^{-2}]$ | apparent viscosity |
| $\Lambda$ | $[s^{-1}]$ | dimensionless resistance factor |
| $\mu$ | $[N.s.m^{-2}]$ | fluid dynamic viscosity |
| $\xi$ | [ ] | shear stress reduction coefficient |
| $\rho$ | $[kg.m^{-3}]$ | fluid density |
| $\tau$ | $[N.m^{-2}]$ | local shear stress |
| $\tau_w$ | $[N.m^{-2}]$ | local wall shear stress |
| $\phi$ | [ ] | any tensorial fluid phase quantity |
| $\phi_s$ | [ ] | sphericity factor |
| $\Phi_{sg}$ | [ ] | total gas/particle drag coefficient |
| $\chi$ | [ ] | tortuosity factor |
| $\psi$ | [ ] | geometric factor |

## Miscellaneous

| | |
|---|---|
| $\nabla$ | del operator |
| $\langle\ \rangle$ | phase average operator |
| $\langle\ \rangle_f$ | intrinsic phase average operator |
| $\{\ \}$ | deviation operator |
| $\tilde{}$ | interchange in unit vectors |
| $\underline{\ }$ | vector (underlined) |
| $\underline{\underline{\ }}$ | diadic (doubly underlined) |

## Acronyms

| | |
|---|---|
| REV | Representative Elementary Volume |
| RUC | Representative Unit Cell |

## Subscripts

| | |
|---|---|
| $f$ | fluid matter |
| $fs$ | fluid-solid interface |
| $h$ | hydraulic |
| $o$ | total solid- and fluid volume |
| $s$ | solid matter |
| $w$ | wall |
| $\|\|$ | parallel to streamwise direction |
| $\perp$ | perpendicular to streamwise direction |
| 0 | lower limit |
| 1 | higher limit |

# Chapter 1

# Introduction

The term *granular porous medium* refers to a material consisting of an unconsolidated solid matrix with interconnected pores, as illustrated in Figure 1.1. One or several solid- and fluid phases may be involved. A porous medium is said to be *permeable* if it is possible for the fluid phase to traverse through the interconnected pore sections. The term *permeability* is therefore used to describe the extent of conductance of fluid flow through the porous medium.

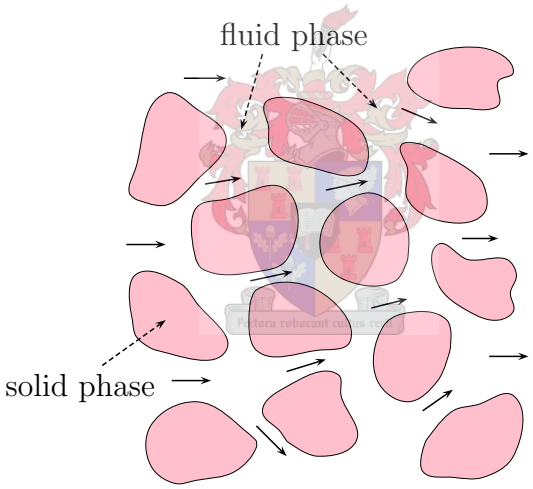


Figure 1.1: A two-dimensional schematic representation of an unbounded granular porous medium. The solid arrows indicate the direction of fluid flow through the pores.

A characteristic bulk property of a porous medium is the *porosity* $\epsilon$ which is defined as the ratio of the void (which may be filled with liquid or gas) volume to the total (void and solid) volume of the porous medium. Granular porous media are classified as *unconsolidated* media and occur either naturally or it is constructed commercially for various engineering applications. Examples are the natural phenomenon of fluid flow through granular soils such as sand, rock and sandstones and water seepage through the subsoil of dams and other construction materials. Sandstone is a natural porous rock formation of very low

porosity ($0.02 < \epsilon < 0.35$). Granular packed beds ($0.25 \leq \epsilon \leq 0.47$) and fluidized beds ($0.35 \leq \epsilon \leq 0.8$) are utilized for various applications in the chemical, pharmaceutical and petroleum industries. Packed columns are widely used in fixed- and fluidized bed reactors, mass and heat transfer operations, separation processes and filtration.

Many years of research have been devoted to predicting the permeability of low to moderate porosity granular porous media. The ability to accurately predict the permeability through any type of granular porous medium, depends on a detailed description of the granular microstructure. A thorough knowledge of the interstitial properties of the porous medium is, however, an arduous task to obtain due to the complex geometry of the porous matrix. As a result there are very few analytical models in the literature for predicting the permeability through granular porous media. The customary procedure to follow recently is to solve the interstitial momentum transport equations through numerical simulations. Instead one seeks simple analytical techniques for predicting the permeability as a function of the porosity without the need to obtain information on the complex interstitial properties of the porous medium.

## 1.1 Granular models from literature

The methods for modelling flow through granular porous media found in the literature may be classified more or less into three categories, i.e. the *capillary tube* or *hydraulic radius* model, the *submerged object* model and models based on a *statistical averaging* approach.

In the capillary tube or hydraulic radius approach the flow through a granular packed bed is regarded as being equivalent to flow through a network of capillary tubes of varying cross-section but with a constant average cross-sectional area. The velocity profile is obtained by solving the Navier-Stokes equation for steady and fully developed flow. An expression is obtained for the pressure drop prediction across the packed bed.

***Ergun (1952)*** proposed a semi-empirical capillary tube model for predicting the pressure drop of a Newtonian fluid across a packed bed for Reynolds numbers ranging from the laminar to the highly turbulent flow regimes. Despite many critical comments by many authors in the past (e.g. Dagan (1989) and Brea et al. (1976)) on the rather unrealistic capillary representation of a packed bed, the Ergun equation proves to be somewhat more successful than the submerged object models, based on the frequent use of the equation to serve as the onset of many other proposed models in the literature. The Ergun equation has been modified by many authors (e.g. Gidaspow (1994), Yu et al. (1968) and Mishra et al. (1975)) to predict the flow behaviour in a fluidized bed. Mehta & Hawley (1969) modified the Ergun equation to take into account the effect of the column wall when the column to particle diameter ratio is small. Bird et al. (2002) was the first to modify the Ergun equation to describe the rheological flow behaviour of non-Newtonian fluids in porous media. The Ergun equation has also been modified extensively (Christopher & Middleman (1965), Kemblowski & Michniewics (1979), Brea et al. (1976)) to account for

non-Newtonian power law flow.

***Macdonald et al. (1979)*** verified the predictive capabilities of the Ergun equation with experimental data from the literature involving granular porous media of various porous microstructures and proposed different coefficient values for the Ergun equation.

***Sabiri & Comiti (1995)*** and ***Chhabra & Srinivas (1991)*** investigated the flow of a non-Newtonian purely viscous power law fluid through granular beds experimentally and proposed an expression for predicting the pressure drop across the bed based on the capillary tube model.

***Chakrabarti et al. (1991)*** investigated the rheology of various concentrations of a commercial polymer solution through beds consisting of spherical particles experimentally by using the capillary tube model.

The submerged object approach regards flow around an assemblage of submerged objects forming a spatial array. The customary procedure to follow in determining the drag force on a typical particle in the assemblage is by modification of the Stokes' drag on a single particle to account for the additional resistance arising from the presence of neighbouring particles.

***Stokes' flow*** (e.g. Chorlton (1967)) involves the steady creeping motion of an incompressible Newtonian fluid with a uniform approaching velocity past an isolated, stationary sphere embedded in a fluid of infinite extent. The drag force on the sphere is determined by solving the Stokes equations.

***Chester (1962)*** pointed out that when the Reynolds number is not negligibly small Stokes' drag for flow past a sphere is inadequate since the inertial terms are not negligible at great distance from the sphere. The drag force obtained from solving Oseen's equations provides a first order expansion of the Reynolds number.

***Hasimoto (1958)*** considered the steady motion of an incompressible Newtonian fluid past a periodic array of small particles in a dilute medium. The drag force on a typical sphere within the array was obtained by modification of the Stokes equations.

***Happel (1958)*** proposed a concentric spherical cell model for predicting the flow of a Newtonian fluid through a random assemblage of spheres of low porosity in the creeping flow regime. The assemblage of spheres is regarded as a periodic array of identical spherical cells. Each cell contains a single sphere surrounded by a fluid envelope with a frictionless boundary. The Stokes' equations subjected to appropriate boundary conditions were solved and by application of Darcy's law the pressure drop prediction across the bed was obtained.

Various statistical averaging methods have been proposed in the literature, e.g. the method involving a spatial volume averaging over a representative elementary volume, the method of homogenization for application to Stokes' flow through periodic structures and purely statistical averaging methods concerning probability density and uncertainty

distribution functions.

***Dagan (1989)*** proposed a purely statistical model for predicting the permeability for steady flow of an incompressible Newtonian fluid through a granular porous medium of low porosity. The porous medium is regarded as a network of three-dimensional planar fissures with interconnected pores and identical constant apertures.

***Du Plessis (1994)*** proposed an analytical model for predicting the pressure gradient for Newtonian flow through granular porous media for all porosities and Reynolds numbers ranging from the Darcy regime to the steady laminar limit of the Forchheimer regime. The pore-scale model is based on a rectangular representation of the average granular porous microstructure.

***Smit & Du Plessis (2000)*** extended the rectangular representative unit cell model of Du Plessis & Masliyah (1991) to provide an analytical pressure drop prediction for non-Newtonian purely viscous power law flow through porous media of various types of porous microstructures, including granular media.

## 1.2 Objective

The capillary tube models are semi-empirical models in which empirical factors are introduced for correlation with experimental data. Many of the submerged object models, on the contrary, are exact analytical models (e.g. the models of Stokes and Hasimoto) and therefore lack the ability to be generalized for a broader field of application. Although the capillary tube model have the ability to be extended for various other fields of applicability, its main draw back is its empiricism. Consequently, the need arises to produce a simple generic analytical model of which the assumptions made within the analytical modelling procedure may easily be adapted to broaden its range of applicability.

Over the past two decades an analytical model has been developed at the University of Stellenbosch for predicting fluid flow through various types of porous media. The original model was proposed in 1988 and has ever since been adapted to improve its predictive capabilities. The objective of this work is to present the most recent improvement of the analytical model for predicting the pressure drop across a *granular* porous medium for Reynolds numbers within the steady laminar flow regime and over a wide range of porosities.

## 1.3 Assumptions

In order to provide a relatively simple, but still realistic, pore-scale model to approximate the complex geometry of the granular porous microstructure, some simplifying assumptions need to be made.

This work concerns three-dimensional, isothermal, steady laminar flow of an incompressible viscous fluid through a granular porous medium. The porous medium is assumed to be homogeneous and isotropic with respect to the average geometrical properties. The porous medium is also assumed to be unbounded. Wall effects due to external boundaries may therefore be neglected and as a result the local porosity may be assumed to be constant. The pore sections are assumed to be inter-connected, but may contain stagnant regions where the fluid remains stationary. The solid constituents are assumed to be uniformly sized, rigid, smooth and randomly distributed in all directions. The traversing fluid is assumed to consist of a single fluid phase, i.e. only saturated fluid flow is considered, with constant physical properties, unless otherwise stated. Both phases will be treated as a continuum and therefore the terms 'particle' and 'grain' will be regarded as equivalent. It is furthermore assumed that the grains remain stationary, which may be justified by the fact that in a packed bed the grains are supported by inter-particle contact (Happel & Brenner (1965)).

## 1.4 Layout of thesis

The commencement of the analytical model to be introduced is the method of volume averaging of the transport equations describing the motion of the fluid through the porous medium. The application of this method to the relevant transport equations is discussed in chapter 2. The granular pore-scale model is introduced in chapter 3 together with a discussion of the laminar flow regimes under consideration. Chapters 4 and 5 are devoted to the analytical modelling of the pore-scale model within the two asymptotic limiting flow regimes discussed in chapter 4. The pore-scale model for Newtonian flow is presented in chapter 6 and compared with the semi-empirical Ergun equation. The rest of this work concerns generalizations of the Newtonian model. In chapter 7 the model is adapted to account for non-Newtonian flow and in chapter 8 the Newtonian model is extended for application in fluidized beds and sandstones. Finally some conclusions are drawn in chapter 9.

# Chapter 2

# Method of Volume Averaging

This chapter concerns the local volume averaging of the momentum equations governing the fluid transport within the pores of the porous medium. The method of volume averaging provides a manner of relating the interstitial flow conditions to the measurable macroscopic flow behaviour.

## 2.1 Interstitial transport equations

The governing equations describing single phase flow of an incompressible Newtonian fluid in an infinitely permeable porous medium are the continuity equation for conservation of mass, i.e.

$$\nabla \cdot \underline{v} \;=\; 0 \;, \tag{2.1}$$

and the Navier-Stokes equation for interstitial momentum transport derived from Newton's second law (e.g. Happel & Brenner (1965))

$$\rho \frac{\partial \underline{v}}{\partial t} \;+\; \nabla \cdot (\rho \, \underline{v} \, \underline{v}) \;=\; -\nabla \mathcal{P} \;+\; \nabla \cdot \underline{\underline{\tau}} \;+\; \rho \, \underline{f}_b \;, \tag{2.2}$$

where $\underline{v}$ is the interstitial fluid velocity at any point within the pore space, $\rho$ is the constant fluid density, $\mathcal{P}$ is the interstitial hydrostatic pressure, $\underline{\underline{\tau}}$ is the local shear stress tensor of a Newtonian fluid and $\underline{f}_b$ denotes the external body forces per unit mass. The terms on the left hand side of equation (2.2) represent the time rate of change in momentum per unit volume of fluid, constituting the inertial forces, and the terms on the right hand side represent the external forces per unit volume contributing to the nett force exerted on the differential fluid element. The external forces include body forces, e.g. gravitation, and pressure and viscous forces exerted on the surface of the fluid element. Assuming that the gravitational force is a conservative force and discarding other external forces, $\underline{f}_b$ may be expressed as $\underline{f}_b = -\nabla gz$ where $z$ denotes an elevation and the gravitation

constant $g$ is assumed to remain constant with variations in $z$. Under these conditions, the terms $-\nabla\mathcal{P}$ and $\rho\underline{f}_b$ may be combined to form a single term, i.e. $-\nabla(\mathcal{P}+\rho\,gz)$. For relatively small values of $z$ the gravitational term may be assumed to be negligible. The pressure $p=\mathcal{P}+\rho\,gz$ will henceforth be referred to as the interstitial dynamic pressure. The Navier-Stokes equation may accordingly be expressed as

$$\rho\,\frac{\partial\,\underline{v}}{\partial\,t}\;+\;\nabla\cdot(\rho\,\underline{v}\,\underline{v})\;=\;-\nabla p\;+\;\nabla\cdot\underline{\underline{\tau}}\,, \tag{2.3}$$

The method of volume averaging over a representative portion of the fluid domain to obtain local measurable macroscopic volume averaged transport equations has been studied by many authors (e.g. Bear & Bachmat (1986), Slattery (1969) and Whitaker (1969)). The next section will shortly address some of the basic principles on which the method is based.

## 2.2 Representative Elementary Volume

A Representative Elementary Volume, abbreviated REV, is defined as an averaging volume $\mathcal{U}_o$ of finite extent within the porous domain (e.g. Whitaker (1999)), consisting of both fluid and solid phases, respectively denoted by $\mathcal{U}_f$ and $\mathcal{U}_s$. A two-dimensional schematic representation of a spherical REV is shown in Figure 2.1.

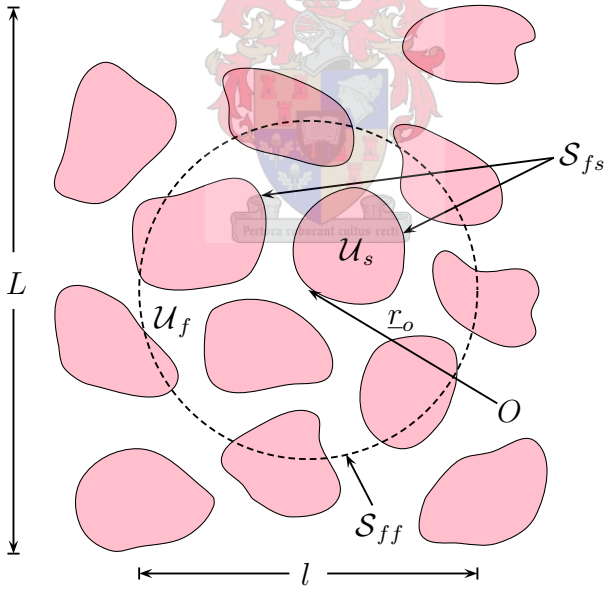


Figure 2.1: A two-dimensional schematic representation of a spherical REV. The dashed line indicates the REV boundary.

An REV is defined at each an every point within the unbounded porous medium. The centroid of each REV is indicated by a position vector $r_o$ relative to some arbitrary origin

$O$, as illustrated in Figure 2.1 for a single REV. Inter-connectivity of the pore space and treating the fluid phase as a continuum are essential requirements for an REV. Although the shape of the REV is not prescribed, it should ensure that the averaging functions are continuous and also continuously differentiable to any order. It is however required that the size, shape and orientation of the REV should remain constant. The REV is chosen to be the smallest possible volume containing sufficient fluid and solid parts to be statistically representative of the local average properties, e.g. the local porosity. The size of the REV is appropriately chosen when small variations in the local volume will not change the values of the local average properties. In terms of the linear dimensions indicated in Figure 2.1, this will require that $l >> d_p$ and $l << L$. The fluid-solid interfaces within the REV are denoted by $\mathcal{S}_{fs}$ and the fluid-fluid interfaces on the REV boundary by $\mathcal{S}_{ff}$. The porosity $\epsilon$ of the REV is assumed to be uniform and constant and is defined by the volumetric ratio

$$\epsilon \equiv \frac{\mathcal{U}_f}{\mathcal{U}_o} . \tag{2.4}$$

## 2.3 Macroscopic volume averaged quantities

The concept of an REV leads to the introduction of various measurable macroscopic volume averaged quantities. The *superficial velocity* $\underline{q}$, also known as the Darcy velocity or specific discharge, is defined as the phase average (Appendix A.1) of the interstitial fluid velocity $\underline{v}$, i.e.

$$\underline{q} = \langle \underline{v} \rangle = \frac{1}{\mathcal{U}_o} \iiint_{\mathcal{U}_f} \underline{v} \, d\mathcal{U} , \tag{2.5}$$

and represents the average velocity that would prevail in a section of the porous medium in which no solid phase is present. For this reason it is customary to use the superficial velocity in the comparison of different flow systems. The *streamwise direction* $\widehat{\underline{n}}$ is defined as the direction of the superficial velocity, that is

$$\widehat{\underline{n}} = \underline{q}/q . \tag{2.6}$$

The *drift velocity* $\underline{u}$ is defined as the intrinsic phase average (Appendix A.1) of the interstitial velocity $\underline{v}$, i.e.

$$\underline{u} = \langle \underline{v} \rangle_f = \frac{1}{\mathcal{U}_f} \iiint_{\mathcal{U}_f} \underline{v} \, d\mathcal{U} , \tag{2.7}$$

and represents the average fluid velocity in the streamwise direction. The relationship between the superficial- and drift velocity is given by

$$\underline{q} = \epsilon \, \underline{u} , \tag{2.8}$$

which is known as the Dupuit-Forchheimer relation. The *deviation* of any fluid phase tensorial quantity $\phi$ at any point within $\mathcal{U}_f$ is denoted by $\{\phi\}$ and defined as

$$\{\phi\} \equiv \phi - \langle\phi\rangle_f \ . \tag{2.9}$$

## 2.4 Macroscopic transport equations

Volume averaging of the continuity equation for an incompressible fluid over a sufficiently large REV (Appendix A.2) leads to

$$\nabla \cdot \underline{q} = 0 \ , \tag{2.10}$$

and the volume averaged Navier-Stokes equation (Appendix A.3) for an incompressible fluid may be expressed as

$$-\nabla \langle p \rangle = \rho \frac{\partial \underline{q}}{\partial t} + \rho \nabla \cdot \left( \underline{q}\,\underline{q}/\epsilon \right) + \rho \nabla \cdot \langle \{\underline{v}\}\{\underline{v}\} \rangle - \nabla \cdot \left\langle \underline{\underline{\tau}} \right\rangle + \frac{1}{\mathcal{U}_o} \iint\limits_{\mathcal{S}_{fs}} \left( \underline{n}\,\{p\} - \underline{n} \cdot \underline{\underline{\tau}} \right) d\mathcal{S} \ . \tag{2.11}$$

where $\underline{n}$ is the inwardly directed unit vector normal to the surface of the solid and $\langle p \rangle$ denotes the average macroscopic pressure. Equation (2.11) predicts the streamwise pressure gradient for unidirectional average flow over any type of porous medium, e.g. granular media, foams and fibre beds. The surface integral contains all the information on the fluid-solid interaction and depends strongly on the porous microstructure. The evaluation of the surface integral is subjected to a detailed and accurate description of the interstitial pressure- and velocity gradients at the fluid-solid interfaces. In order to circumvent the complex geometry of the solid constituents, a pore-scale model resembling the porous microstructure will be introduced in the following chapter to approximate and quantify the surface integral for the particular case of a granular porous medium.

# Chapter 3

# Rectangular Granular Pore-Scale Model

This chapter introduces the concept of a pore-scale model for closure modelling of the interstitial fluid-solid interaction to analytically quantify the pressure gradient prediction over a granular porous medium.

## 3.1 Rectangular Representative Unit Cell

A rectangular Representative Unit Cell, abbreviated RUC, was originally introduced by Du Plessis & Masliyah (1988) for isotropic sponge-like media. A rectangular RUC is defined as the smallest rectangular control volume, $U_o$, into which the local average properties of the REV may be embedded. The granular RUC model was introduced by Du Plessis & Masliyah (1991) after which some of the model assumptions were improved by Du Plessis (1994). The latter model will henceforth be referred to as the existing RUC model. The granular RUC model is schematically illustrated in Figure 3.1. The fluid filled volume within the RUC is denoted by $U_f$ and $U_s$ denotes the volume of the solid phase. The RUC is assumed to be homogeneous and isotropic in accordance with the average geometry of the porous medium. The assumption of average geometrical isotropy allows the introduction of a cubic RUC of linear dimension $d$, defined as the average length scale over which similar changes in geometrical and physical properties take place. The solid cube represents the average geometric properties of the granular solid microstructure. The length of the cube is denoted by $d_s$. The cubic geometry of the RUC model is introduced for mathematical simplicity and serves as an approximation for flow through an assemblage of grains with arbitrary shape. The solid cube is assumed to be stationary and is positioned so that a vector normal to any of the cube's faces is parallel to a normal vector on the corresponding face of the RUC. Due to the parallel alignment of the solid cubes' faces with that of the RUC, one of the fluid channels will always be aligned with the streamwise direction, leaving the remaining two channels to be directed in transverse

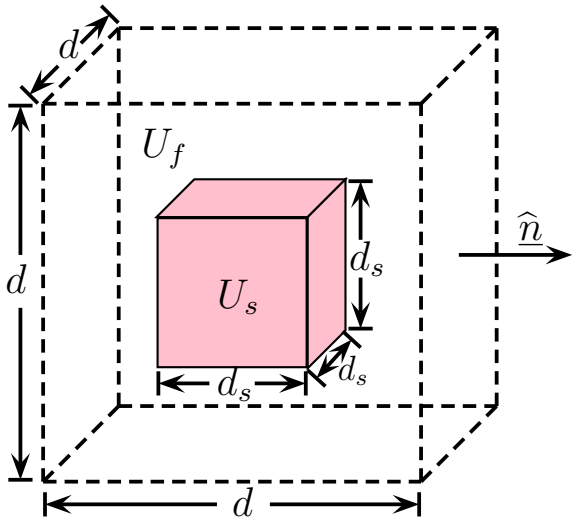


Figure 3.1: Cubic geometry of the RUC model for modelling the fluid flow through an isotropic granular porous medium. The streamwise direction is indicated by $\hat{n}$.

directions, that means, directions perpendicular to the streamwise direction. Any property referring to the streamwise direction will henceforth be denoted by a subscript $\parallel$ and any property related to a transverse direction by $\perp$. The porosity $\epsilon$ of the RUC is assumed to be equivalent to the porosity of the REV and is defined as

$$\epsilon = \frac{U_f}{U_o} . \tag{3.1}$$

The fluid filled volume $U_f$ and the volume of the solid cube $U_s$ may be expressed in terms of the linear dimensions $d$ and $d_s$ as follows

$$U_f = \epsilon U_o = \epsilon d^3 , \tag{3.2}$$

$$U_s = d_s^3 , \tag{3.3}$$

which lead to the following relationship between the linear dimensions of the RUC in terms of the porosity $\epsilon$:

$$d_s = (1-\epsilon)^{\frac{1}{3}} d . \tag{3.4}$$

## 3.2 Staggered and non-staggered arrays

The relative transverse positioning of neighbouring RUC's in the streamwise direction leads to the introduction of two arrays yielding different fluid flow phenomena. The array in which maximum possible staggering of the solid cubes in a straight streamtube of width $d$ occurs in the streamwise direction, is referred to as a *fully staggered array* and the array in which no staggering occurs in any of the three principal directions, is referred to as a

*regular array*. This section forms an extension of the existing RUC model since the latter model did not consider an array in which splitting of the stream-tube occurs neither one in which stagnant regions are present.

### 3.2.1 Fully staggered array

A typical two-dimensional RUC within a streamwisely fully staggered array is schematically illustrated in Figure 3.2.

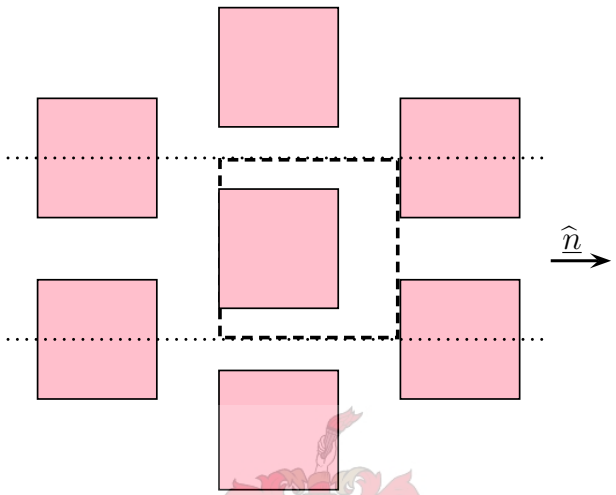


Figure 3.2: A two-dimensional schematic representation of a fully staggered array. The boundaries of a typical RUC is indicated by the bold dashed lines and the dotted lines represent a stream-tube.

In a fully staggered array the streamwise flux is split and then deviated in opposite transverse directions to traverse past the solid cube opposing the motion of the fluid in the streamwise direction. The streamwise flux reunites on the lee side of this cube and proceeds to flow in the streamwise direction before the next solid obstacle causes the streamwise flux to split again and the process repeats itself. A fully staggered array contains no stagnant regions and no staggering occurs in the two transverse directions. Also shown in Figure 3.2 is a stream-tube, represented by the dotted lines, that serves as a fluid envelope through which the fluid flows in the streamwise direction. Since the stream-tube consists of a bundle of streamlines which may not cross, it is assumed that all the fluid enters the RUC through the upstream face and exits through the downstream face with no fluid exchange across the transverse facing surfaces of the RUC. Figure 3.3 is a three-dimensional schematic representation of an RUC within a fully staggered array.

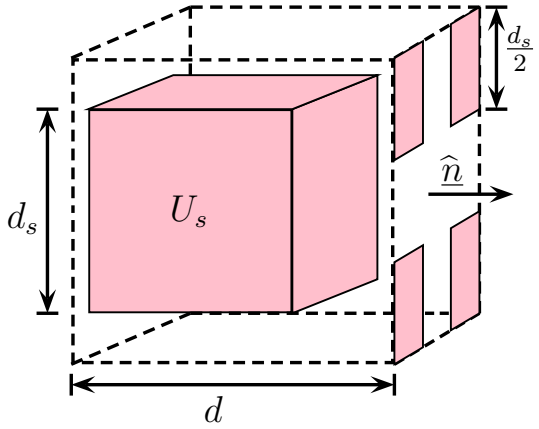


Figure 3.3: A three-dimensional schematic representation of an RUC within a fully staggered array.

Figure 3.4 represents a two-dimensional upstream view of the RUC associated with a fully staggered array. It may be visualized that the fluid is flowing out of the paper around the cube at the rear and then transversally to exit past the forward quarter cubes.

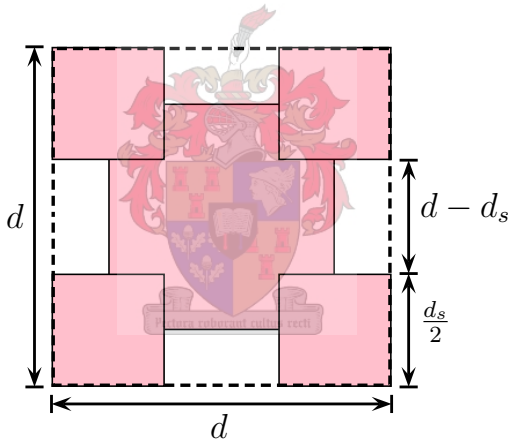


Figure 3.4: A two-dimensional upstream view of an RUC associated with a fully staggered array.

### 3.2.2 Regular array

Figure 3.5 is a two-dimensional schematic representation of a typical RUC within a regular array. Also shown is the stream-tube associated with such an array.

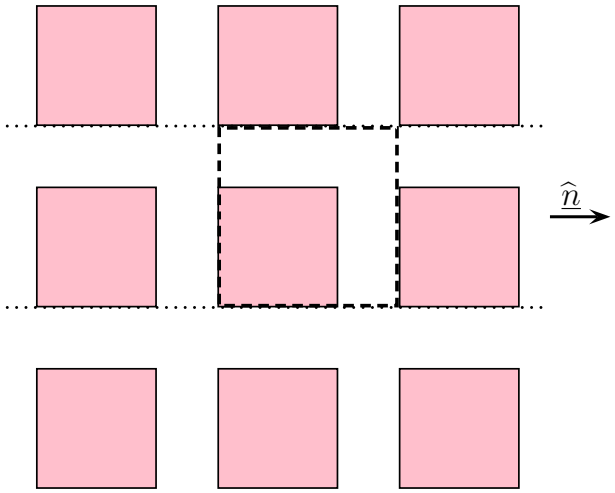


Figure 3.5: A two-dimensional schematic representation of a regular array. The boundaries of a typical RUC is indicated by the bold dashed lines and the dotted lines represent a stream-tube.

In a regular array the fluid enters and leaves the RUC in the streamwise direction without being deviated in a transverse direction, that is, in a regular array no staggering occurs. A regular array contains stagnant regions where the fluid remains stationary between any two neighbouring cubes in the streamwise direction. Note that in each of the three principal directions normal to the cube faces no staggering occurs. A three-dimensional schematic representation of an RUC within a regular array is shown in Figure 3.6.

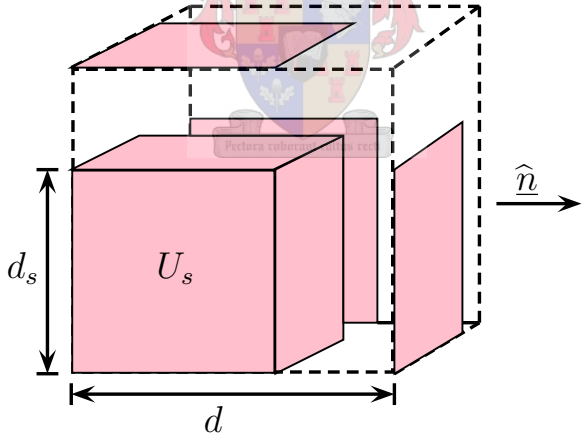


Figure 3.6: A three-dimensional schematic representation of an RUC within a regular array.

Figure 3.7 shows a two-dimensional upstream view of a regular array. The fluid may be visualized to be flowing out of the paper, past the cubes which are positioned directly behind each other in the streamwise direction.

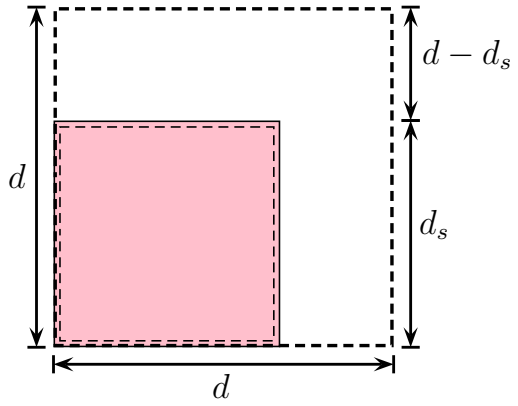


Figure 3.7: A two-dimensional upstream view of an RUC associated with a regular array.

## 3.3 Piece-wise straight streamlines

The adopted rectangular geometry and the isotropy requirement of the RUC model allow for the facing surfaces of any two neighbouring cubes to be a uniform distance $d - d_s$ apart, yielding pair-wise sets of equal parallel plates. In conjunction with the parallel plate configuration, piece-wise straight streamlines, between and parallel to the plates, are assumed to prevail within all the flow channels, as illustrated in Figure 3.8 for the respective arrays.

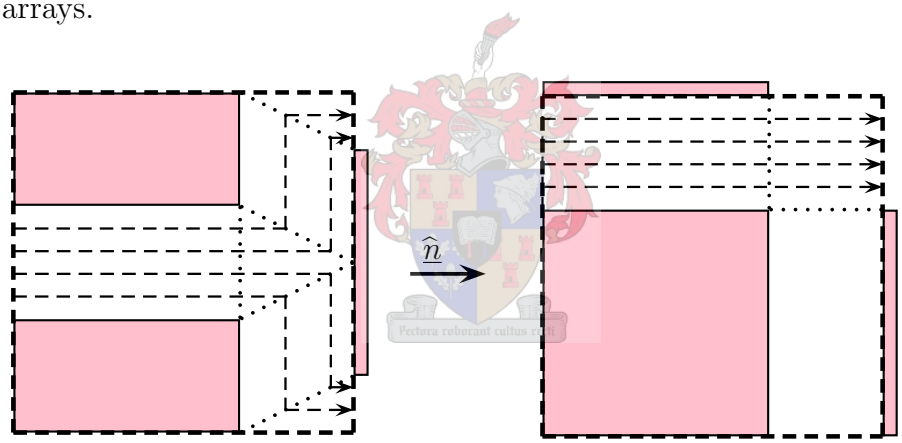


(a) Fully staggered array (b) Regular array

Figure 3.8: A two-dimensional representation of the piece-wise straight streamlines associated with (a) a fully staggered array and (b) a regular array. The dashed lines represent the streamlines and the bold dashed lines a typical RUC.

The splitting of the stream-tube into two equal but directionally opposite transverse fluid volumes within a fully staggered array is clearly illustrated by the streamlines in Figure 3.8 (a). Figure 3.8 (b) shows the stagnant volume, indicated by the absence of streamlines, present between any two neighbouring cubes in the streamwise direction within a regular array.

## 3.4 Volume partitioning

The piece-wise straight streamlines allow for the fluid domain within an RUC to be partitioned into different sub-volumes depending on the orientation of the particular fluid volume with respect to the streamwise direction and the presence of surfaces adjacent to the specific fluid volume under consideration. The concept of volume partitioning of the fluid domain was not considered in the existing RUC model. The volume partitioning of the fluid domain within the RUC presented in Figure 3.6 for a regular array is shown in Figure 3.9. As opposed to the other figures shown thus far, the shaded volumes within Figure 3.9 represent fluid volumes. The solid volumes are not shown.

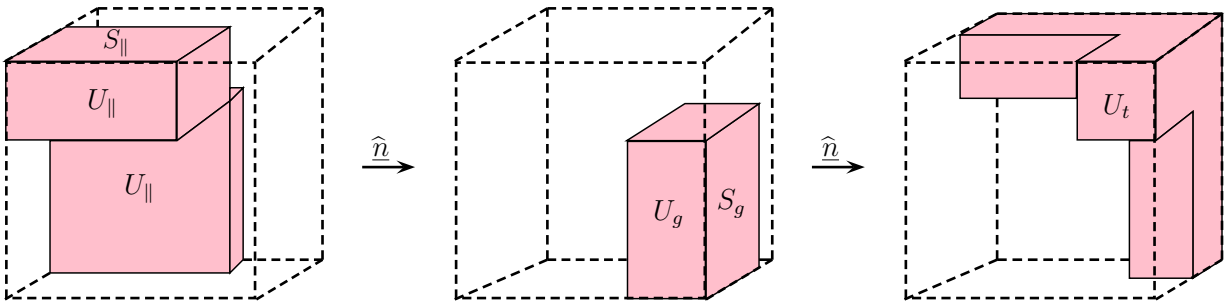


Figure 3.9: A three-dimensional volume partitioning of the fluid domain within the RUC presented in Figure 3.6 for a regular array. The shaded volumes represent fluid volumes, solid volumes are not shown.

The fluid volume in the channels parallel to the streamwise direction and adjacent to solid surfaces is denoted by $U_\parallel$ and is referred to as a streamwise volume. The solid surfaces adjacent to $U_\parallel$ are denoted by $S_\parallel$ and are referred to as the streamwise surfaces. The fluid volume in the stagnant regions between any two neighbouring cubes in the streamwise direction, is denoted by $U_g$ and is referred to as a stagnant volume. The solid surfaces adjacent to $U_g$ are denoted by $S_g$ and are referred to as the stagnant surfaces. The fluid volume involving no shear stresses due to the absence of adjacent solid surfaces is denoted by $U_t$ and is referred to as a transfer volume. Similarly, volume partitioning may be applied to the fluid domain within the RUC presented in Figure 3.3 for a fully staggered array. The volume partitioning of a fully staggered array is not shown because of the complexity of illustrating it graphically. As opposed to the stagnant region within a regular array, a fully staggered array is characterized by a fluid volume in which the fluid flows in directions perpendicular to the streamwise direction. These fluid volumes, denoted by $U_\perp$, are adjacent to solid surfaces and are referred to as the transverse volumes. The solid surfaces adjacent to $U_\perp$ are denoted by $S_\perp$ and are referred to as the transverse surfaces. The total fluid volume $U_f$ contained within an RUC associated with any of the two arrays may thus be expressed as

$$U_f \;=\; U_\parallel \;+\; U_\perp \;+\; U_g \;+\; U_t \;, \tag{3.5}$$

and the total fluid-solid interfaces $S_{fs}$ may accordingly be expressed as

$$S_{fs} \;=\; S_{\parallel} \;+\; S_{\perp} \;+\; S_g \;. \tag{3.6}$$

For a fully staggered array $U_g = S_g = 0$ and for a regular array $U_\perp = S_\perp = 0$. The expressions for the three-dimensional surface- and volume partitioning of the respective arrays are presented in Table 3.1 in terms of the linear dimensions $d$ and $d_s$. The expressions presented in Table 3.1 denote the total volume (or surface area) associated with the specified volume (or surface).

| | Array | |
|---|---|---|
| Parameter | Fully staggered | Regular |
| $U_o$ | $d^3$ | |
| $U_s$ | $d_s^3$ | |
| $U_f$ | $d^3 - d_s^3$ | |
| $U_t$ | $(d-d_s)^2\,(d+2d_s)$ | |
| $U_{\parallel}$ | $2\,d_s^2(d-d_s)$ | |
| $S_{\parallel}$ | $4\,d_s^2$ | |
| $U_\perp$ | $d_s^2(d-d_s)$ | 0 |
| $S_\perp$ | $2\,d_s^2$ | 0 |
| $U_g$ | 0 | $d_s^2(d-d_s)$ |
| $S_g$ | 0 | $2\,d_s^2$ |

Table 3.1: Three-dimensional surface- and volume partitioning for the RUC's associated with a fully staggered- and regular array.

The volume partitioning of the fluid domain allows for the introduction of a streamwise average pore velocity $\underline{w}_{\parallel}$ (Du Plessis (1994)), defined as

$$\underline{w}_{\parallel} \;=\; \frac{1}{U_{\parallel}+U_t} \iiint\limits_{U_f} \underline{v}\, dU \tag{3.7}$$

and relates as follows to the superficial velocity $\underline{q}$,

$$\underline{w}_{\parallel} \;=\; \frac{\underline{q}\, d^2}{A_{p_{\parallel}}} \;, \tag{3.8}$$

where $A_{p_\parallel}$ is the streamwise cross-sectional flow area available for fluid discharge through the RUC, i.e.

$$A_{p_\parallel} \;=\; d^2 - d_s^2 \;. \tag{3.9}$$

It thus follows that

$$\underline{w}_\parallel \;=\; \frac{\underline{q}\, d^2}{d^2 - d_s^2} \;. \tag{3.10}$$

As listed in Table 3.1, different expressions are obtained for $U_\parallel$ and $U_\perp$ implying that the average pore velocities within these two fluid volumes should differ. A coefficient $\beta$ is therefore introduced to account for the different average velocities in the streamwise and transverse channels and is defined as

$$\beta \equiv \frac{w_\perp}{w_\parallel} \;, \tag{3.11}$$

with $w_\perp$ the magnitude of the transverse average pore velocity. A geometric factor $\psi$, defined as

$$\psi \;=\; \frac{U_f}{U_\parallel + U_t} \;=\; \frac{U_\parallel + U_t + U_\perp + U_g}{U_\parallel + U_t} \;, \tag{3.12}$$

was introduced by Lloyd et al. (2004). This factor yields the same result for a both a fully staggered- and non-staggered array, i.e.

$$\psi \;=\; \frac{\epsilon}{(1 - (1-\epsilon)^{2/3})} \;. \tag{3.13}$$

The reason for the introduction of the geometric factor $\psi$ will be addressed in the following chapter.

## 3.5 Volume averaging of transport equations over an RUC

Volume averaging of the Navier-Stokes equation for incompressible flow over a typical RUC may be expressed as

$$-\nabla \langle p \rangle \;=\; \rho \frac{\partial\, \underline{q}}{\partial\, t} \;+\; \rho \nabla \cdot \left( \underline{q}\, \underline{q}/\epsilon \right) \;+\; \rho \nabla \cdot \langle \{\underline{v}\}\, \{\underline{v}\} \rangle \;-\; \nabla \cdot \left\langle \underline{\underline{\tau}} \right\rangle + \frac{1}{U_o} \iint\limits_{S_{fs}} \left( \underline{n}\, \{p\} - \underline{n} \cdot \underline{\underline{\tau}} \right) dS \;, \tag{3.14}$$

where $\underline{n}$ denotes the inwardly directed unit vector normal to one of the cube faces. Together with the volume averaged continuity equation of an incompressible fluid, that is,

$$\nabla \cdot \underline{q} \;=\; 0 \;, \tag{3.15}$$

these equations describe the fluid transport through an RUC, which represents the average geometric and physical properties of the granular porous medium. Equation (3.14) provides an expression for the streamwise pressure gradient over the linear dimension $d$ of the RUC. The momentum dispersion term, $\rho\nabla\cdot\langle\{\underline{v}\}\{\underline{v}\}\rangle$, may be expressed as follows in terms of the superficial velocity $\underline{q}$ (Appendix A.3):

$$\rho\nabla\cdot\langle\{\underline{v}\}\{\underline{v}\}\rangle \;=\; \rho\nabla\cdot\left\langle\underline{q}\,\underline{q}\right\rangle - \frac{2}{\epsilon}\,\rho\nabla\cdot\left\langle\underline{q}\,\underline{q}\right\rangle + \frac{1}{\epsilon^2}\,\rho\nabla\cdot\left\langle\underline{q}\,\underline{q}\right\rangle\;, \tag{3.16}$$

It thus follows that

$$\begin{aligned}-\nabla\langle p\rangle \;=\; \rho\,\frac{\partial\,\underline{q}}{\partial\,t} \;+\; \rho\,\nabla\cdot\left(\underline{q}\,\underline{q}/\epsilon\right) \;+\; \rho\nabla\cdot\left\langle\underline{q}\,\underline{q}\right\rangle - \frac{2}{\epsilon}\,\rho\nabla\cdot\left\langle\underline{q}\,\underline{q}\right\rangle + \frac{1}{\epsilon^2}\,\rho\nabla\cdot\left\langle\underline{q}\,\underline{q}\right\rangle \\ -\nabla\cdot\left\langle\underline{\underline{\tau}}\right\rangle \;+\; \frac{1}{U_o}\iint\limits_{S_{fs}}\left(\underline{n}\,\{p\} - \underline{n}\cdot\underline{\underline{\tau}}\right)dS\;.\end{aligned} \tag{3.17}$$

For a Newtonian fluid of constant viscosity $\mu$, it follows that $\nabla\cdot\left\langle\underline{\underline{\tau}}\right\rangle = \mu\nabla^2\underline{q}$, yielding

$$\begin{aligned}-\nabla\langle p\rangle \;=\; \rho\,\frac{\partial\,\underline{q}}{\partial\,t} \;+\; \rho\,\nabla\cdot\left(\underline{q}\,\underline{q}/\epsilon\right) \;+\; \rho\nabla\cdot\left\langle\underline{q}\,\underline{q}\right\rangle - \frac{2}{\epsilon}\,\rho\nabla\cdot\left\langle\underline{q}\,\underline{q}\right\rangle + \frac{1}{\epsilon^2}\,\rho\nabla\cdot\left\langle\underline{q}\,\underline{q}\right\rangle \\ -\mu\nabla^2\underline{q} \;+\; \frac{1}{U_o}\iint\limits_{S_{fs}}\left(\underline{n}\,\{p\} - \underline{n}\cdot\underline{\underline{\tau}}\right)dS\;.\end{aligned} \tag{3.18}$$

All the terms in equation (3.18), except the surface integral, are macroscopic terms. The term $-\mu\nabla^2\underline{q}$ represents the macroscopic viscous shear at external walls, which may be neglected since the porous medium is assumed to be unbounded. Justified by approximated experimental conditions (Dybbs & Edwards (1982)), a uniform superficial velocity field $\underline{q}$ may be assumed. Since a uniform average velocity field implies macroscopic conservation of momentum, all the terms resulting from the interstitial rate of change in momentum should vanish macroscopically, which is indeed the case when $\underline{q}$ is assumed to be uniform in equation (3.18). It thus follows that for steady flow of an incompressible viscous fluid through a homogeneous porous medium in which a uniform average velocity field is assumed, the streamwise pressure gradient may be expressed as

$$-\nabla\langle p\rangle \;=\; \frac{1}{U_o}\iint\limits_{S_{fs}}\left(\underline{n}\,p - \underline{n}\cdot\underline{\underline{\tau}}\right)dS\;. \tag{3.19}$$

Equation (3.19) represents a force balance between the external pressure gradient for fluid transport through the RUC and the pressure and viscous forces exerted by the solid cube on the traversing fluid. The first term in the surface integral denotes the inertial pressure forces exerted by the solid cube on the traversing fluid due to a pressure variation over the upstream and downstream facing surfaces of the cube. The pressure variation results

from a change in momentum across the streamwise facing surfaces of the cube. Note that these inertial pressure forces are interstitial forces which contribute to the external pressure gradient, as opposed to the macroscopic inertial forces that vanished due to the assumption of a uniform average velocity field. Interstitially changes in momentum occur, which become significant at higher Reynolds numbers, but macroscopically momentum is conserved. The second term in the surface integral denotes the viscous forces exerted by the solid cube on the traversing fluid due to shear stresses at the fluid-solid interfaces. Since the Reynolds number is defined as the ratio of the inertial forces to the viscous forces, the contribution of the pressure- and viscous forces to the streamwise pressure gradient depends on the magnitude of the Reynolds number. The Reynolds number used in the RUC model is a particle Reynolds number $Re_p$, defined in terms of the length $d_s$ of the solid cube, i.e.

$$Re_p = \frac{\rho\, q\, d_s}{\mu} \ . \tag{3.20}$$

The following chapters concern closure modelling of the surface integral of equation (3.19) in order to analytically quantify the fluid-solid interaction in the limit of very low Reynolds number flow and in the steady laminar limit of the inertial flow regime to obtain a general expression for the streamwise pressure gradient over a wide range of Reynolds numbers through application of an asymptote matching technique.

## 3.6 Classification of laminar flow regimes

Three laminar flow regimes will be considered, namely the asymptotic limit of low Reynolds number flow in the Darcy or creeping flow regime, the steady laminar limit of the inertial or Forchheimer flow regime and the transition regime in between which is characterized by the development of boundary layers. The steady laminar limit is followed by an unsteady laminar flow regime and at even higher Reynolds numbers the boundary layer becomes turbulent (Dybbs & Edwards (1982)). Since only steady flow is considered, the latter two regimes fall beyond the scope of this work.

### 3.6.1 Limit of low Reynolds number flow

The Darcy or creeping flow regime corresponds to a pore Reynolds number $Re < 1$ (Dybbs & Edwards (1982)). The analytical modelling procedure of the RUC model in this regime will concern pore Reynolds numbers within the asymptotic limit, i.e. $Re \approx 0.1$. The analogue between the streamlines associated with flow past a sphere and a cube in the limit of low Reynolds number flow is schematically shown in Figure 3.10. The piece-wise straight streamlines assumed by the RUC model for flow past a cube is clearly illustrated.

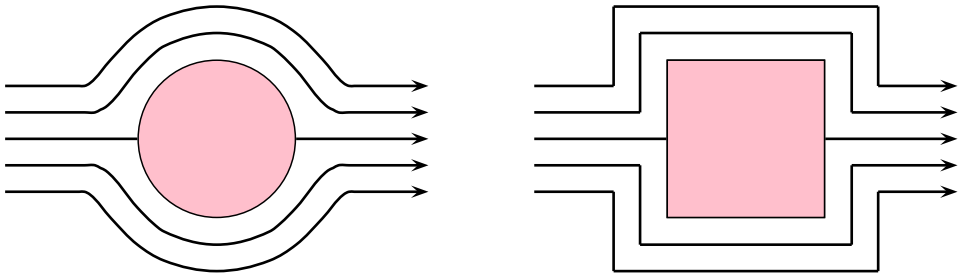

Flow past a sphere ($Re \approx 0.1$) Flow past a cube ($Re \approx 0.1$)

Figure 3.10: A two-dimensional schematic representation of the streamlines associated with flow past a sphere and a cube in the limit of low Reynolds number flow.

In this limit the viscous forces predominate over the inertial pressure forces and consequently the flow pattern is strongly influenced by the granular microstructure. The advantage of modelling fluid flow through the pores within this limit is that a fully developed velocity profile may be assumed to prevail throughout all the pore sections. The entrance effects arising from the gradual build-up of a developing velocity profile may thus be neglected.

### 3.6.2 Transition regime

The transition from the Darcy to the Forchheimer regime is due to the development of boundary layers near the solid surfaces within the pores. This regime is associated with $1 < Re < 100$ (Dybbs & Edwards (1982)). In the transition regime both the inertial and viscous forces contribute to the streamwise pressure gradient. The flow conditions in this regime are not modelled explicitly as it would require an enormous computational effort. The applied asymptote matching is assumed to be reasonably accurate in predicting the transitional effects.

### 3.6.3 Steady laminar limit of the inertial flow regime

The steady laminar limit of the inertial flow regime corresponds to $Re > 100$ (Dybbs & Edwards (1982)). At Reynolds numbers just before the commencement of the inertial flow regime, the boundary layer begins to separate from the downstream stagnation point on the lee side of the solids grains. The boundary layer moves further downstream as the Reynolds number increases until the steady laminar limit is reached at which a separation zone is formed on lee side of the solids grains. The analogue between the separation zone for flow past a sphere and a cube within the steady laminar limit of the inertial flow regime is schematically illustrated in Figure 3.11.

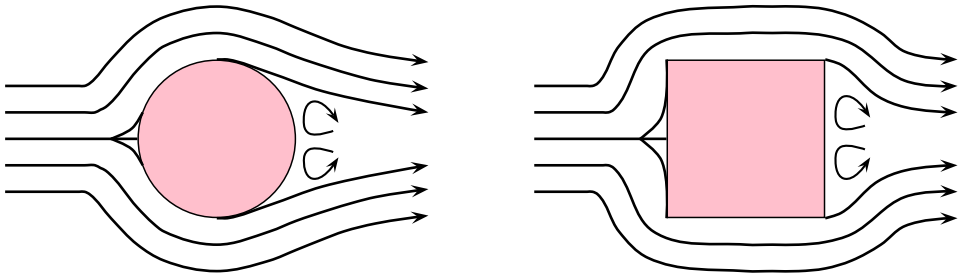

Flow past a sphere ($Re > 100$) Flow past a cube ($Re > 100$)

Figure 3.11: A two-dimensional schematic representation of the streamlines associated with flow past a sphere and a cube in the steady laminar limit of the inertial flow regime.

In the separation zone a low fluid velocity persists whereas, on the boundary of the separation zone, the fluid velocity is relatively high. As a result of the significant difference in flow velocities an interstitial recirculation pattern is generated within the separation zone. The entire square surface on the lee side of the solid is therefore exposed to a relatively low pressure. The resulting streamwise pressure difference between the upstream and downstream facing surfaces of the solid grains depends on the size of the separation zone which, in turn, depends on the position of the point of separation. The point of separation is again determined by the shape or form of the solid obstacle. This is the reason why the pressure force resulting from the pressure difference across a single isolated solid grain is referred to in the literature as form drag. For a laminar boundary layer separation occurs about midway between the front and rear of the solid (Roberson & Crowe (1985)). As a result of the separation of the boundary layer from the surface of the solid, the surface area on which the shear stresses act, is diminished substantially. Consequently, in the steady laminar limit of the inertial flow regime the pressure forces predominate over the viscous shear forces.

# Chapter 4

# Low Reynolds Number Flow Regime

This chapter involves the analytical closure modelling of the fluid-solid interaction within the RUC for predicting the streamwise pressure gradient in the asymptotic limit of low Reynolds number flow.

## 4.1 Closure modelling at low to moderate porosities

The assumption of flow between parallel plates is only valid for low to moderate porosities where neighbouring cubes are present. At high porosities neighbouring cubes are absent so that the parallel plate configuration no longer persists and the assumption of flow between parallel plates is no longer valid. The RUC model within the limit of low Reynolds number flow will therefore be classified as a low to moderate porosity model (i.e. $\epsilon < 0.8$). Fully developed laminar flow of a Newtonian fluid is assumed to prevail piece-wise throughout all pore sections. The closure modelling procedure with the three-dimensional granular RUC model to be presented in this work closely follows the work of Lloyd et al. (2004) for two-dimensional Newtonian flow perpendicular to a unidirectional fibre bed, although some discrepancies occur (Appendix B). The streamwise pressure gradient resulting from volume averaging of the transport equations in which a uniform velocity field $\underline{q}$ is assumed (Chapter 3), is given by

$$-\nabla \langle p \rangle = \frac{1}{U_o} \iint_{S_{fs}} \left( \underline{n}\, p - \underline{n} \cdot \underline{\underline{\tau}} \right) dS \,. \tag{4.1}$$

It was established by Lloyd (2003) that for low porosity media in the creeping flow regime the pressure term in the surface integral of equation (4.1) contains a viscous effect which contributes significantly to the streamwise pressure gradient. Although the viscous forces predominate over the inertial pressure forces in this regime, the pressure term should not be neglected. The shear stresses on the surfaces within the transverse channels are accompanied by transverse pressure gradients. These pressure gradients are contained within

the pressure term in the surface integral of equation (4.1). The commencement of the closure modelling procedure is the evaluation of the surface integral over the streamwise-, transverse- and stagnant surfaces within and adjacent to the RUC, yielding

$$-\nabla \langle p \rangle = \frac{1}{U_o} \iint_{S_\parallel} \underline{n}\, p\, dS + \frac{1}{U_o} \iint_{S_\perp + S_g} \underline{n}\, p\, dS - \frac{1}{U_o} \iint_{S_\parallel} \underline{n} \cdot \underline{\underline{\tau}}\, dS - \frac{1}{U_o} \iint_{S_\perp} \underline{n} \cdot \underline{\underline{\tau}}\, dS - \frac{1}{U_o} \iint_{S_g} \underline{n} \cdot \underline{\underline{\tau}}\, dS \,. \tag{4.2}$$

The parallel alignment of the streamwise surfaces of neighbouring cubes in the transverse directions results in a vectorial cancelation of the pressure on the streamwise surfaces, that is,

$$\frac{1}{U_o} \iint_{S_\parallel} \underline{n}\, p\, dS = \underline{0} \,. \tag{4.3}$$

Although streamlines may appear in the stagnant volume $U_g$ of a regular array, the corresponding velocities will be very small (Lloyd (2003)). Assuming therefore that the shear stresses on $S_g$ are negligible, it follows that

$$\frac{1}{U_o} \iint_{S_g} \underline{n} \cdot \underline{\underline{\tau}}\, dS = \underline{0} \,. \tag{4.4}$$

Equation (4.2) there-upon simplifies to

$$-\nabla \langle p \rangle = \frac{1}{U_o} \iint_{S_\perp + S_g} \underline{n}\, p\, dS - \frac{1}{U_o} \iint_{S_\perp} \underline{n} \cdot \underline{\underline{\tau}}\, dS - \frac{1}{U_o} \iint_{S_\parallel} \underline{n} \cdot \underline{\underline{\tau}}\, dS \,. \tag{4.5}$$

The quasi-periodic structure of the RUC model in the streamwise direction, i.e. each upward transverse channel is to be followed by an opposite downward transverse channel, plays an important role in the further analysis of the remaining surface integrals regarding the particular location of the RUC in the streamwise direction. It is therefore of utmost importance that all possible locations of the RUC in the streamwise direction should be considered. The two typical choices of RUC's chosen to accomplish the latter requirement are illustrated in Figures 4.1 and 4.2 for a fully staggered- and regular array, respectively. The upstream and downstream facing surfaces of the RUC with corner points AAAA cut through solid parts and the upstream and downstream facing surfaces of the RUC with corner points BBBB do not cut through any solid parts. $S_{\perp AA}$ and $S_{\perp BB}$ respectively denotes the fluid-solid interfaces adjacent to $U_\perp$ of the RUC with corner points AAAA and BBBB in the fully staggered array shown in Figure 4.1. Similarly, $S_{gAA}$ and $S_{gBB}$ respectively denotes the fluid-solid interfaces adjacent to $U_g$ of the RUC with corner points AAAA and BBBB in the regular array shown in Figure 4.2.

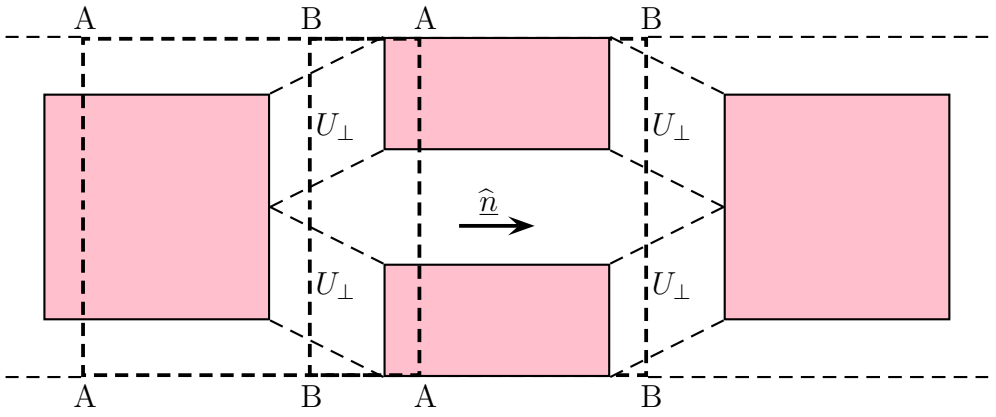


Figure 4.1: Schematic illustration of the two typical choices of RUC's in a fully staggered array to consider all possible locations in the streamwise direction.

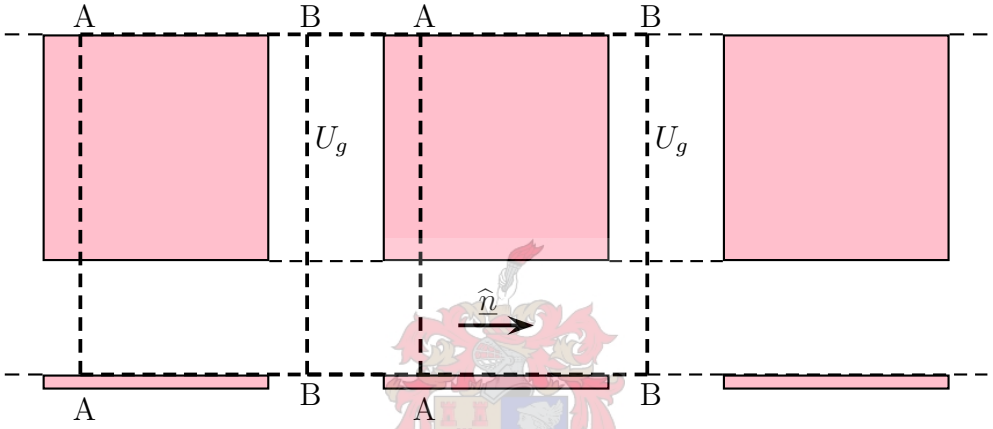


Figure 4.2: Schematic illustration of the two typical choices of RUC's in a regular array to consider all possible locations in the streamwise direction.

The relative frequency of occurrence of the RUC with corner points AAAA in the streamwise direction is $d_s/d$ and the relative frequency of occurrence of the RUC with corner points BBBB in the streamwise direction is $(d-d_s)/d$. If the transverse and stagnant surface integrals of equation (4.5) are weighed according to these relative frequencies of occurrence, over a streamwise displacement $d$, it follows that

$$-\nabla\langle p\rangle = \frac{d_s}{d}\cdot\frac{1}{U_o}\iint\limits_{S_{\perp AA}+S_{gAA}} \underline{n}\,p\,dS + \frac{d-d_s}{d}\cdot\frac{1}{U_o}\iint\limits_{S_{\perp BB}+S_{gBB}} \underline{n}\,p\,dS$$
$$-\frac{d_s}{d}\cdot\frac{1}{U_o}\iint\limits_{S_{\perp AA}} \underline{n}\cdot\underline{\underline{\tau}}\,dS - \frac{d-d_s}{d}\cdot\frac{1}{U_o}\iint\limits_{S_{\perp BB}} \underline{n}\cdot\underline{\underline{\tau}}\,dS - \frac{1}{U_o}\iint\limits_{S_\parallel} \underline{n}\cdot\underline{\underline{\tau}}\,dS\,. \qquad (4.6)$$

Assuming that the pressure $p$ on all facing pairs of transverse and stagnant surfaces are

equal, results in a vectorial cancelation of the pressures on these surfaces, that is

$$\frac{d_s}{d} \cdot \frac{1}{U_o} \iint\limits_{S_{\perp AA} \,+\, S_{gAA}} \underline{n}\, p \, dS \;=\; \underline{0}\,. \tag{4.7}$$

The RUC with corner points BBBB in the fully staggered array contains two transverse channels in which the fluid flows in opposite directions perpendicular to the streamwise direction. The shear stresses opposing the motion of the fluid on the surfaces adjacent to fluid volumes in these channels cancel vectorially. It thus follows that

$$\frac{d - d_s}{d} \cdot \frac{1}{U_o} \iint\limits_{S_{\perp BB}} \underline{n} \cdot \underline{\underline{\tau}}\, dS \;=\; \underline{0}\,. \tag{4.8}$$

Equation (4.6) there-upon simplifies to

$$-\nabla \langle p \rangle \;=\; \frac{d - d_s}{d} \cdot \frac{1}{U_o} \iint\limits_{S_{\perp BB} \,+\, S_{gBB}} \underline{n}\, p \, dS \;-\; \frac{d_s}{d} \cdot \frac{1}{U_o} \iint\limits_{S_{\perp AA}} \underline{n} \cdot \underline{\underline{\tau}}\, dS \;-\; \frac{1}{U_o} \iint\limits_{S_{\parallel}} \underline{n} \cdot \underline{\underline{\tau}}\, dS\,. \tag{4.9}$$

Defining $\tau_w$ as the magnitude of the local shear stress tensor $\underline{\underline{\tau}}$ on the solid surfaces, i.e. the wall shear stress, leads to

$$-\nabla \langle p \rangle \;=\; \frac{d - d_s}{d} \cdot \frac{1}{U_o} \iint\limits_{S_{\perp BB} \,+\, S_{gBB}} \underline{n}\, p \, dS \;+\; \frac{d_s}{d} \cdot \frac{1}{U_o} \iint\limits_{S_{\perp AA}} \tau_w \, dS \;+\; \frac{1}{U_o} \iint\limits_{S_{\parallel}} \tau_w \, dS\,. \tag{4.10}$$

Since fully developed flow is assumed within the asymptotic limit of low Reynolds numbers, the wall shear stress $\tau_w$ is assumed to be uniform and piece-wise constant over all the fluid-solid interfaces $S_{fs}$. The assumption of flow between parallel plates an equal distance $d - d_s$ apart allows for the interstitial velocity field within each channel section to be described by plane Poiseuille flow. The fully developed parabolic velocity profile associated with plane Poiseuille flow, together with the piece-wise straight streamlines assumed by the RUC model are illustrated in Figure 4.3 for a fully staggered- and regular array.

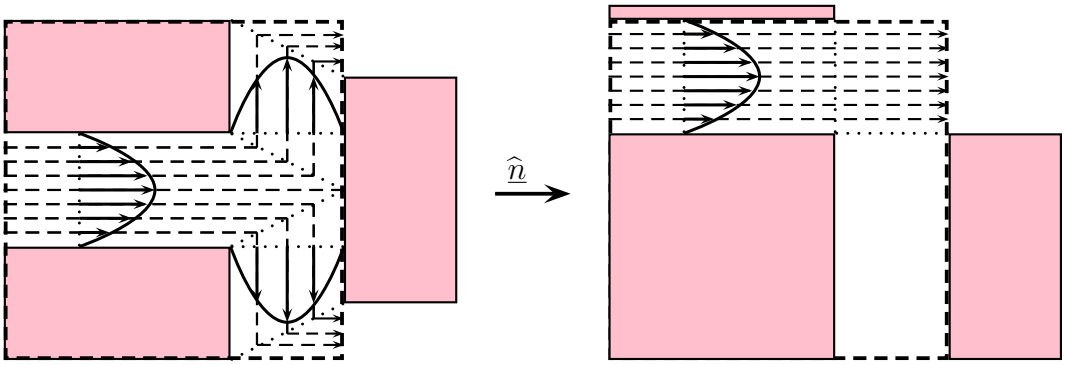


(a) Fully staggered array (b) Regular array

Figure 4.3: A two-dimensional schematic representation of the fully developed parabolic velocity profile together with the piece-wise straight streamlines associated with (a) a fully staggered and (b) a regular array. Only half of the neighbouring solid volumes are shown for clearer representation of the fluid channels.

Let $\tau_{w_\parallel}$ denote the wall shear stresses on the streamwise surfaces $S_\parallel$ and $\tau_{w_\perp}$ denote the wall shear stresses on the transverse surfaces $S_\perp$. The wall shear stress of a Newtonian fluid on the streamwise surfaces resulting from plane Poiseuille flow may be expressed as

$$\tau_{w_\parallel} \;=\; \frac{6\,\mu\,w_\parallel}{d-d_s}\;. \tag{4.11}$$

In a fully staggered array the streamwise flux divides to circumvent the solid obstacles causing the staggering in the streamwise direction. As a result the fluid flows in opposite directions within the transverse channels leading to a reduction in the wall shear stresses in the transverse channels of a fully staggered array due to the splitting of the streamtube. The latter effect is accounted for by the introduction of a coefficient $\xi$. The wall shear stresses on the transverse surfaces may accordingly be expressed as

$$\tau_{w_\perp} \;=\; \beta\,\xi\tau_{w_\parallel} \;=\; \frac{6\,\mu\,\beta\,\xi\,w_\parallel}{d-d_s}\;, \tag{4.12}$$

where $\beta$ is defined as in equation (3.11). The streamwise pressure gradient there-upon yields

$$-\nabla\langle p\rangle \;=\; \frac{d-d_s}{d}\cdot\frac{1}{U_o}\iint\limits_{S_{\perp BB}\;+\;S_{gBB}} \underline{n}\,p\,dS \;+\; \frac{\tau_{w_\parallel}S_\parallel + (d_s/d)\,\tau_{w_\perp}S_\perp}{U_o}\,\widehat{\underline{n}}\;. \tag{4.13}$$

In the limit of low porosities, that is, where the assumptions of the RUC model are satisfied,

$$\frac{d_s}{d} \;\approx\; 1\;. \tag{4.14}$$

It thus follows that

$$-\nabla \langle p \rangle \;=\; \frac{d-d_s}{d} \cdot \frac{1}{U_o} \iint\limits_{S_{\perp BB} \,+\, S_{gBB}} \underline{n}\, p \, dS \;+\; \frac{S_{\parallel} + \beta\, \xi\, S_{\perp}}{U_o}\, \tau_{w_{\parallel}}\, \widehat{\underline{n}}\,. \tag{4.15}$$

The remaining surface integral was shown by Lloyd (2003), to be expressible in terms of the gradient of the average pressure. The same procedure as for two-dimensional arrays of squares can be applied to three-dimensional arrays in the following way: Splitting the surface integral of equation (4.15) into one applicable to a fully staggered array and the other applicable to a regular array, yields

$$\begin{aligned} \frac{d-d_s}{d} \cdot \frac{1}{U_o} \iint\limits_{S_{\perp BB} \,+\, S_{gBB}} \underline{n}\, p \, dS \;&=\; \frac{d-d_s}{d} \cdot \frac{1}{U_o} \iint\limits_{S_{\perp BB}} \underline{n}\, p \, dS \;+ \\ &\quad \frac{d-d_s}{d} \cdot \frac{1}{U_o} \iint\limits_{S_{gBB}} \underline{n}\, p \, dS\,. \end{aligned} \tag{4.16}$$

The surface integral applicable to a fully staggered array may be expressed as

$$\begin{aligned} \frac{d-d_s}{d} \cdot \frac{1}{U_o} \iint\limits_{S_{\perp BB}} \underline{n}\, p \, dS \;&=\; \frac{(d-d_s)}{d} \left[ \frac{d_s^2}{U_o} \left( \Delta p + \delta p \right) \right] \widehat{\underline{n}} \\ &=\; -\frac{U_{\perp} + U_g}{U_f} \nabla \langle p \rangle \\ &=\; \left( \frac{U_{\parallel} + U_t}{U_f} - 1 \right) \nabla \langle p \rangle \;, \end{aligned} \tag{4.17}$$

where $\Delta p$ is the total change in pressure in the streamwise volume and $\delta p$ is the total change in pressure in the transverse volume. The above result (Lloyd (2003)) is obtained from the fact that

$$\frac{\Delta p + \delta p}{d}\, \widehat{\underline{n}} \;=\; -\frac{U_o}{U_f} \nabla \langle p \rangle \;. \tag{4.18}$$

The surface integral applicable to a regular array may be expressed as

$$\begin{aligned} \frac{d-d_s}{d} \cdot \frac{1}{U_o} \iint\limits_{S_{gBB}} \underline{n}\, p \, dS \;&=\; \frac{(d-d_s)}{d} \left[ \frac{d_s^2}{U_o} \Delta p \right] \widehat{\underline{n}} \\ &=\; -\frac{U_{\perp} + U_g}{U_f} \nabla \langle p \rangle \\ &=\; \left( \frac{U_{\parallel} + U_t}{U_f} - 1 \right) \nabla \langle p \rangle \;, \end{aligned} \tag{4.19}$$

resulting from the fact that

$$\frac{\Delta p}{d}\,\underline{\widehat{n}} \;=\; -\frac{U_o}{U_f}\,\nabla\langle p\rangle \;. \tag{4.20}$$

The streamwise pressure gradient applicable to both a fully staggered and a regular array may thus be expressed as

$$-\nabla\langle p\rangle \;=\; \left(\frac{U_\parallel + U_t}{U_f} - 1\right)\nabla\langle p\rangle \;+\; \frac{S_\parallel \;+\; \beta\,\xi\,S_\perp}{U_o}\,\tau_{w_\parallel}\;\underline{\widehat{n}}\;, \tag{4.21}$$

or after simplification

$$-\nabla\langle p\rangle \;=\; \left(\frac{U_f}{U_\parallel + U_t}\right)\frac{S_\parallel \;+\; \beta\,\xi\,S_\perp}{U_o}\,\tau_{w_\parallel}\;\underline{\widehat{n}}\;. \tag{4.22}$$

The streamwise pressure gradient may there-upon be expressed as

$$\begin{aligned}
-\nabla\langle p\rangle \;&=\; \frac{S_\parallel \;+\; \beta\,\xi\,S_\perp}{U_0}\,\psi\,\tau_{w_\parallel}\;\underline{\widehat{n}} && \text{(Eqn. (3.12))}\\
&=\; \frac{S_\parallel \;+\; \beta\,\xi\,S_\perp}{U_0}\,\psi\,\left(\frac{6\,\mu\,w_\parallel}{d-d_s}\right)\;\underline{\widehat{n}} && \text{(Eqn. (4.11))}\\
&=\; \frac{S_\parallel \;+\; \beta\,\xi\,S_\perp}{d^3}\,\psi\,\frac{6\,d^2\,\mu\,\underline{q}}{(d-d_s)(d^2-d_s^2)} && \text{(Eqn.(3.10)}\,,\; U_0 = d^3)\\
&=\; \frac{S_\parallel \;+\; \beta\,\xi\,S_\perp}{d}\,\frac{\epsilon}{(1-(1-\epsilon)^{2/3})}\,\frac{6\,\mu\,\underline{q}}{(d-d_s)(d^2-d_s^2)} && \text{(Eqn. (3.13))}\\
&=\; 12\,(2+\beta\,\xi)\,\frac{\epsilon}{(1-(1-\epsilon)^{2/3})}\,\frac{d_s^2\,\mu\,\underline{q}}{d\,(d-d_s)\,(d^2-d_s^2)} && (S_\parallel = 4d_s^2\,,\; S_\perp = 2d_s^2)\\
&=\; \frac{12\,(2+\beta\,\xi)}{d_s^2}\,\frac{\epsilon\,(1-\epsilon)^{4/3}}{(1-(1-\epsilon)^{1/3})\,(1-(1-\epsilon)^{2/3})^2}\,\mu\,\underline{q}\;. && \text{(Eqn. (3.4))}
\end{aligned} \tag{4.23}$$

For a porous medium of local uniform porosity

$$\nabla\langle p\rangle \;=\; \epsilon\nabla\langle p\rangle_f \;. \tag{4.24}$$

A well-known expression for relating the external pressure drop to the superficial velocity is Darcy's empirical law for steady unidirectional creeping flow of a Newtonian fluid through an unbounded isotropic granular porous medium of uniformly sized particles, i.e.

$$\frac{\Delta p}{L} \;=\; \frac{\mu}{k}\,q\;, \tag{4.25}$$

where $\Delta p$ is the pressure drop across the porous medium of length $L$ and $k$ is the Darcy or hydrodynamic permeability. For unidirectional flow in the positive $x$-direction of a Cartesian coordinate system, the streamwise pressure drop for Newtonian flow may, analogously to Darcy's equation, be expressed as

$$-\frac{\mathrm{d}p}{\mathrm{d}x} \;=\; \mu f_{00}\,q\;, \tag{4.26}$$

where $f_{00}$ is the shear factor of which the first subscript denotes the asymptotic limit of low Reynolds number flow and the second subscript denotes the asymptotic limit of low porosity. It thus follows that the shear factor $f_{00}$ relates to the hydrodynamic permeability, which is dependent on the porous microstructure, as follows

$$f_{00} \;=\; \frac{1}{k}\,. \tag{4.27}$$

The shear factor $f_{00}$ may consequently be expressed as

$$f_{00} \;=\; \frac{12\,(2+\beta\,\xi)(1-\epsilon)^{4/3}}{d_s^2\,(1-(1-\epsilon)^{1/3})\,(1-(1-\epsilon)^{2/3})^2}\,. \tag{4.28}$$

The dimensionless shear factor $F_{00} = f_{00}\,d_s^2$, describing the flow of a Newtonian fluid through both a fully staggered- and a non-staggered regular array, is thus given by

$$F_{00} \;=\; \frac{12\,(2+\beta\,\xi)(1-\epsilon)^{4/3}}{(1-(1-\epsilon)^{1/3})\,(1-(1-\epsilon)^{2/3})^2}\,, \tag{4.29}$$

or in terms of the dimensionless hydrodynamic permeability $\mathcal{K} = k/d_s^2$,

$$\mathcal{K} \;=\; \frac{\left(1-(1-\epsilon)^{1/3}\right)\left(1-(1-\epsilon)^{2/3}\right)^2}{12\,(2+\beta\,\xi)(1-\epsilon)^{4/3}}\,. \tag{4.30}$$

The transverse pore sections of a fully staggered array, in which the fluid flows in opposite directions, are assumed to be equal in volume. Therefore it is assumed that, similarly as in the case of two-dimensional flow, $\xi = \frac{1}{2}$ for a fully staggered array. For a regular array $\xi = 1$, since in a regular array no splitting of the streamtube occurs. Due to the fact that a regular array does not contain any transverse channels, it follows that for a regular array $\beta = 0$. The determination of the value of $\beta$ for a fully staggered array requires further analysis and will be addressed in the following subsection.

### 4.1.1 Evaluation of the coefficient $\beta$

The RUC associated with a fully staggered array can be partitioned into four symmetric parts, as illustrated in Figure 4.4. Consider one of the four symmetric parts of the RUC presented in Figure 4.4. The bottom left hand part is arbitrarily chosen for illustration purposes. Let $\Delta s$ denote the displacement of the centroid of the fluid due to the shifting thereof to circumvent obstacles for streamwise discharge. Figure 4.5 illustrates the transverse displacement $\Delta s$ for fluid discharge through the RUC corresponding to the bottom left hand part of Figure 4.4. Let $\Delta x$ and $\Delta y$ respectively denote the transverse displacement of the centroid of the fluid in the x- and y-directions of a Cartesian coordinate system, as shown in Figure 4.5.

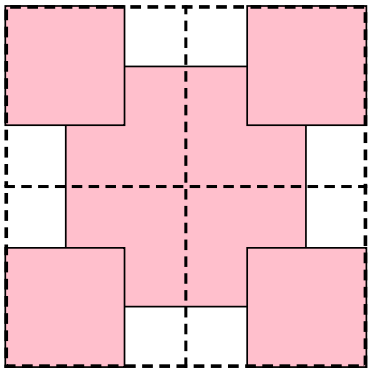

Figure 4.4: A two-dimensional illustration of the partitioning of the RUC associated with a fully staggered array into four symmetric parts.

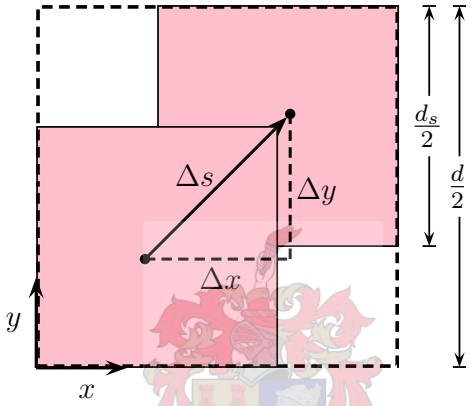


Figure 4.5: Illustration of the transverse displacement $\Delta s$ of the centroid of the fluid for discharge through the RUC corresponding to the bottom left hand part of the RUC shown in Figure 4.4.

The fluid volume in the transverse channels $U_\perp$ may be expressed as

$$U_\perp \;=\; A_{p_\perp} \Delta s \;, \tag{4.31}$$

where $A_{p_\perp}$ denote the cross-sectional flow area available for fluid discharge through the transverse channels within the RUC. Conservation of mass requires that

$$Q \;=\; w_\parallel A_{p_\parallel} \;=\; w_\perp A_{p_\perp} \;, \tag{4.32}$$

where $Q$ denotes the volumetric flow rate. From equations (4.31), (4.32) and (3.11) it follows that $\beta$ may be expressed as

$$\beta \;=\; \frac{A_{p_\parallel} \Delta s}{U_\perp} \;. \tag{4.33}$$

The displacement $\Delta s$ may be obtained by determining the position of the centroid of the fluid before and after the transverse shift (Appendix C), yielding

$$\Delta s \;=\; \frac{\sqrt{2}\, d_s^2}{d + d_s}\,. \tag{4.34}$$

It thus follows that the value of $\beta$ for a fully staggered array, yields

$$\beta \;=\; \frac{(d^2 - d_s^2)}{d_s^2 d_f}\frac{\sqrt{2}\, d_s^2}{d + d_s} \;=\; \sqrt{2}\,. \tag{4.35}$$

Since each of the four symmetric parts of the RUC shown in Figure 4.4, yields the same value for $\beta$ and contributes evenly to the nett effect of the flow field, $\beta = \sqrt{2}$ may be taken as the average value for $\beta$ for a fully staggered array.

### 4.1.2 Isotropic RUC model

The resulting expressions for the dimensionless shear factor $F_{00}$ and the dimensionless hydrodynamic permeability $\mathcal{K}$ for a fully staggered- and a regular array are presented in Table 4.1.

| Array | $F_{00}$ | $\mathcal{K}$ |
|---|---|---|
| Fully staggered | $\dfrac{32.5\,(1-\epsilon)^{4/3}}{\left(1-(1-\epsilon)^{1/3}\right)\left(1-(1-\epsilon)^{2/3}\right)^2}$ | $\dfrac{\left(1-(1-\epsilon)^{1/3}\right)\left(1-(1-\epsilon)^{2/3}\right)^2}{32.5\,(1-\epsilon)^{4/3}}$ |
| Regular | $\dfrac{24\,(1-\epsilon)^{4/3}}{\left(1-(1-\epsilon)^{1/3}\right)\left(1-(1-\epsilon)^{2/3}\right)^2}$ | $\dfrac{\left(1-(1-\epsilon)^{1/3}\right)\left(1-(1-\epsilon)^{2/3}\right)^2}{24\,(1-\epsilon)^{4/3}}$ |

Table 4.1: Expressions for the dimensionless shear factor $F_{00}$ and the dimensionless hydrodynamic permeability $\mathcal{K}$ for a staggered and non-staggered array.

It should be noted that the RUC model is a theoretical model which provides a simple hypothetical approximation of the actual complex granular porous microstructure. The RUC can not be regarded as a repetitive building block, since it is practically impossible to construct an isotropic array. An isotropic medium requires the random distribution of a large number of grains to obtain staggering in all directions. The construction of a streamwisely staggered array results in non-staggeredness in the other two principle directions perpendicular to the streamwise direction. Neither a fully staggered array nor a regular array is therefore isotropic. A fully staggered array is staggered only in the streamwise direction. In the other two principal directions perpendicular to the streamwise direction no staggering occurs, which corresponds to a regular array. The RUC model is

assumed to be isotropic with respect to the *average* geometric properties of the granular porous medium. Consequently, an isotropic RUC model is introduced by taking the average of one fully staggered array and two regular arrays, i.e.

$$F_{00} = \frac{1 \times \left[12\left(2 + (1/\sqrt{2})\right)\right] + 2 \times \left[12\left(2 + 0\right)\right]}{3} \times \left[\frac{(1-\epsilon)^{4/3}}{\left(1 - (1-\epsilon)^{1/3}\right)\left(1 - (1-\epsilon)^{2/3}\right)^2}\right] . \quad (4.36)$$

The existing RUC model also adopted the assumption of average geometrical isotropy, but the assumption was never mathematically justified as above. The final present RUC model for steady laminar flow of an incompressible Newtonian fluid through isotropic homogeneous granular porous media of low to moderate porosity in the limit of low Reynolds number flow, expressed as $F_{00}$, $f_{00}\, d^2$ and $\mathcal{K}$, are presented in Table 4.2.

| Dimensionless parameter | Isotropic RUC model |
|---|---|
| $F_{00}$ | $\dfrac{26.8\,(1-\epsilon)^{4/3}}{\left(1-(1-\epsilon)^{1/3}\right)\left(1-(1-\epsilon)^{2/3}\right)^2}$ |
| $f_{00}\, d^2$ | $\dfrac{26.8\,(1-\epsilon)^{2/3}}{\left(1-(1-\epsilon)^{1/3}\right)\left(1-(1-\epsilon)^{2/3}\right)^2}$ |
| $\mathcal{K}$ | $\dfrac{\left(1-(1-\epsilon)^{1/3}\right)\left(1-(1-\epsilon)^{2/3}\right)^2}{26.8\,(1-\epsilon)^{4/3}}$ |

Table 4.2: Dimensionless expressions for the RUC model in the limit of low Reynolds number flow.



## 4.2 Comparison with granular models from literature

### 4.2.1 Hydraulic diameter

The hydraulic diameter is a length scale most commonly used for direct comparison between flow through systems of different geometrical structure. The hydraulic diameter $D_h$ for capillary tube flow of uniform cross-section is defined as

$$D_h = 4R_h , \quad (4.37)$$

where $R_h$ denotes the hydraulic radius, defined as

$$R_h = \frac{\text{cross-sectional area available for flow}}{\text{wetted perimeter}} . \quad (4.38)$$

For flow through porous media $R_h$ may also be expressed as (Bird et al. (2002))

$$R_h \;=\; \frac{\text{void volume/volume of bed}}{\text{wetted surface/volume of bed}} \;=\; \frac{\epsilon}{a}\,, \tag{4.39}$$

where $a$ is referred to as the specific surface and relates to the total solid surface per volume of particles $a_v$, i.e. the solid specific surface, through

$$a \;=\; a_v(1-\epsilon)\,. \tag{4.40}$$

The solid specific surface $a_v$ is used to extend the definition of the hydraulic radius to account for beds of non-uniformly sized particles in order to obtain an average diameter. In effect, the assemblage of non-uniformly sized particles is replaced with an assemblage of uniformly sized particles, having the same ratio of total solid surface per volume of particles as the original assemblage, but not the same number of particles. Therefore the actual particle diameter does not enter into the determination of the hydraulic radius. The (average) hydraulic diameter may consequently be expressed in terms of the specific surface as follows

$$D_h \;=\; \frac{6}{a_v}\,. \tag{4.41}$$

The reason for the latter definition for the hydraulic diameter is to obtain the desired result of

$$D_h \;=\; \frac{6}{a_v} \;=\; 6\,\frac{(4/3)\,\pi R^3}{4\,\pi R^2} \;=\; 2\,R \;=\; D_p\,, \tag{4.42}$$

for an assemblage of uniformly sized spherical particles of radius $R$ and diameter $D_p$. In RUC notation it follows that for an assemblage of uniformly sized cubes of length $d_s$,

$$D_h \;=\; \frac{6}{a_v} \;=\; 6\,\frac{d_s^3}{6\,d_s^2} \;=\; d_s\,. \tag{4.43}$$

From equations (4.39) to (4.41) it follows that the relationship between the hydraulic radius and the hydraulic diameter may be expressed in terms of the porosity as

$$R_h \;=\; \frac{\epsilon\,D_h}{6\,(1-\epsilon)}\,. \tag{4.44}$$

The present RUC model is to be compared with other granular models from the literature. Based on the results of equations (4.42) and (4.43), it will henceforth be assumed that the diameter of a sphere in an assemblage of uniformly sized spherical particles is equal to the length of the cube $d_s$ in the RUC model.

### 4.2.2 Dimensionless permeability and shear factor

The models to be compared with the present RUC model for predicting flow in the low Reynolds number flow regime are presented in Table 4.3. All these models consider three-dimensional, steady, laminar flow of an incompressible Newtonian fluid through a homogeneous isotropic granular porous medium.

| Model | Model type | Packing material |
|---|---|---|
| Blake-Kozeny | Capillary | Spheres |
| Macdonald et al. (1979) | Empirical verification | Spheres |
| Dagan (1989) | Statistical averaging | Cubes |
| Happel (1958) | Concentric cell | Spheres |
| Existing RUC | Spatial averaging | Cubes |

Table 4.3: Granular models for predicting flow in the low Reynolds number flow regime.

The Blake-Kozeny equation (Appendix D.1) concerns fully developed laminar flow of a Newtonian fluid through a packed bed of smooth uniformly sized spherical particles in die Darcy regime. The flow through the interstices of the packed column of uniform diameter is regarded as flow through a bundle of uniform parallel capillary tubes. To account for the tortuous flow path actually followed by the traversing fluid, Carman (1937) introduced a tortuosity factor into the Blake-Kozeny equation. The dimensionless hydrodynamic permeability $\mathcal{K}$ as predicted by the Blake-Kozeny equation, may be expressed as

$$\mathcal{K} = \frac{\epsilon^3}{150\,(1-\epsilon)^2}\,, \tag{4.45}$$

and is valid for $\epsilon < 0.5$. Macdonald et al. (1979) suggested a coefficient value of 180 for the Blake-Kozeny equation, instead of the value of 150, which corresponds to the coefficient value proposed by Carman (1937) in the Carman-Kozeny-Blake equation (Appendix D.2). His proposal was based on a large number of experimental results. The dimensionless hydrodynamic permeability $\mathcal{K}$, as suggested by the empirical verification of Macdonald et al. (1979), may thus be expressed as

$$\mathcal{K} = \frac{\epsilon^3}{180\,(1-\epsilon)^2}\,. \tag{4.46}$$

Dagan (1989) proposed a model based on a statistical volume averaging approach for predicting the permeability through a granular porous medium of low porosity. The porous medium is regarded as a network of three-dimensional planar fissures with interconnected

pores of uniform aperture. The random orientation of the fissures is described by a probability distribution function. Fully developed laminar flow is assumed to prevail throughout all pore sections. The hydrodynamic permeability as predicted by the model of Dagan (1989), in which a uniform superficial velocity field is assumed, is given by

$$k \;=\; \frac{\epsilon\, b^2}{18}\;, \tag{4.47}$$

where $b$ denotes the constant aperture between the fissures. For flow between parallel plates a distance $b$ apart, it follows that

$$D_h \;=\; 2\, b\;. \tag{4.48}$$

From equations (4.37), (4.40) and (4.41), it follows that

$$b \;=\; \frac{\epsilon\, D_h}{3\,(1-\epsilon)}\;. \tag{4.49}$$

The dimensionless hydrodynamic permeability $\mathcal{K}$ as predicted by the model of Dagan (1989), may thus be expressed as

$$\mathcal{K} \;=\; \frac{\epsilon^3}{162\,(1-\epsilon)^2}\;. \tag{4.50}$$

Happel (1958) proposed a concentric spherical cell model for predicting the permeability through a random assemblage of spheres in the creeping flow regime over the entire porosity range. The spherical shape was chosen since many particles approximate the spherical form. The assemblage of spheres is regarded as a periodic array consisting of identical spherical unit cells of which each cell contains a single solid sphere surrounded by a fluid envelope. The solid sphere is positioned concentrically with the outer spherical fluid envelope. The concentric spheres are assumed to be stationary with a traversing fluid entering the cell with a uniform approaching velocity $\underline{q}$. The fluid is free to pass over the outer surface of the cell. The outside surface of each cell is assumed to be frictionless, that is, the normal velocity and the tangential stresses on the outer sphere are assumed to be zero. No friction occurs between adjacent fluid envelopes. The porosity of the spherical cell is assumed to be equal to the porosity of the entire assemblage. The pressure gradient prediction over the packed bed was determined by solving the Stokes's equations subjected to the boundary conditions ensuring frictionless outer surfaces. The dimensionless hydrodynamic permeability $\mathcal{K}$ as predicted by the model of Happel (1958), may be expressed as

$$\mathcal{K} \;=\; \frac{\left(3 - \frac{9}{2}(1-\epsilon)^{1/3} + \frac{9}{2}(1-\epsilon)^{5/3} - 3\,(1-\epsilon)^2\right)}{18\,(1-\epsilon)\,(3 + 2(1-\epsilon)^{5/3})}\;. \tag{4.51}$$

The dimensionless hydrodynamic permeability $\mathcal{K}$ as predicted by the existing RUC model is given by

$$\mathcal{K} \;=\; \frac{\epsilon\left(1-(1-\epsilon)^{1/3}\right)\left(1-(1-\epsilon)^{2/3}\right)}{41\,(1-\epsilon)^{4/3}}\;. \tag{4.52}$$

A graphical comparison for the permeability prediction of the models presented in Table 4.3 with the present low porosity RUC model is shown in Figure 4.6.

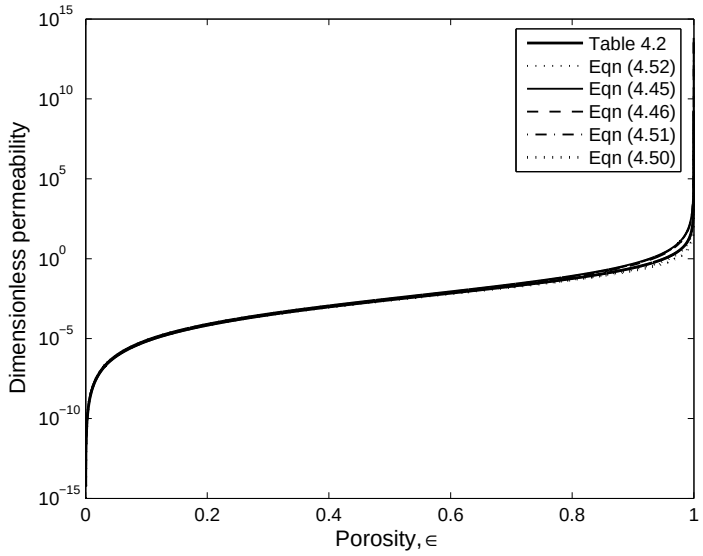


Figure 4.6: Comparison between hydrodynamic permeability predictions.

Graphically it appears as if there is very little difference between the present and existing RUC models. However, from an analytical point of view the difference between the models is quite significant. The fundamental differences between the two models are the following: The present RUC model mathematically justifies the assumption of average geometrical isotropy, which was not accounted for in the existing model. The contribution of the transverse pressure term in the surface integral of equation (4.1) to the streamwise pressure gradient, caused by the transverse shear stresses, was neglected in the existing model. The square in the numerator of the expression for $\mathcal{K}$ of the present RUC model in Table 4.2, which is absent in the expression for the existing model, is the result of this discrepancy. The existing RUC model considered only a staggered array in which no splitting of the streamtube occurs and no stagnant regions are present, which is the reason for the difference in coefficient values produced by the two models. The close correspondence between all the models in Figure 4.6 show that the capillary models (Blake-Kozeny and Macdonald), the submerged object model (Happel) and the models based on volume averaging (RUC models and Dagan) are all adequate models for modelling laminar flow through granular porous medium of low to moderate porosities. It is very satisfactory that the present RUC model agree so well with the other models which follow different modelling strategies. The validity of the analytical closure modelling procedure with the pore-scale RUC model is therefore justified in this manner. Since the models are all low to moderate porosity models, except for the extended range of the spherical cell model, the discrepancies observed at $\epsilon > 0.8$ are expected and may be attributed to the different physical flow process occurring at high porosities due to the absence of neighbouring grains. At high porosities a flow *by* situation occurs instead of flow *through*.

### 4.2.3 Coefficient $A$ in the Blake-Kozeny equation

Another way of comparison between the models presented in Table 4.3 is to provide predictions for the coefficient $A$ in the Blake-Kozeny equation as a function of porosity. The expressions for the coefficient $A$ as proposed by the present and existing RUC models are respectively given by

$$A = \frac{26.8\,\epsilon^3}{(1-\epsilon)^{2/3}\left(1-(1-\epsilon)^{1/3}\right)\left(1-(1-\epsilon)^{2/3}\right)^2}\,, \tag{4.53}$$

and

$$A = \frac{41\,\epsilon^2}{(1-\epsilon)^{2/3}\left(1-(1-\epsilon)^{1/3}\right)\left(1-(1-\epsilon)^{2/3}\right)}\,. \tag{4.54}$$

The spherical cell model of Happel (1958) yields the following expression for the coefficient $A$ as a function of porosity

$$A = \frac{18\,\epsilon^3\left(3+2\,(1-\epsilon)^{5/3}\right)}{(1-\epsilon)\left(3-\frac{9}{2}(1-\epsilon)^{1/3}+\frac{9}{2}(1-\epsilon)^{5/3}-3\,(1-\epsilon)^2\right)}\,. \tag{4.55}$$

For beds of randomly packed uniformly sized spherical particles, $0.38 \leq \epsilon \leq 0.47$ (Happel & Brenner (1965), Kaviany (1995)). The porosity value chosen for comparison between the model predictions for the coefficient $A$ is taken as the average value of $\epsilon = 0.38$ and $\epsilon = 0.47$ rounded up to the second decimal, i.e. $\epsilon = 0.43$. The values for $A$ evaluated at $\epsilon = 0.43$ as predicted by the models presented in Table 4.3 are given in Table 4.4. The dependence of the coefficient $A$ on the porosity is graphically illustrated in Figure 4.7.

| Model | Coefficient $A$, $\epsilon = 0.43$ |
|---|---|
| Blake-Kozeny | 150 |
| Carman-Kozeny-Blake | 180 |
| Macdonald et al. (1979) | 180 |
| Dagan (1989) | 162 |
| Happel (1958) | 165 |
| Existing RUC model | 206 |
| Present RUC model | 186 |

Table 4.4: Comparison between the value of the coefficient $A$ at $\epsilon = 0.43$.

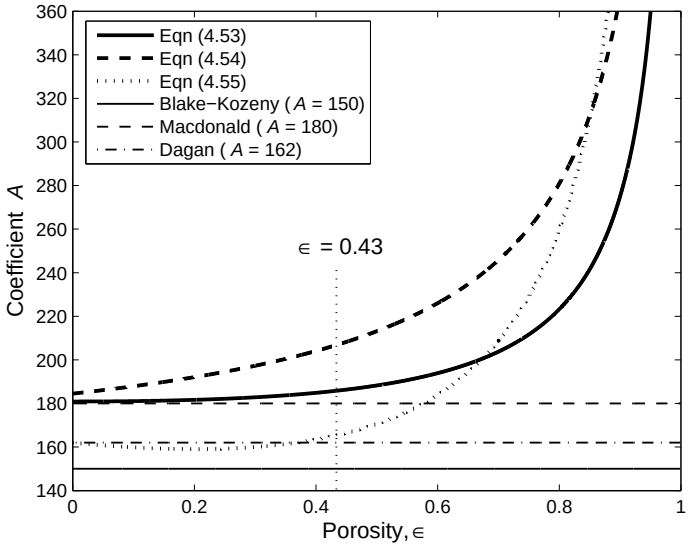


Figure 4.7: Dependence of the coefficient $A$ on porosity.

For porosities ranging from $\epsilon = 0.34$ to $\epsilon = 0.48$, empirical values for $A$ ranging from $A = 157$ to $A = 180$ has been obtained, with an average value of $A = 169$ (Macdonald et al. (1979)). For the same porosity range the values for $A$ predicted by the present RUC model range from 183.5 to 187 with an average value of 185. According to a survey of Kemblowski & Michniewics (1979), the values suggested for the coefficient $A$ for flow of Newtonian fluids through granular beds, range from $A = 150$ to $A = 200$, but the majority of references suggest the value of $A = 180$ and most commonly used are the values of $A = 180$, determined by Carman (1937), and $A = 150$, proposed by Ergun (1952). It is encouraging that the value of $A = 186$ for $\epsilon = 0.43$, suggested by the present RUC model, verges upon this range and the excellent correspondence with the value of $A = 180$, suggested by Carman (1937) and Macdonald et al. (1979), is very satisfying and clearly shows the improvement on the existing RUC model ($A = 206$).

### 4.2.4 High porosity model

In the limit of low Reynolds number flow the RUC model increasingly loses its validity as the porosity $\epsilon$ approaches unity due to the failure of the applicability of the assumption of flow between parallel plates. Churchill & Usagi (1972) introduced an asymptote matching technique in which two expressions, each of which dominates in its own region of applicability, may be matched to obtain a general expression over the entire range of parameter values. By application of this technique it is possible to match the RUC model with a model for predicting flow conditions in the asymptotic limit of high porosities. Two high porosity models from the literature which are adequate for this purpose is the well-known drag model of Stokes (e.g. Chorlton (1967)) and the model of Hasimoto (1958). As opposed to the low porosity models which provide an expression for the pressure drop

prediction over an assemblage of submerged grains, the high porosity models provide an expression for the drag force on a single grain within the assemblage, due to the absence of neighbouring grains. At high porosities a different physical flow process occurs: the grains are far enough apart so that the disturbances produced by an individual grain on the flow behaviour is not affected by the disturbances produced by its neighbours. Stokes' flow concerns the steady motion of an unbounded incompressible Newtonian fluid with a uniform approaching velocity $q$ past an isolated stationary sphere of radius $R$ in the creeping flow regime. The equation resulting from omission of the inertial terms from the Navier-Stokes equation, together with the continuity equation, are known as the Stokes' equations. The drag force $\mathcal{F}$ exerted by the sphere on the fluid is obtained by solving the Stokes' equations subjected to a no-slip boundary condition, yielding

$$\mathcal{F} \;=\; 6\,\pi\,\mu\,R\,q\;. \tag{4.56}$$

Equation (4.56) applies for $\epsilon \approx 1$. From equation (4.26) it follows that the relation between the shear factor $f_{01}$ and the drag force $\mathcal{F}$ may be expressed as

$$-\frac{\mathrm{d}p}{\mathrm{d}x} \;=\; \mu f_{01}\,q \;=\; \frac{\mathcal{F}}{d^3}\;, \tag{4.57}$$

where the first subscript of the shear factor $f_{01}$ denotes the asymptotic limit of low Reynolds number flow and the second subscript denotes the asymptotic limit of high porosity. Assuming that the diameter of the sphere is equivalent to the length of the cube in the RUC model, i.e. $2R = d_s$, yields

$$f_{01} \;=\; \frac{3\,\pi\,(1-\epsilon)}{d_s^2}\;, \tag{4.58}$$

or in terms of the dimensionless shear factor $F_{01}$ the Stokes' drag may be described as

$$F_{01} \;=\; 3\,\pi\,(1-\epsilon)\;. \tag{4.59}$$

The Stokes' drag serves as a basis for the introduction of many other high porosity models from the literature. An example is the model of Hasimoto (1958) concerning the steady motion of an incompressible Newtonian fluid past a periodic array of small particles in a dilute medium. A periodic array of uniform spheres is constructed by repeating a basic unit cell with spheres placed at the corners of each cell. Hasimoto replaced each sphere by a point force, retarding the motion of the fluid, and modified the Stokes equations to compensate for the discontinuous force field by means of the Dirac delta function and Fourier series. A no-slip boundary condition is assumed at the surface of each sphere. The flow past three different types of cubic lattices is considered, namely simple, body-centered and face-centered cubic lattices. The drag force for flow past a single sphere of radius $R$ in a body-centered or face-centered cubic array is given by

$$\mathcal{F} \;=\; \frac{6\,\pi\,\mu\,R\,q}{1-1.791\,(1-\epsilon)^{1/3}} \;+\; O\left(R^3\right)\;. \tag{4.60}$$

For dilute suspensions, that is $\epsilon \approx 1$, the series expansion,

$$\frac{1}{1-1.791(1-\epsilon)^{1/3}} \approx 1+1.791\,(1-\epsilon)^{1/3}+O\left((1-\epsilon)^{2/3}\right) , \tag{4.61}$$

can be used (Happel & Brenner (1965)) to approximate equation (4.41), yielding

$$\mathcal{F} = 6\,\pi\,\mu\,R\,q\left(1+1.791\,(1-\epsilon)^{1/3}\right) + O\left((1-\epsilon)^{2/3}\right) . \tag{4.62}$$

Neglecting the higher order terms, the drag force may be expressed in terms of the shear factor $f_{01}$ as follows

$$f_{01} = \frac{3\,\pi\,(1-\epsilon)}{d_s^2}\left(1+1.791\,(1-\epsilon)^{1/3}\right) , \tag{4.63}$$

or in terms of the dimensionless shear factor $F_{01}$ the model of Hasimoto (1958) may be described as

$$F_{01} = 3\,\pi\,(1-\epsilon)\left(1+1.791\,(1-\epsilon)^{1/3}\right) . \tag{4.64}$$

Since external boundary effects are neglected in this work, the physical flow process in which the grains move at a uniform average velocity through a stationary fluid or the grains remain stationary in the presence of a traversing fluid with a uniform average velocity, may be treated as mathematically equivalent (Happel (1958)).

### 4.2.5 Asymptote matching of low and high porosity models

Application of the asymptote matching technique of Churchill & Usagi (1972) yields the following general expression for the shear factor in the limit of low Reynolds number flow, $F_0$, applicable over the entire porosity range

$$F_0 = \left((F_{00})^s+(F_{01})^s\right)^{1/s} , \tag{4.65}$$

where $s$ denotes a shifting parameter. The numerical value of the shifting parameter determines how closely the matching curve follows the two asymptotic limits in the transition regime. For simplicity the value $s=1$ is chosen which yields a simple superposition of the two asymptotic limits. Asymptote matching of the RUC model with Stokes' drag model yields

$$F_0 = \frac{26.8\,(1-\epsilon)^{\frac{4}{3}}}{\left(1-(1-\epsilon)^{\frac{1}{3}}\right)\left(1-(1-\epsilon)^{\frac{2}{3}}\right)^2} + 3\,\pi\,(1-\epsilon) , \tag{4.66}$$

and matching the RUC model with the model of Hasimoto (1958) one obtains

$$F_0 = \frac{26.8\,(1-\epsilon)^{\frac{4}{3}}}{\left(1-(1-\epsilon)^{\frac{1}{3}}\right)\left(1-(1-\epsilon)^{\frac{2}{3}}\right)^2} + 3\,\pi\,(1-\epsilon)\left(1+1.791\,(1-\epsilon)^{1/3}\right) . \tag{4.67}$$

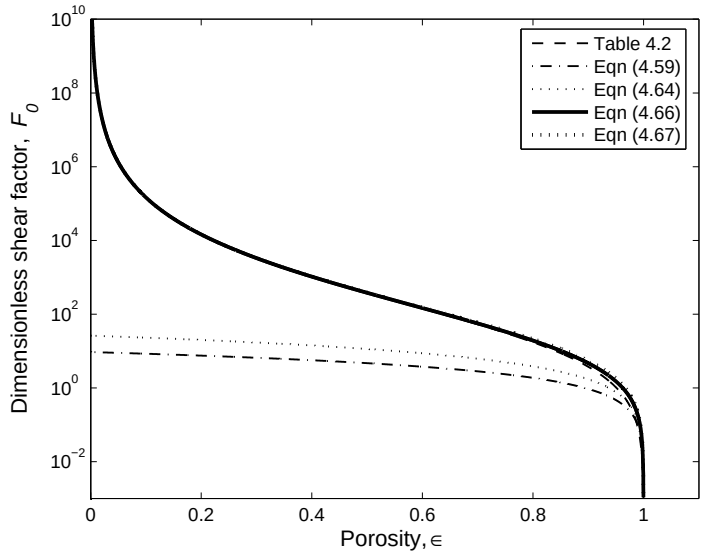


Figure 4.8: Asymptote matching of the RUC model with high porosity models.

The asymptote matching of the RUC model with the Stokes' drag and the model of Hasimoto (1958) is shown in Figure 4.8 for all porosity values. Compared to the matching curves, the RUC model slightly under-predicts the frictional effects at $\epsilon \approx 1$. No physical explanation can be given regarding this matter, since the assumptions of the RUC model are all invalid in this high porosity regime. Also note the small difference between the two matching curves. Both the RUC/Stokes and RUC/Hasimoto models may therefore be regarded as adequate in predicting flow in the limit of low Reynolds number flow through granular porous media over the entire porosity range.

### 4.2.6 The Kozeny constant

The Kozeny constant $k_{koz}$ (Appendix D.2), defined as

$$k_{koz} \;=\; k_0 \left(\frac{L_e}{L}\right)^2 \;, \tag{4.68}$$

was introduced by Carman (1937) through modification of the Blake-Kozeny equation with the velocity relationship,

$$u \;=\; \frac{q}{\epsilon}\frac{L_e}{L} \;, \tag{4.69}$$

where $L_e$ is the length of a tortuous channel, $L$ is the length of a straight channel and $k_0$ is an empirical shape factor which depends on the shape of the cross-section of the channel. Happel & Brenner (1965) defines the Kozeny constant as "a dimensionless number which, presumably, has the same numerical value for all random porous media, independently of

the size of the particles and the porosity" and presents the Kozeny constant alternatively as

$$k_{koz} = \frac{\epsilon R_h^2}{k} = \frac{\epsilon^3}{36 \mathcal{K} (1-\epsilon)^2} . \tag{4.70}$$

The specific surface $a_v$ is introduced into the definition for the hydraulic diameter (equation (4.41)) to account for assemblages of non-uniformly sized particles. The purpose is to replace the assemblage of non-uniformly sized particles with an assemblage of uniformly sized particles, having the same ratio of total solid surface per volume of particles as the original assemblage, but not the same number of particles. This is the reason for the actual particle diameter not entering into the definition of the hydraulic radius. The hydraulic diameter in effect determines an average diameter for the assemblage of non-uniformly sized particles. Since it is assumed in this work that the spherical particle diameter is equivalent to the length $d_s$ of the solid cube in the RUC model, it follows that equation (4.70) will indeed yield the same $k_{koz}$-value for an assemblage of spheres and cubes of the same porosity. The constancy of $k_{koz}$ is supported by a considerable volume of experimental data and can be predicted theoretically to a considerable degree of accuracy (Happel & Brenner (1965)). Experimentally $k_o$ lies within the range 2.0 to 2.5 for flow through rectangular, elliptical and annular shapes. For pipe flow $k_o$ ranges between 2.0 and 3.0 (Carman (1937)) and for flow between parallel plates $k_o = 3.0$ (Kemblowski & Michniewics (1979)). Due to the very small variation in $k_o$ for flow through channels of various cross-sections, the value of $k_o$ may be regarded as reasonably independent of shape (Happel & Brenner (1965)), leading to more or less constant $k_{koz}$-values as predicted by equation (4.68). Table 4.5 compares the $k_{koz}$-values predicted by the present RUC model (equation (4.70)) to the empirical values for $k_{koz}$ presented by Carman (1937) for flow though an assemblage of cubes and the cell model of Happel (1958) for flow through an assemblage of spheres.

| | Kozeny constant, $k_{koz}$ | | |
|---|---|---|---|
| Porosity, $\epsilon$ | Carman (cubes) | Present RUC (cubes) | Happel (spheres) |
| 0.344 | 5.29 | 5.10 | 4.48 |
| 0.397 | 4.71 | 5.13 | 4.54 |
| 0.448 | 4.21 | 5.17 | 4.62 |

Table 4.5: Dependence of the Kozeny constant $k_{koz}$ on low porosity values.

Sufficient experimental data on beds consisting of a variety of non-spherical particles indicate that $k_{koz} \approx 5.0$, independent of shape and porosity, from $\epsilon = 0.26$ to $\epsilon = 0.8$ (Happel (1958)). For packed beds of uniformly sized spherical particles the Carman-Kozeny-Blake equation within the range $\epsilon = 0.26$ to $\epsilon = 0.48$, gives excellent correlation

with a Kozeny constant of $k = 4.8$ (Happel & Brenner (1965)). Table 4.5 shows the excellent predictive capability of the present RUC model for obtaining $k_{koz} \approx 5.0$ in the appropriate porosity range. Figure 4.9 compares the porosity dependence of the Kozeny constant as predicted by the present RUC model with the predictive capability of the spherical cell model of Happel (1958).

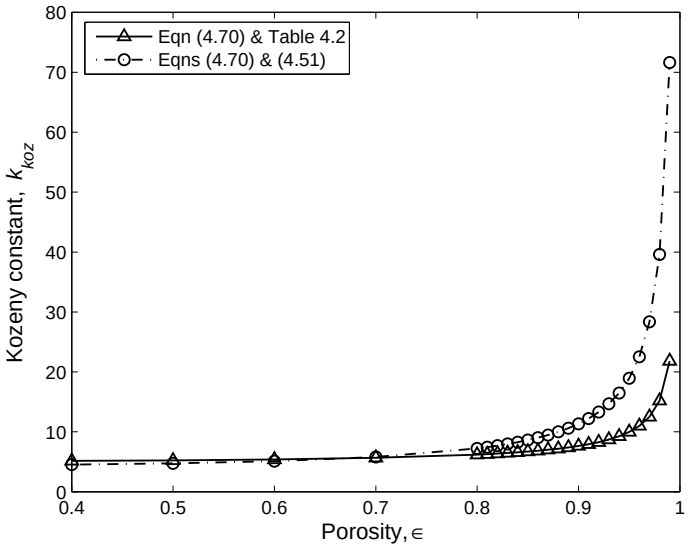


Figure 4.9: Porosity dependence of the Kozeny constant $k_{koz}$.

The correspondence between the $k_{koz}$-values predicted by the models for $\epsilon$ ranging between 0.4 and 0.8 is very satisfactory. The reason for agreement of the values in this region is because the RUC model is a low to moderate porosity model whilst the spherical cell model is applicable over the entire porosity range. This also explains the reason for the discrepancies observed between the two models at porosities above 0.8. Table 4.6 shows the effect of matching the present RUC model with the high porosity models of Stokes' and Hasimoto (1958) on the values of the Kozeny constant. A graphical comparison between the $k_{koz}$-values presented in Table 4.6 is shown in Figure 4.10. The values proposed by the RUC/Hasimoto model are in slightly better agreement with the values of the spherical cell model as the values predicted by the RUC/Stokes model. This is due to the larger frictional effects predicted by the model of Hasimoto (1958) at $\epsilon < 1$ than the Stokes' drag, since the model of Hasimoto (1958) considers a cubic array of particles and the Stokes' drag only a single isolated particle. The latter effect, however, presents a minor difference. The good correspondence of both models with the spherical cell model renders both the RUC/Stokes and RUC/Hasimoto models adequate in predicting the values of the Kozeny constant for all porosities larger than 0.4.

| | Kozeny constant, $k_{koz}$ | | | |
|---|---|---|---|---|
| Porosity, $\epsilon$ | Happel (spheres) | Present RUC (cubes) | RUC / Stokes (cubes / spheres) | RUC / Hasimoto (cubes / spheres) |
| 0.99 | 71.63 | 21.81 | 47.22 | 57.02 |
| 0.90 | 11.34 | 7.64 | 9.55 | 11.13 |
| 0.80 | 7.22 | 6.20 | 6.87 | 7.57 |
| 0.70 | 5.79 | 5.66 | 5.96 | 6.32 |
| 0.60 | 5.11 | 5.39 | 5.53 | 5.71 |
| 0.50 | 4.74 | 5.23 | 5.29 | 5.39 |
| 0.40 | 4.54 | 5.14 | 5.16 | 5.21 |

Table 4.6: Porosity dependence of the Kozeny constant.

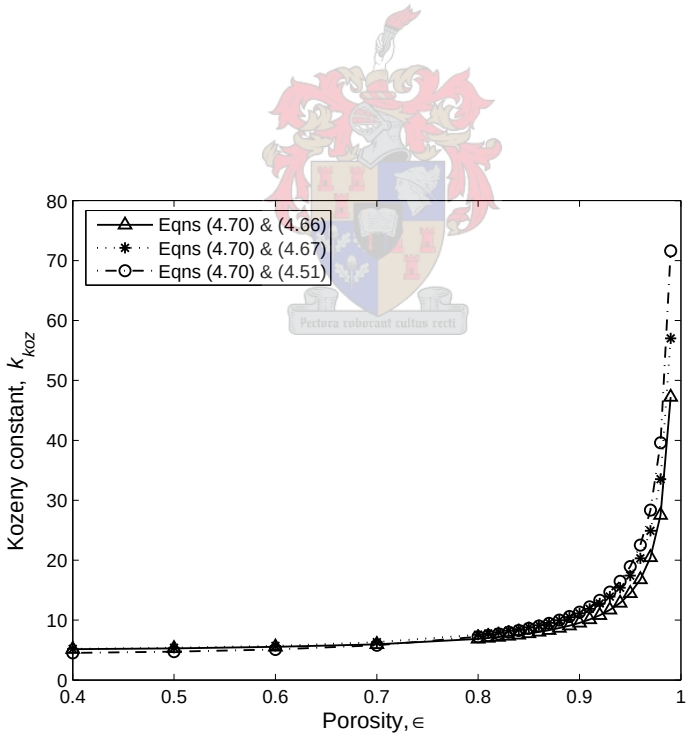


Figure 4.10: Porosity dependence of the Kozeny constant for different models presented.

# Chapter 5

# Laminar inertial flow regime

This chapter involves the analytical closure modelling of the fluid-solid interaction within the RUC for predicting the streamwise pressure gradient in the steady laminar limit of the inertial flow regime where turbulence is not yet present.

## 5.1 Closure modelling at moderate to high porosities

Du Plessis & Van der Westhuizen (1993) modelled the pressure integral in the Forchheimer regime for laminar crossflow through prismatic porous media by an internal form drag condition, analogous to the external form drag condition for flow past a single obstacle in the inertial flow regime. The same modelling procedure was applied to flow through granular porous media (Du Plessis (1992)). It was assumed that the solid cube is subject to a pressure deficit of $\frac{1}{2}\rho v_p^2 c_d$, resulting from the interstitial flow recirculation within the separation zone. The velocity $v_p$ denotes the magnitude of the average pore velocity as opposed to the uniform approaching velocity far away from the solid in the case of flow past an isolated sphere. The reason for the introduction of the average pore velocity was to incorporate the effect of neighbouring solids on the pressure gradient. A value of $\sqrt{2}$ was proposed for the drag coefficient $c_d$ to account for the larger average transverse channel velocity due to the less pore space available for transverse flow than for flow in the streamwise direction. A different analytical closure modelling procedure, analogous to the procedure presented in Du Plessis (1994), will be presented in this work.

The microscopic inertial effects will be modelled through consideration of interstitial flow recirculation within the separation zone on the lee side of the solid cube with respect to the streamwise direction. In order to account for the influence, albeit assumed to be minimal, of the proximity of other cubes on the separation zone, the RUC model within the laminar limit of the inertial flow regime will be regarded as a moderate to high porosity model (i.e. $\epsilon > 0.5$). The flow within this limit, as within the low Reynolds number flow regime, will be assumed to be Newtonian. The streamwise pressure gradient resulting from volume averaging of the transport equations in which a uniform velocity field $\underline{q}$ is

assumed (Chapter 3), leads to

$$-\nabla \langle p \rangle \;=\; \frac{1}{U_o} \iint\limits_{S_{fs}} \left( \underline{n}\, p - \underline{n} \cdot \underline{\underline{\tau}} \right) dS \; . \tag{5.1}$$

In the steady laminar limit of the inertial flow regime the shear stresses yield viscous forces proportional to $|\underline{q}|^{1.5}$ (Du Plessis (1992)) when the inertial effects are modelled through consideration of flow development within the boundary layers. Modelling of the microscopic inertial effects in the laminar limit through interstitial recirculation yields a proportionality of $|\nabla p| \propto |\underline{q}|^2$. Since the latter proportionality lies well above the former, it will be assumed that the viscous forces may be neglected in the steady laminar limit of the inertial flow regime, yielding

$$-\nabla \langle p \rangle \;=\; \frac{1}{U_o} \iint\limits_{S_{fs}} \underline{n}\, p \, dS \; . \tag{5.2}$$

Although the streamlines change dramatically from the Darcy to the inertial flow regime, resulting from the development of boundary layers and local flow separation, the volume partitioning of the fluid domain presented in chapter 3 will be used as an approximation for the partitioning of the fluid domain within this limit in order to proceed with the closure modelling procedure made available by the RUC model. The evaluation of the surface integral of equation (5.2) over the respective surfaces, resulting from volume partitioning of the fluid domain, leads to

$$-\nabla \langle p \rangle \;=\; \frac{1}{U_o} \iint\limits_{S_{\parallel}} \underline{n}\, p \, dS \;+\; \frac{1}{U_o} \iint\limits_{S_{\perp}} \underline{n}\, p \, dS \;+\; \frac{1}{U_o} \iint\limits_{S_g} \underline{n}\, p \, dS \; . \tag{5.3}$$



At increasing porosities, the stagnant regions diminish and may therefore be discarded at very high porosities. Consequently, only high porosity fully staggered arrays will be considered within this limit. It thus follows that

$$-\nabla \langle p \rangle \;=\; \frac{1}{U_o} \iint\limits_{S_{\parallel}} \underline{n}\, p \, dS \;+\; \frac{1}{U_o} \iint\limits_{S_{\perp}} \underline{n}\, p \, dS \; . \tag{5.4}$$

The parallel alignment of the streamwise surfaces of neighbouring cubes in the transverse directions, albeit assumed to be very far apart, results in the vectorial cancellation of the pressure on the streamwise surfaces, yielding

$$-\nabla \langle p \rangle \;=\; \frac{1}{U_o} \iint\limits_{S_{\perp}} \underline{n}\, p \, dS \; . \tag{5.5}$$

The importance of the need to consider all possible locations of the RUC in the streamwise direction was already mentioned in the closure modelling procedure for flow in the low Reynolds number flow regime and needs to be addressed once again. The two possible choices of RUC's, considering all possible locations of an RUC associated with a fully staggered array in the streamwise direction, are shown in Figure 5.1. The upstream and downstream facing surfaces of the RUC with corner points AAAA cut through solid parts and the corresponding faces of the RUC with corner points BBBB do not cut through any solid parts. $S_{\perp AA}$ and $S_{\perp BB}$ respectively denote the fluid-solid interfaces in $U_\perp$ of the RUC with corner points AAAA and BBBB.

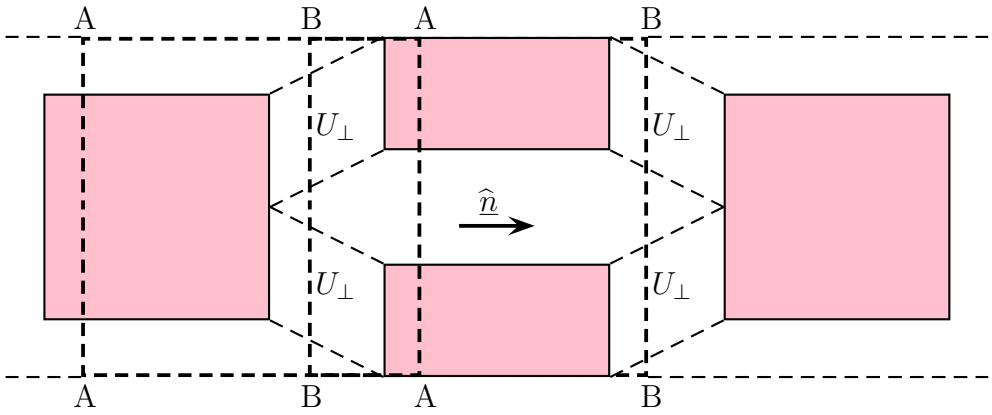


Figure 5.1: Schematic illustration of the two typical choices of RUC's in a fully staggered array to consider all possible locations in the streamwise direction.

Repeating the weighting procedure for the relative frequency of occurrence of the two possible RUC's, shown in Figure 5.1, over a streamwise displacement $d$, leads to

$$-\nabla \langle p \rangle \;=\; \frac{d_s}{d} \cdot \frac{1}{U_o} \iint\limits_{S_{\perp AA}} \underline{n}\, p \, dS \;+\; \frac{d - d_s}{d} \cdot \frac{1}{U_o} \iint\limits_{S_{\perp BB}} \underline{n}\, p \, dS \; . \tag{5.6}$$

Assuming that the pressure $p$ on all facing pairs of transverse surfaces are equal, results in a vectorial cancellation of the pressures on these surfaces, that is

$$-\nabla \langle p \rangle \;=\; \frac{d - d_s}{d} \cdot \frac{1}{U_o} \iint\limits_{S_{\perp BB}} \underline{n}\, p \, dS \; . \tag{5.7}$$

At very high porosities, it follows that

$$\frac{d - d_s}{d} \;\approx\; 1 \; , \tag{5.8}$$

yielding

$$-\nabla \langle p \rangle \;=\; \frac{1}{U_o} \iint\limits_{S_{\perp BB}} \underline{n}\, p \, dS \; . \tag{5.9}$$

The resulting surface integral represents the streamwise pressure drop over a solid cube contained within an RUC associated with a high porosity fully staggered array. For further analysis of the surface integral of equation (5.9), consider Figure 5.2, representing only the top half of the fully staggered array presented in Figure 5.1 for clearer illustration purposes. The interstitial recirculation within the separation zone on the lee side of the solid cube with respect to the streamwise direction is clearly illustrated. Let $S_{\perp_U}$ denote the upstream square surface of the cube and $S_{\perp_D}$ the downstream facing surface. The vectors $\underline{n}_U$ and $\underline{n}_D$ denote the corresponding inwardly directed unit vectors normal to $S_{\perp_U}$ and $S_{\perp_D}$, respectively. Point A represents the stagnation point on the upstream facing surface of the cube and point B on $S_{\perp_D}$ represents the separation point of the dividing streamline. Point C denotes the inflection point on the dividing streamline adjacent to the separation zone of interstitial recirculation.

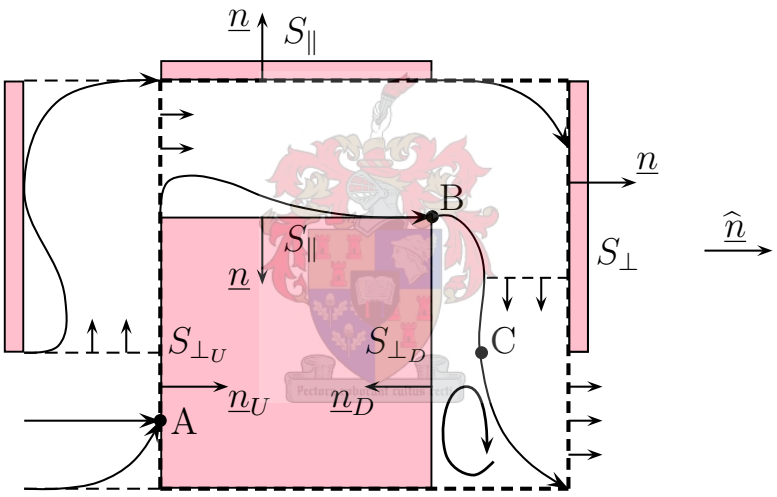


Figure 5.2: A two-dimensional schematic representation of the interstitial recirculation present within the separation zone on the lee side of the solid cube with respect to the streamwise direction. The bold dashed lines indicate the RUC boundaries.

Splitting the transverse surface integral accordingly into the upstream and downstream transverse facing surfaces yields

$$-\nabla \langle p \rangle \;= \frac{1}{U_o} \iint\limits_{S_{\perp_D}} \underline{n}_D \, p_D \, dS \;+\; \frac{1}{U_o} \iint\limits_{S_{\perp_U}} \underline{n}_U \, p_U \, dS \; , \tag{5.10}$$

where $p_D$ denotes the pressure on $S_{\perp_D}$ and $p_U$ the pressure on $S_{\perp_U}$. Due to the relatively low velocities within the separation zone, the pressure on the downstream surface $S_{\perp_D}$ is assumed to be constant. It thus follows that

$$-\nabla \langle p \rangle \;=\; \frac{d_s^2}{U_o}\, p_D\, \underline{n}_D \;+\; \frac{\underline{n}_U}{U_o} \iint\limits_{S_{\perp_U}} p_U \, dS \;. \tag{5.11}$$

The pressure $p_U$ will be approximated by applying Bernoulli's equation along the dividing streamline from the stagnation points A and B to the inflection point C. Bernoulli's equation was, however, derived for non-viscous vortex free flow and the present modelling procedure opposingly regards the flow of a viscous fluid. The applicability of Bernoulli's equation is motivated by the fact that the dividing streamline along which the equation is applied, is *adjacent* to the region of recirculation and the viscosity of the fluid in the *vicinity* of the inflection point C is assumed to be negligible. Although the applicability of Bernoulli's equation is a somewhat rough estimate for approximating the pressure on $S_{\perp_U}$, fluids such as water and air which are most frequently used for modelling purposes, are low viscosity fluids which renders the approximation to be less harsh. Therefore, applying Bernoulli's equation along the dividing streamline from the stagnation point A to the inflection point C and assuming that the difference in elevation between the two points is negligible, leads to

$$\frac{p_A}{\rho} \;+\; \frac{v_A^2}{2} \;=\; \frac{p_C}{\rho} \;+\; \frac{v_C^2}{2} \;, \tag{5.12}$$

where $v_A$ and $v_C$ respectively denotes the magnitude of the interstitial fluid velocities at the stagnation point A and the inflection point C. Since $v_A = 0$ and since it may be assumed that the pressure at the separation point B also prevails within the separation zone (Roberson & Crowe (1985)), i.e. $p_C = p_D$, it follows that

$$p_U \;=\; p_A \;=\; p_D + \frac{1}{2}\,\rho\, v_C^2 \;, \tag{5.13}$$

yielding the following expression for the streamwise pressure gradient

$$-\nabla \langle p \rangle \;=\; \frac{d_s^2}{U_o}\, p_D\, \underline{n}_D \;+\; \frac{\underline{n}_U}{U_o} \iint\limits_{S_{\perp_U}} p_D \, dS \;+\; \frac{\underline{n}_U}{U_o} \iint\limits_{S_{\perp_U}} \frac{1}{2}\rho\, v_C^2 \, dS \;. \tag{5.14}$$

Since, $\underline{n}_U = -\underline{n}_D = \widehat{\underline{n}}$, the first two terms of equation (5.14) cancel, yielding

$$-\nabla \langle p \rangle \;=\; \frac{\widehat{\underline{n}}}{U_o} \iint\limits_{S_{\perp_U}} \frac{1}{2}\,\rho\, v_C^2 \, dS \;. \tag{5.15}$$

At relatively high velocities the interstitial flow field approximates a uniform velocity profile, so that it seems reasonable to assume that the actual velocity at the inflection point C may be approximated by the average transverse pore velocity, i.e.

$$v_C \;\approx\; w_\perp \;=\; \beta\, w_\parallel \;, \tag{5.16}$$

The value of $\beta$ for a fully staggered array is again taken as $\beta = \sqrt{2}$ (chapter 4), since at high velocities, the partial occupation of the region of flow recirculation in the transverse channel has negligible effect on the ratio of the average pore velocities $w_\perp$ and $w_\parallel$. The streamwise pressure gradient may there-upon be expressed as

$$\begin{aligned}
-\nabla \langle p \rangle &= \frac{\rho\, w_\parallel^2 S_{\perp_U}}{U_o}\, \widehat{n} \\
&= \frac{\rho\, w_\parallel \underline{w}_\parallel\, d_s^2}{d^3} && (U_0 = d^3\,,\; S_{\perp_U} = d_s^2) \\
&= \frac{\rho\, q\, \underline{q}\, d\, d_s^2}{(d^2 - d_s^2)^2} && (\text{Eqn. } (3.10)) \\
&= \frac{\rho\, q\, \underline{q}\, (1-\epsilon)}{d_s \left(1 - (1-\epsilon)^{2/3}\right)^2} && (\text{Eqn. } (3.4)) \\
&= \frac{\mu\, \underline{q}\, (1-\epsilon)}{d_s^2 \left(1 - (1-\epsilon)^{2/3}\right)^2} Re_p && (\text{Eqn. } (3.20))
\end{aligned} \tag{5.17}$$

For unidirectional flow of a Newtonian fluid in the positive $x$-direction of a Cartesian coordinate system through a porous medium of local uniform porosity the streamwise pressure drop may, analogously to Forchheimer's extension of Darcy's law (Forchheimer (1901)) in which the higher order velocity term dominates, be expressed as

$$-\frac{\mathrm{d}p}{\mathrm{d}x} \;=\; \mu\, f_1\, q \;. \tag{5.18}$$

Here $f_1$ denotes the shear factor in laminar limit of the inertial flow regime which may may consequently be expressed as

$$f_1 \;=\; \frac{(1-\epsilon)}{d_s^2\, \epsilon \left(1 - (1-\epsilon)^{2/3}\right)^2} Re_p \;. \tag{5.19}$$

The dimensionless shear factor $F_1 = f_1\, d_s^2$, describing the flow of a Newtonian fluid through granular media of high porosity, is thus given by

$$F_1 \;=\; \frac{(1-\epsilon)}{\epsilon \left(1 - (1-\epsilon)^{2/3}\right)^2} Re_p \;. \tag{5.20}$$

Equation (5.20) is equivalent to the expression proposed by the existing RUC model for flow in the steady laminar limit of the inertial flow regime. The validity of applying the technique of volume partitioning of the fluid domain in the laminar limit is therefore justified since the volume partitioning technique was not applied in the modelling procedure of the existing RUC model within this regime.

## 5.2 Comparison with granular models from literature

### 5.2.1 Shear factor

There are very few models in the literature regarding flow through porous media in the Forchheimer regime due to the complex nature of the flow characteristics, especially where turbulence is involved. A well-known semi-empirical model for predicting the pressure gradient for the flow of a Newtonian fluid through packed beds of smooth uniformly sized spherical particles in the Forchheimer regime, where highly turbulent flow was assumed to be present, is the empirical Burke-Plummer equation (Appendix D.3). The Burke-Plummer equation is based on the capillary-tube representation of turbulent flow through a packed bed and may be expressed in terms of the dimensionless shear factor $F_1$ as follows

$$F_1 = \frac{1.75\,(1-\epsilon)}{\epsilon^3} Re_p \,, \tag{5.21}$$

and is valid for $\epsilon < 0.5$. Macdonald et al. (1979) suggested a coefficient value of 1.80 for the Burke-Plummer equation, instead of the value of 1.75. His proposal was based on extensive experimental data. The dimensionless shear factor $F_1$ as suggested by the empirical verification of Macdonald et al. (1979), may consequently be expressed as

$$F_1 = \frac{1.8\,(1-\epsilon)}{\epsilon^3} Re_p \,. \tag{5.22}$$

A graphical comparison between the present RUC model, the Burke-Plummer equation and the empirical verification of Macdonald et al. (1979) is shown in Figure 5.3 for $\epsilon = 0.43$ and Reynolds numbers within the Forchheimer regime. Although the RUC model for predicting flow in the laminar inertial flow regime is a high porosity model, it seems that the assumptions made within the analytical modelling procedure apply equally well to porosities within the packed bed region. The excellent correspondence of the RUC model with the Burke-Plummer equation and with the empirical verification of Macdonald et al. (1979) over the entire Reynolds number range indicated in Figure 5.3, i.e. $10 < Re_p < 1000$, demonstrates the ability of the RUC model to predict flow behaviour in the laminar inertial flow regime.

### 5.2.2 Coefficient $B$ in the Burke-Plummer equation

The present RUC model may alternatively be compared to the Burke-Plummer equation by providing an expression for predicting the coefficient $B$ in the Burke-Plummer equation (Appendix D.3) as a function of porosity i.e.

$$B = \frac{\epsilon^2}{\left(1-(1-\epsilon)^{2/3}\right)^2} \,. \tag{5.23}$$

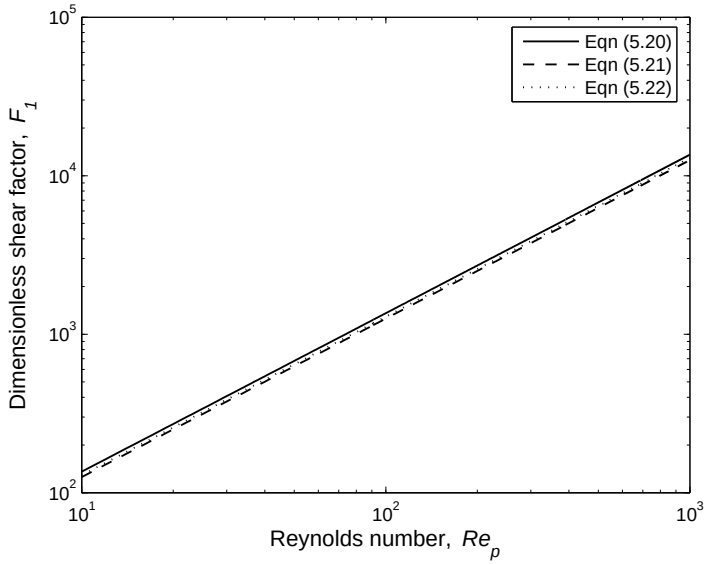


Figure 5.3: Comparison of the dimensionless resistance factor $F_1$ for $\epsilon = 0.43$.

A comparison between the coefficient values predicted by the analytical and semi-empirical models is given in Table 5.1 for $\epsilon = 0.43$. The latter porosity value is chosen as the average value corresponding to a granular packed bed.

| Model | Coefficient $B$, $\epsilon = 0.43$ |
|---|---|
| Burke-Plummer | 1.75 |
| Macdonald | 1.80 |
| Present RUC | 1.89 |

Table 5.1: Comparison of the coefficient $B$ for $\epsilon = 0.43$.

The porosity dependence of equation (5.23), together with the constant values proposed by the semi-empirical models, are graphically shown in Figure 5.4. For porosities ranging from 0.34 to 0.48 values for $B$ ranging from 1.49 to 1.77 with an average value of 1.63 have been obtained experimentally (Macdonald et al. (1979)). For the same range of porosities the RUC model predicts values for $B$ ranging from 1.85 to 1.97 with an average value of 1.91. The objective of the RUC model with its simplifying assumptions was by no means to predict exact values, but rather to obtain values of the same order of magnitude as the experimental values. In this respect the range of values predicted by the RUC model is very pleasing, especially the very good correspondence with the value proposed by Macdonald et al. (1979) at $\epsilon = 0.43$.

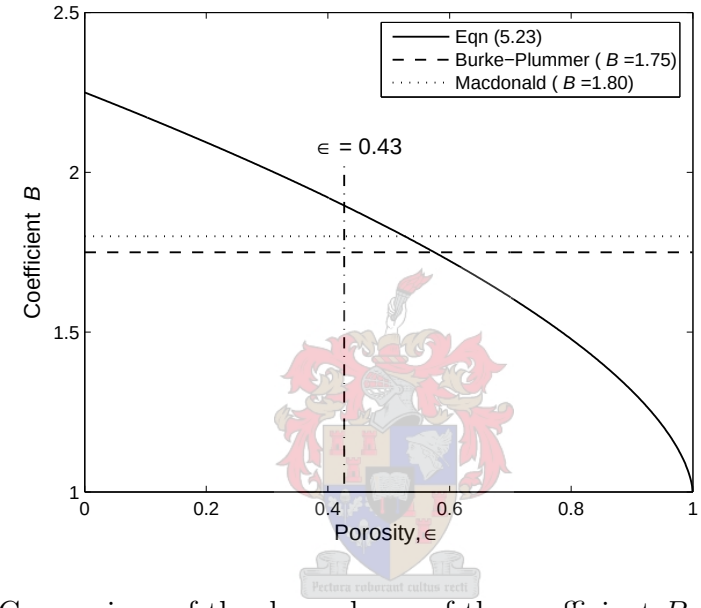


Figure 5.4: Comparison of the dependence of the coefficient $B$ on the porosity.

# Chapter 6

# Asymptote matching of laminar limits

The RUC model proposed for the dimensionless shear factor in the asymptotic limit of low Reynolds number flow and in the laminar limit of the inertial flow regime may be matched according to the asymptote matching technique introduced by Churchill & Usagi (1972) through application of the formula

$$F \;=\; (F_0^s + F_1^s)^{1/s} \;, \tag{6.1}$$

to obtain an overall shear factor $F$ applicable over the entire steady laminar flow regime. In order to obtain an analytical model for direct comparison with the semi-empirical Ergun equation (Appendix D.4), which is simply a superposition of two asymptotic limits, the shifting parameter $s$ is chosen to be unity. A more accurate predictive expression may be obtained for values of the $s$ greater than unity. Substituting for the corresponding shear factors as predicted by the present RUC model into equation (6.1), yields

$$F \;=\; \frac{26.8\,(1-\epsilon)^{4/3}}{\left(1-(1-\epsilon)^{1/3}\right)\left(1-(1-\epsilon)^{2/3}\right)^2} \;+\; \frac{(1-\epsilon)}{\epsilon\left(1-(1-\epsilon)^{2/3}\right)^2} Re_p \;, \tag{6.2}$$

For unidirectional flow of a Newtonian fluid in the positive $x$-direction of a Cartesian coordinate system through a porous medium of local uniform porosity the streamwise pressure drop may, analogously to Forchheimer's extension of Darcy's law, be expressed as

$$-\frac{\mathrm{d}p}{\mathrm{d}x} \;=\; \mu\, F\, q \;, \tag{6.3}$$

where, for $s = 1$, the overall shear factor is given by

$$F \;=\; F_0 + F_1 \;. \tag{6.4}$$

The pressure drop prediction proposed by the present RUC model thus leads to

$$-\frac{\mathrm{d}p}{\mathrm{d}x} \;=\; \frac{26.8\,(1-\epsilon)^{4/3}}{d_s^2\left(1-(1-\epsilon)^{1/3}\right)\left(1-(1-\epsilon)^{2/3}\right)^2}\,\mu\,q \;+\; \frac{(1-\epsilon)}{\epsilon\,d_s\left(1-(1-\epsilon)^{2/3}\right)^2}\,\rho\,q^2\;. \qquad (6.5)$$

If the RUC/Hasimoto model is introduced for the lower limit in equation (6.1) then the overall shear factor becomes

$$F \;=\; \frac{26.8\,(1-\epsilon)^{\frac{4}{3}}}{\left(1-(1-\epsilon)^{\frac{1}{3}}\right)\left(1-(1-\epsilon)^{\frac{2}{3}}\right)^2} \;+\; 3\,\pi\,(1-\epsilon)\,\left(1+1.791\,(1-\epsilon)^{1/3}\right) + \frac{(1-\epsilon)}{\epsilon\left(1-(1-\epsilon)^{\frac{2}{3}}\right)^2}Re_p\;, \qquad (6.6)$$

with the corresponding pressure drop prediction given by

$$-\frac{\mathrm{d}p}{\mathrm{d}x} \;=\; \frac{26.8\,(1-\epsilon)^{\frac{4}{3}}}{\left(1-(1-\epsilon)^{\frac{1}{3}}\right)\left(1-(1-\epsilon)^{\frac{2}{3}}\right)^2}\,\mu\,q \;+\; 3\,\pi\,(1-\epsilon)\,\left(1+1.791\,(1-\epsilon)^{1/3}\right)\,\mu\,q + \frac{(1-\epsilon)}{\epsilon\,d_s\left(1-(1-\epsilon)^{2/3}\right)^2}\,\rho\,q^2\;. \qquad (6.7)$$

Equations (6.5) and (6.7) are unified expressions for predicting the pressure drop for the flow of an incompressible Newtonian fluid through a homogeneous isotropic granular porous medium within the entire steady laminar flow regime.

## 6.1 Comparison with the Ergun equation

The semi-empirical Ergun equation provides an expression for the pressure drop prediction for the flow of an incompressible Newtonian fluid through a packed bed with uniformly sized spherical particles for Reynolds numbers ranging from the laminar to the highly turbulent flow regime, i.e.

$$\frac{\Delta p}{L} \;=\; 150\,\frac{(1-\epsilon)^2}{\epsilon^3}\frac{\mu\,q}{D_h^2} \;+\; 1.75\,\frac{(1-\epsilon)}{\epsilon^3}\frac{\rho\,q^2}{D_h}\;, \qquad (6.8)$$

where $\Delta p$ denotes the pressure drop over a bed of length $L$. The Ergun equation usually provides good agreement with experimental data for $\epsilon < 0.5$. Expressed in terms of the overall shear factor the Ergun equation yields

$$F \;=\; \frac{150\,(1-\epsilon)^2}{\epsilon^3} \;+\; \frac{1.75\,(1-\epsilon)}{\epsilon^3}Re_p\;, \qquad (6.9)$$

and the empirical verification of Macdonald et al. (1979) produces

$$F \;=\; \frac{180\,(1-\epsilon)^2}{\epsilon^3} \;+\; \frac{1.8\,(1-\epsilon)}{\epsilon^3} Re_p \;. \tag{6.10}$$

In Figure (6.1) results of the present RUC model is compared with the Ergun equation and the empirical verification of Macdonald et al. (1979) over the entire Reynolds number range.

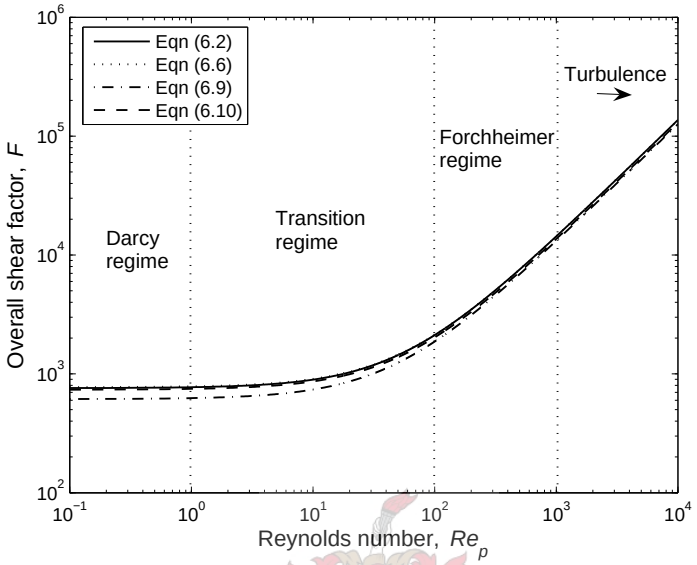


Figure 6.1: Comparison of the present RUC model with the Ergun equation.

The excellent correspondence of the present RUC model with the empirical verification of Macdonald et al. (1979) is rather astonishing, since the analytical model and the semi-empirical Ergun equation follow completely different modelling approaches. The agreement of the RUC model with the semi-empirical models at $Re_p > 1000$ renders doubt on the early onset of turbulence in porous media. The asymptote matching technique provides a gradual transition from the Darcy to the inertial flow regime and proves to be a very skilful technique for the matching of two asymptotic limits to obtain a unified expression for predicting flow conditions over the entire matching domain. The present RUC model may thus be regarded as a theoretical derivation of the semi-empirical Ergun equation. Despite the frequent use and modification of the Ergun equation in the literature, it has received a great amount of criticism due to its lack of inter-connectedness (Dullien (1979)) and its limited applicability (Kaviany (1995)). The major advantage of the RUC model over the Ergun equation is that it contains no empirical factors. The coefficients introduced into the model are all based purely on sound physical principles. The pore-space of the RUC model is interconnected and provides a more realistic approximation for flow through granular beds. Since a difference between the RUC model and the RUC/Hasimoto model is hardly discernable from Figure (6.1), it may be concluded that the RUC model, without the asymptote matching with the high porosity model of Hasimoto in the low Reynolds number flow regime, is adequate for modelling flow conditions

over the entire Reynolds number flow regime. When flow behaviour in the low Reynolds number flow regime alone is considered, the RUC/Hasimoto is the most promising model.

## 6.2 Critical Reynolds number

The Reynolds number associated with the location of the centre of the transition region between the Darcy and Forchheimer regime, is called the critical Reynolds number, denoted by $Re_c$. The critical Reynolds number may be determined from equation (6.2) and the resulting expression as a function of porosity is given by

$$Re_c = \frac{26.8\,\epsilon\,(1-\epsilon)^{1/3}}{(1-(1-\epsilon)^{1/3})}\,. \tag{6.11}$$

Equation (6.11) defines a critical Reynolds number range of $0.1 \leq Re_c \leq 75$ for a porosity range of $0.1 \leq \epsilon \leq 1$. This range of critical Reynolds numbers correspond exactly with the Reynolds number range proposed by Dullien (1979) above which Darcy's law is no longer valid for various porous media. Happel & Brenner (1965) state that the critical Reynolds number at which separation first occurs in flow around a sphere is $Re_c = 17$. For porosities in the range $0.9 \leq \epsilon \leq 0.95$ equation (6.11) yields a range of critical Reynolds numbers of $15 \leq Re_c \leq 21$. The value of $Re_c = 17$ falls exactly within this range, underscoring the statement by Happel & Brenner (1965).

# Chapter 7

# Non-Newtonian flow

A very large category of fluids used for industrial applications does not obey Newton's law of viscosity, which implies that the shear stress is no longer linearly proportional to the shear rate. These structurally complex fluids of molecular weights larger than 5000 are referred to as non-Newtonian fluids (Bird et al. (2002)). The viscosity of these fluids depends strongly on the velocity gradient and is therefore a function of the characteristics of the porous medium and the rheological properties of the fluid. In contrast to incompressible Newtonian fluids, which solely require a measurement of the viscosity, non-Newtonian fluids require measurements of the viscosity together with possible second order effects such as normal stresses and viscoelastic responses. Non-Newtonian fluids find application in, for instance, the processing, pharmaceutical and petroleum industries and in biological fields. Specific applications of the flow of non-Newtonian liquids through porous media include the filtration of polymer solutions and the flow of aqueous polymer solutions through sand in secondary oil recovery operations (Christopher & Middleman (1965)). The velocity gradient dependent viscosity function takes on a variety of forms and therefore non-Newtonian fluids may be divided into three broad categories (Harris (1977), Skelland (1967)): (1) purely viscous or time-independent fluids , (2) time-dependent fluids and (3) viscoelastic fluids. The purely viscous non-Newtonian fluids may in turn be subdivided into the following groups: (i) shear-thinning or pseudoplastic fluids, (ii) shear-thickening or dilatant fluids and (iii) viscoplastic fluids. The shear-thinning fluids are characterized by a decrease in apparent viscosity with increasing shear rate, whilst the shear-thickening fluids exhibit an increase in apparent viscosity with increasing shear rate. The viscoplastic fluids are characterized by an additional finite yield stress which is required to initiate the flow. The time-dependent fluids are those for which the shear rate is a function of both the magnitude and the duration of the shear stress at isothermal conditions. Liquids for which the apparent viscosity increases with the duration of the shear stress are referred to as rheopectic fluids and those for which the apparent viscosity decreases with the duration of the shear stress are referred to as thixotropic fluids. Viscoelastic fluids possess both viscous and elastic properties. These fluids exhibit partial recovery of deformation upon removal of stress and are associated with normal stress effects. In reality the classification of non-Newtonian fluids given above is by no means distinct or sharply defined since these fluids actually exhibit combinations of the

respective rheological flow characteristics; the classification simply serves as an aid for mathematical modelling purposes. Various models are available in the literature for describing the non-Newtonian flow behaviour within the distinctive categories. Only purely viscous shear-thinning fluids will be considered in this work, due to the following reasons: The RUC model only concerns inelastic time-independent fluids. Time-dependent fluids are seldom utilized in engineering design procedures and if required, purely viscous fluids could be applied to time-dependent materials under isothermal steady flow conditions. Furthermore, the elastic properties of viscoelastic fluids are insignificant for fluid flow through channels of fixed cross section in the laminar flow regime (Skelland (1967)). Examples of purely viscous shear-thinning fluids are polymer and rubber solutions, greases, soap, paints, gelatine, clay, milk, blood and liquid cement. A generalized expression for model-ling the shear stress of both Newtonian and non-Newtonian fluids (Appendix E) is given by:

$$\tau_{yx} \;=\; \eta\left(\dot{\gamma}\right)\left|\dot{\gamma}\right| \,, \tag{7.1}$$

where $\tau_{yx}$ is the magnitude of the shear stress tensor $\underline{\underline{\tau}}$ for unidirectional fluid discharge in the positive $x$-direction. The simplest and most commonly used model to describe the rheological flow behaviour of purely viscous shear-thinning fluids for intermediate shear rates is the empirical Ostwald-de-Waele power law model (Skelland (1967)). The dependence of the apparent viscosity $\eta$ on the shear rate $\dot{\gamma}$ may be obtained from empirical viscometry data and expressed as

$$\eta\left(\dot{\gamma}\right) \;=\; K\left|\dot{\gamma}\right|^{n-1} \qquad \text{for} \qquad n < 1 \,. \tag{7.2}$$

Here $K$ and $n$ are constants characterizing the fluid and respectively referred to as the consistency and behaviour indices. Since $n$ is less than unity for shear-thinning fluids it is evident that the apparent viscosity decreases with increasing shear rate, which is defined as

$$\dot{\gamma} \;=\; \frac{\mathrm{d}v}{\mathrm{d}y} \,, \tag{7.3}$$

with $v$ the actual speed of the fluid. The power law model may thus be expressed as

$$\tau_{yx} \;=\; K\left|\dot{\gamma}\right|^{n} \,. \tag{7.4}$$

The behaviour index $n$ is the slope of the logarithmic plot of shear stress $\tau_{yx}$ versus shear rate $\dot{\gamma}$ which ranges from unity, resembling Newtonian flow behaviour, to zero. The consistency index $K$ is calculated from the intercept on the $\tau_{yx}$ axis at unit shear rate (Skelland (1967)). The effect of normal stresses cannot be predicted or interpreted by the power law model (Savins (1970)). For $n = 1$ the shear stress expression for describing Newtonian fluids is obtained (Appendix E).

## 7.1 RUC model for purely viscous power law flow

The RUC model was generalized for the first time by Du Plessis (1996) to predict the flow of purely viscous power law fluids through a variety of porous microstructures, including isotropic granular porous media. This section is based on the work of Smit & Du Plessis (1997) and (2000) which concerns the evaluation of the RUC model of Du Plessis & Masliyah (1991) for power law flow through isotropic granular porous media with published experimental data. The results of this chapter have been published (Woudberg et al. (2006)). The expression obtained for the streamwise pressure gradient for Newtonian flow in the low Reynolds number flow regime (equation (4.22)) is given by

$$-\nabla \langle p \rangle \;=\; \left(\frac{U_f}{U_{\parallel} + U_t}\right) \frac{S_{\parallel} \,+\, \beta\, \xi S_{\perp}}{U_o}\, \tau_{w_{\parallel}}\, \underline{\widehat{n}}\,. \tag{7.5}$$

The latter expression may be generalized to account for non-Newtonian purely viscous flow by introducing the dependency of the apparent viscosity into the expression for the wall shear stress. The wall shear stress for power law flow between parallel plates a distance $2B$ apart, in which a no-slip boundary condition and fully developed flow are assumed (Appendix E.1) may be expressed as

$$\tau_{w_{\parallel}} \;=\; K \left(\frac{2n+1}{n}\right)^n \left(\frac{2w_{\parallel}}{d - d_s}\right)^n \qquad , \qquad n < 1\,. \tag{7.6}$$

Substituting for $\tau_{w_{\parallel}}$ into equation (7.5) yields

$$-\nabla \langle p \rangle \;=\; \left(\frac{U_f}{U_{\parallel} + U_t}\right) \frac{S_{\parallel} \,+\, \beta\, \xi S_{\perp}}{U_o}\, K \left(\frac{2n+1}{n}\right)^n \left(\frac{2w_{\parallel}}{d - d_s}\right)^n \underline{\widehat{n}}\,. \tag{7.7}$$

The following generalization of the pressure gradient for flow though a porous medium of local uniform porosity was introduced by Du Plessis (1996),

$$-\epsilon \nabla \langle p \rangle_f \;=\; K \mathcal{F}_n q^{n-1} \underline{q}\,, \tag{7.8}$$

so that for unidirectional discharge in the positive $x$-direction of a Cartesian coordinate system the streamwise pressure drop may be expressed as

$$-\epsilon \frac{\mathrm{d}p}{\mathrm{d}x} = K \mathcal{F}_n\, q^n\,. \tag{7.9}$$

Here $\mathcal{F}_n$ is the shear factor used in Du Plessis (1996) and relates to the shear factor used in the present RUC model $f_n$ by

$$f_n \;=\; \frac{\mathcal{F}_n}{\epsilon}\,. \tag{7.10}$$

The streamwise pressure drop may there-upon be expressed as

$$-\frac{\mathrm{d}p}{\mathrm{d}x} = K f_n q^n \tag{7.11}$$

where

$$f_n = f_{n_0} \; + \; f_{n_1} \; , \tag{7.12}$$

resulting from application of the asymptote matching technique of Churchill & Usagi (1972) with $s = 1$. The shear factor for power law flow in the limit of low Reynolds numbers, $f_{n_0}$, as proposed by the present generalized RUC model is thus given by

$$f_{n_0} \; = \; \frac{1}{k_n} \; = \; \frac{2^n (4.47)(1-\epsilon)^{(n+3/3)}}{d_s^{n+1} \left(1-(1-\epsilon)^{1/3}\right)^n \left(1-(1-\epsilon)^{2/3}\right)^{n+1}} \left(\frac{2n+1}{n}\right)^n \; , \tag{7.13}$$

where $k_n$ denotes the generalized hydrodynamic permeability. The expression obtained for the streamwise pressure gradient in the laminar limit of the inertial flow regime is given by

$$-\nabla \langle p \rangle \; = \; \frac{\rho \, w_{\parallel}^2 S_{\perp_U}}{U_o} \, \underline{\widehat{n}} \; . \tag{7.14}$$

Since the viscous forces are negligible in the steady laminar limit, the same expression holds for the shear factor as for Newtonian flow (equation (5.19)) and by application of equation (7.11) the following expression is obtained for the shear factor for power law flow in the laminar limit of the inertial flow regime,

$$f_{n_1} \; = \; \frac{\rho \, q^{2-n} (1-\epsilon)}{d_s \, \epsilon \, K \left(1-(1-\epsilon)^{\frac{2}{3}}\right)^2} \; . \tag{7.15}$$

It thus follows that the overall shear factor for purely viscous power law flow applicable over the entire steady laminar flow regime, $f_n$, may be expressed as

$$f_n \; = \; \frac{2^n (4.47)(1-\epsilon)^{(n+3/3)}}{d_s^{n+1} \left(1-(1-\epsilon)^{1/3}\right)^n \left(1-(1-\epsilon)^{2/3}\right)^{n+1}} \left(\frac{2n+1}{n}\right)^n \left[1 + \frac{(1-(1-\epsilon)^{2/3})}{12\,(4.47)\,\epsilon} Re_{p_n}\right] \; , \tag{7.16}$$

where the generalized particle Reynolds number $Re_{p_n}$, defined in terms of the cube length $d_s$, is given by

$$Re_{p_n} \; = \; \frac{12 \, \rho \, d_s^n \, q^{2-n}}{K(1-\epsilon)^{n/3}} \frac{(1-(1-\epsilon)^{1/3})^n}{(1-(1-\epsilon)^{2/3})^{2-n}} \left(\frac{n}{2\,(2n+1)}\right)^n \; . \tag{7.17}$$

The reason for expressing the Reynolds number $Re_{p_n}$, as in equation (7.17), is simply to be able to express the friction factor $f_n$ in the particular way that it is presented in

equation (7.16). Expressing $f_n$ in terms of the linear dimension $d$ of the RUC, yields

$$f_n = \frac{2^n(4.47)(1-\epsilon)^{2/3}}{d^{n+1}(1-(1-\epsilon)^{1/3})^n(1-(1-\epsilon)^{2/3})^{n+1}}\left(\frac{2n+1}{n}\right)^n\left[1+\frac{(1-(1-\epsilon)^{2/3})}{12\,(4.47)\,\epsilon}Re_{p_n}\right], \tag{7.18}$$

with the corresponding cell Reynolds number given by

$$Re_{p_n} = \frac{12\,\rho\,d^n\,q^{2-n}}{K}\frac{\left(1-(1-\epsilon)^{1/3}\right)^n}{(1-(1-\epsilon)^{2/3})^{2-n}}\left(\frac{n}{2\,(2n+1)}\right)^n. \tag{7.19}$$

The expression for the overall shear factor $f_n$ proposed by Smit & Du Plessis (1997) is given by

$$f_n = \frac{2^n\,6\,(1-\epsilon)^{2/3}}{d^{n+1}(1-(1-\epsilon)^{1/3})^n(1-(1-\epsilon)^{2/3})^n}\left(\frac{2n+1}{n}\right)^n\left[1+\frac{1}{72}Re_{p_n}\right], \tag{7.20}$$

with the Reynolds number given by equation (7.19).

### 7.1.1 Comparison with empirical models from literature

This section involves the evaluation of the present RUC model for power law flow at intermediate shear rates described by equations (7.11), (7.18) and (7.19) by comparing the predicted pressure drop to various semi-empirical models and experimental data from the literature. A graphical comparison between the present RUC model and the existing model proposed by Smit & Du Plessis (1997) will not be shown in this section since the two models prove to be graphically indistinguishable. However, from an analytical point of view, as discussed in chapter 4.2.2, the difference between the models is quite significant. Sabiri & Comiti (1995) experimentally investigated the flow of a purely viscous power law fluid through a densely packed bed of glass spheres and proposed an expression for predicting the pressure drop for Reynolds numbers ranging from the creeping flow to the inertial flow regimes ($0.17 < Re < 35$). The friction factor $f_{mod}$ based on the capillary representation of a packed bed, that is

$$f_{mod} = \frac{16}{Re_p}\left[1+\frac{2\,d_p}{3D(1-\epsilon)}\right]^{1+n_i} + 2\left\{\left[1-\left(1-\frac{d_p}{D}\right)^2\right]0.0413+0.0968\left(1-\frac{d_p}{D}\right)^2\right\}, \tag{7.21}$$

is evaluated against the experimental friction factor

$$f_{exp} = \frac{\Delta p}{H}\frac{2\,\epsilon^3}{\rho\,q^2\,T^3(1-\epsilon)\,a_{vd}}, \tag{7.22}$$

with the Reynolds number for tube flow given by

$$Re_p = \frac{\rho\,\epsilon^{2n_i-2}\,T^{2-n_i}\,q^{2-n_i}}{2^{n_i-3}K_i\left[(3n_i+1)/4n_i\right]^{n_i}(1-\epsilon)^{n_i}\,a_{vd}^{n_i}}. \tag{7.23}$$

The indices $n_i$ and $K_i$ respectively denote the behaviour and consistency indices of the power law model, $d_p$ is the spherical particle diameter, $D$ is the column diameter, $T$ denotes the tortuosity, $a_{vd}$ is the dynamic specific surface area and $\Delta p$ is the pressure drop measured over a bed height $H$. An aqueous solution of carboximethylcellulose sodium salt (CMC) has been used of which the rheological behaviour is described by the following series of equations for the shear stress $\tau$ for power law flow:

$$i = 1: \quad \tau = 0.116\,\dot{\gamma}^{0.771} \quad \text{for} \quad 38 < \dot{\gamma} < 450\,s^{-1} \tag{7.24}$$

$$i = 2: \quad \tau = 0.262\,\dot{\gamma}^{0.634} \quad \text{for} \quad 400 < \dot{\gamma} < 3500\,s^{-1}\,. \tag{7.25}$$

The values of the indices $n$ and $K$ were obtained from the empirical flow curve data of shear stress versus shear rate. The shear rate $\dot{\gamma}$ in the laminar flow regime relates to the superficial velocity $q$ and the tortuosity $T$ as follows

$$\dot{\gamma} = \frac{3n_i + 1}{2\,n_i}\frac{q\,T}{\epsilon^2}(1-\epsilon)\,a_{vd}\,. \tag{7.26}$$

The characteristic fluid-, particle- and bed parameters are presented in Table 7.1.

| Test fluid | Packing material | $d_p$ (mm) | $\epsilon$ | $\rho$ (kg.m$^{-3}$) | $T$ | $a_{vd}$ (m$^{-1}$) | $D$ (m) |
|---|---|---|---|---|---|---|---|
| CMC | Glass spheres | 2.92 | 0.36 | 1021 | 1.44 | 2055 | 0.06 |

Table 7.1: Characteristic fluid-, particle- and bed parameters (Sabiri & Comiti (1995)).

The values of $T$ and $a_{vd}$ were obtained form pressure drop measurements of a Newtonian fluid (water). In order to compare the RUC model to the experimental data of Sabiri & Comiti (1995), the values of the friction factors $f_{exp}$ and $f_{mod}$, were digitized from a plot of $f_{exp}$ versus $f_{mod}$ by Smit (1997). The Reynolds number values were obtained by using the parameter values presented in Table 7.1 and solving for $Re_p$ from equation (7.21). The values of the superficial velocity $q$ could then in turn be solved from equation (7.23). Finally, the experimental pressure drop values were computed from equation (7.22). The values of the resistance factor $f_n$ of the present RUC model (equation (7.18)) were obtained by using the same computed $q$-values and power law indices and also the same parameter values as presented in Table 7.1. The pressure drop values predicted by the present RUC model were obtained from equation (7.11). Figure 7.1 compares the predictive analytical pressure drop to the experimental pressure drop data of Sabiri & Comiti (1995). Although the pressure drop data of Sabiri & Comiti (1995) are for Reynolds numbers ranging from the creeping flow to the inertial flow regime, the most data points lie within the creeping flow regime and therefore a graph of experimental versus analytical pressure drop was found to be the most appropriate manner to compare theory and experiment. Figure

7.1 shows the deviation of the experimental values relative to the predicted values. The fact that all the experimental data lie very close to the solid line is very encouraging and substantiate the predictive capability of the RUC model.

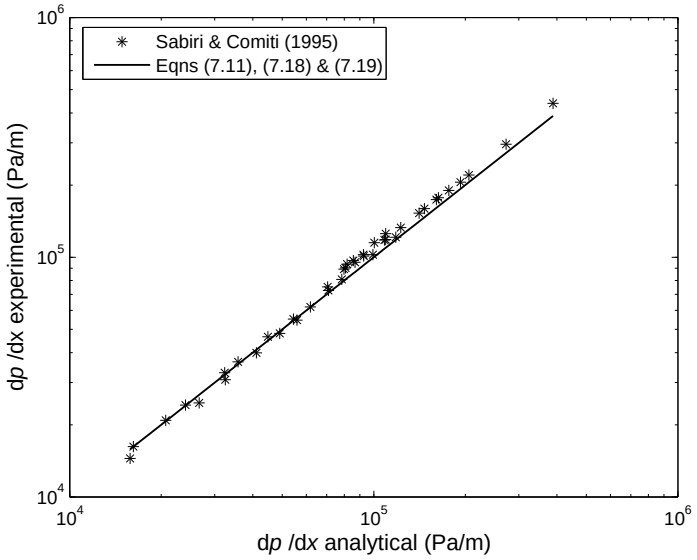


Figure 7.1: Comparison between the predicted analytical pressure drop proposed by the present RUC model and the empirical pressure drop data of Sabiri & Comiti (1995).

Chhabra & Srinivas (1991) experimentally investigated the flow of purely viscous power law fluids through packed beds of non-spherical particles, e.g. Rashig rings and gravel chips, for porosities ranging from 0.472 to 0.704 and Reynolds numbers mostly within the Darcy regime ($0.0016 < Re < 2.5$). The main emphasis of their work was the effect of particle shape on the pressure drop. The rheological properties of aqueous solutions of carboxymethyl cellulose (CMC) were modelled through application of the power law model, i.e.

$$\tau = K\dot{\gamma}^n \; . \tag{7.27}$$

The values of $K$ and $n$ were obtained form a curve relating the shear stress to the shear rate by using a non-linear regression approach. The experimental pressure drop data is obtained from an adaptation of the empirical Ergun equation for non-spherical particles and non-Newtonian flow behaviour and presented as

$$f \;=\; \frac{D_p}{\rho\, q^2}\left(\frac{\Delta p}{L}\right)\frac{\epsilon^3}{1-\epsilon}\; . \tag{7.28}$$

Here the Reynolds number $Re'$ is defined as (Kemblowski & Michniewics (1979))

$$Re^{'} \;=\; \frac{\rho\, q^{2-n} D_p^n}{K(1-\epsilon)^n}\left(\frac{4n}{3n+1}\right)^n\left(\frac{15\sqrt{2}}{\epsilon^2}\right)^{1-n}\; , \tag{7.29}$$

with $\Delta p$ the pressure drop measured over a bed height $L$. To account for non-spherical particles the spherical particle diameter $D_p$ is defined as $D_{pe}\phi_s$ where $D_{pe}$ is the effective or equivalent diameter, i.e. the diameter of a sphere of identical volume and $\phi_s$ denotes a sphericity factor. The values of the sphericity factor for the two Raschig ring sizes and the gravel chips are obtained from experimental data concerning the flow of a Newtonian fluid, namely glucose syrup, at Reynolds numbers within the Darcy regime and by application of the adapted empirical Ergun equation, i.e.

$$f = \frac{150}{Re'} + 1.75 \, . \tag{7.30}$$

The experimental bed- and fluid properties, together with the sphericity factor $\phi_s$ of the three types of particles, are presented in Table 7.2.

| Liquid no. | Test liquid | $n$ | $K$ (Pa.s$^n$) | $\rho$ (kg.m$^{-3}$) | $D_{pe}$ (mm) | $\phi_s$ | $\epsilon$ | Particle* |
|---|---|---|---|---|---|---|---|---|
| 1 | Water | 1.0 | 0.00105 | 1000 | 6.119 | 0.580 | 0.472 | C |
| 2 | Water | 1.0 | 0.00105 | 1000 | 7.769 | 0.330 | 0.654 | B |
| 3 | 2.0% CMC | 0.69 | 0.468 | 1000 | 11.675 | 0.301 | 0.704 | A |
| 4 | 2.2% CMC | 0.56 | 1.079 | 1000 | 6.119 | 0.580 | 0.472 | C |
| 5 | 2.1% CMC | 0.62 | 0.697 | 1000 | 7.769 | 0.330 | 0.654 | B |
| 6 | 2.8% CMC | 0.49 | 3.617 | 1000 | 7.769 | 0.330 | 0.654 | B |
| 7 | 2.8% CMC | 0.49 | 3.768 | 1000 | 11.675 | 0.301 | 0.704 | A |
| 8 | 2.8% CMC | 0.49 | 3.770 | 1000 | 6.119 | 0.580 | 0.472 | C |
| 9 | 2.4% CMC | 0.56 | 1.465 | 1000 | 6.119 | 0.580 | 0.472 | C |
| 10 | 2.4% CMC | 0.57 | 1.272 | 1000 | 11.675 | 0.301 | 0.704 | A |

*Particle: A - Raschig rings (13 mm); B - Raschig rings (8 mm); C - Gravel chips;

Table 7.2: Bed- and fluid properties (Chhabra & Srinivas (1991)).

For comparison between the RUC model and the experimental data of Chhabra & Srinivas (1991), the values of the friction factor $f$ and the corresponding Reynolds number values were digitized from a plot of $f$ versus $Re'$ by Smit (1997). The values of the superficial velocity $q$ were obtained by using the parameter values presented in Table 7.2 and solving for $q$ from equation (7.29). The experimental pressure drop values were computed from equation (7.28). The values of the pressure drop predicted by the present RUC model were obtained from equation (7.11) by using the same computed $q$-values and the same parameter values as presented in Table 7.2. A comparison between the analytical pressure drop as predicted by the present RUC model and the empirical pressure drop data of Chhabra & Srinivas (1991) is shown in Figure 7.2. The pressure drop as predicted by

the Ergun equation (equation (7.30)), in which the non-spherical shape of the particles is accounted for by the sphericity factor, is also shown in Figure 7.2. It is evident from the favourable correspondence between the experimental data of Chhabra & Srinivas (1991) and the proposed RUC model that the latter gives acceptable pressure drop predictions for power law flow through granular porous media for the parameter values presented in Table 7.2 and Reynolds numbers within the Darcy regime ($0.0016 < Re < 2.5$). The Ergun equation, adjusted to account for non-spherical particles, successfully correlates the experimental data for power law flow through beds of non-spherical particles in the low Reynolds number flow regime and also corresponds very well with the RUC model.

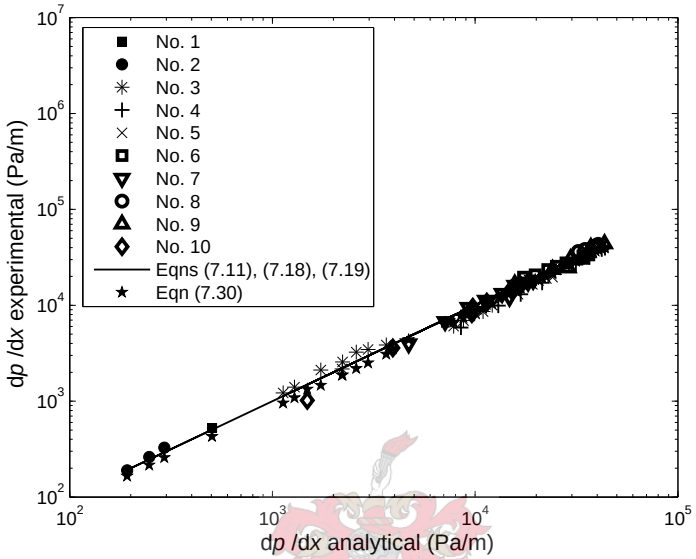


Figure 7.2: Comparison between the predicted analytical pressure drop proposed by the present RUC model and the empirical pressure drop data of Chhabra & Srinivas (1991).

Smit (1997) proposed the following dimensionless resistance factor, $\Lambda$, expressed as a linear function of the cell Reynolds number $Re$, analogous to the Ergun equation

$$\Lambda \;=\; fRe \;=\; A_E + B_E Re\,. \tag{7.31}$$

Here the friction factor $f$ for power law flow through granular porous media (Appendix E.2), is given by

$$f \;=\; -\frac{\mathrm{d}p}{\mathrm{d}x}\frac{d\left(1-(1-\epsilon)^{2/3}\right)^2\left(1-(1-\epsilon)^{1/3}\right)}{\rho\, q^2} \tag{7.32}$$

and the cell Reynolds number $Re$ is defined as

$$Re \;=\; \frac{2^n\,\rho\, q^{2-n}\, d^n}{K}\frac{\left(1-(1-\epsilon)^{1/3}\right)^n}{\left(1-(1-\epsilon)^{2/3}\right)^{2-n}}\,. \tag{7.33}$$

The streamwsie pressure drop predicted by the present RUC model for Reynolds numbers within the entire steady laminar flow regime may accordingly be expressed as

$$-\frac{\mathrm{d}p}{\mathrm{d}x} = \frac{2^n(4.47)}{d^{n+1}}\left(\frac{2n+1}{n}\right)^n \frac{K\,q^n(1-\epsilon)^{2/3}}{\left(1-(1-\epsilon)^{1/3}\right)^n\left(1-(1-\epsilon)^{2/3}\right)^{n+1}} \times \left[1 + \frac{\left(1-(1-\epsilon)^{2/3}\right)}{\epsilon\,2^{2n}(4.47)}\left(\frac{n}{2n+1}\right)^n Re\right] . \quad (7.34)$$

Christopher & Middleman (1965) modified the Blake-Kozeny equation (Appendix D.1) to account for non-Newtonian power law flow through packed beds within the creeping flow regime ($10^{-6} - 10^{-2}$). Analogous to the derivation for the average streamwise channel velocity for power law flow between parallel plates (equation (E.15)), an expression for the average tube velocity $u$ has been obtained for power law flow through long straight capillaries by modification of the Hagen-Poiseuille flow equation (Bird et al. (2002)), i.e.

$$u = \frac{n}{3n+1} R^{1+1/n}\left(\frac{\Delta p}{2\,K\,L_e}\right)^{1/n} , \quad (7.35)$$

where $R(=2R_h)$ is the radius of the capillary tube. Based on the assumptions of the Blake-Kozeny equation together with the proposal that the channel length $L$ may be replaced with $25L/12$, leads to

$$\frac{\Delta p}{L} = \frac{25\,K}{2\,D_h^{n+1}}\left(\frac{3(3n+1)}{n}\right)^n \frac{(1-\epsilon)^{n+1}}{\epsilon^{2n+1}} q^n . \quad (7.36)$$

The pressure drop expressed in terms of the the linear dimension $d$ of the RUC model yields

$$\frac{\Delta p}{L} = \frac{25\,K}{2\,d^{n+1}}\left(\frac{3(3n+1)}{n}\right)^n \frac{(1-\epsilon)^{(2n+2)/3}}{\epsilon^{2n+1}} q^n . \quad (7.37)$$

Kemblowski & Michniewics (1979) modified the Carman-Kozeny-Blake equation (Appendix D.2) to account for non-Newtonian power law flow through granular packed beds within the creeping flow regime. According to them the assumptions of the Blake-Kozeny equation are too simplistic and in their opinion the relation $L_e = (25/12)L$ has no physical meaning since, for fluid flow on the surface of a sphere, the maximum possible value which the ratio $L_e/L$ can reach is $\pi/2$. They also state that the modification of the Blake-Kozeny equation by Christopher & Middleman (1965) for modelling the flow of power law fluids through granular porous media yields an incorrect relation between $u$ and $L_e$ in equation (7.35) since $u$ occurs to the first power and $L_e$ to the power $1/n$. The allocation of the tortuosity factor has a rather significant effect in the case of power law flow and is therefore important. Kemblowski & Michniewics (1979) used the following

expression as a starting point for the average channel velocity of a power law fluid through a channel of arbitrary cross-section

$$u \;=\; \frac{4n}{3n+1}\frac{R_h}{k_o}\left(\frac{\Delta p}{K}\frac{R_h}{L_e}\right)^{1/n} \quad , \tag{7.38}$$

which is equivalent to equation (7.35). Substituting for the expressions for $R_h$, $u$ and $L_e$ as proposed by Carman (1937), yields

$$\frac{\Delta p}{L} \;=\; \left(\frac{3n+1}{4n}\right)^n \frac{6\sqrt{2}\,15^n(\sqrt{2})^n K\,q^n}{D_h^{n+1}}\frac{(1-\epsilon)^{n+1}}{\epsilon^{2n+1}} \; . \tag{7.39}$$

The pressure drop expressed in terms of the the linear dimension $d$ of the RUC model, is given by

$$\frac{\Delta p}{L} \;=\; \left(\frac{3n+1}{4n}\right)^n \frac{6\sqrt{2}\,15^n(\sqrt{2})^n K\,q^n}{d^{n+1}}\frac{(1-\epsilon)^{(2n+2)/3}}{\epsilon^{2n+1}} \; . \tag{7.40}$$

Brea et al. (1976) investigated the flow of non-Newtonian purely viscous fluids through granular packed beds for Reynolds numbers ranging from the laminar to the turbulent flow regimes. The Blake-Kozeny equation was modified to describe the steady non-Newtonian flow behaviour of slurries (titanium dioxide in water) through fixed beds of uniformly sized spherical particles. The wall shear stress describing the laminar flow in a capillary tube of any purely viscous non-Newtonian fluid is expressed as

$$\tau_w \;=\; \frac{R_h\Delta p}{L_e} \;=\; K^{'}\left[\frac{2\,u}{R_h}\right]^{n^{'}} \quad , \tag{7.41}$$

where $K^{'}$ and $n^{'}$ are the empirical rheological parameters. It is assumed, analogously to the modelling strategy of Christopher & Middleman (1965), that $L_e$ may be replaced with $\chi L$, where $\chi$ is a empirical tortuosity factor. From sufficient experimental data a value of $\chi = 20/9$ was determined leading to a coefficient value of $A = 160$. Together with the expressions for $R_h$ and $u$ used in the Blake-Kozeny equation, the following expression is obtained for the pressure drop of a power law fluid

$$\frac{\Delta p}{L} \;=\; \frac{40\,K\,12^n\,q^n\,(1-\epsilon)^{n+1}}{3\,\epsilon^{2n+1}D_h^{n+1}} \; . \tag{7.42}$$

The pressure drop expressed in terms of the the linear dimension $d$ of the RUC model yields

$$\frac{\Delta p}{L} \;=\; \frac{40\,K\,12^n\,q^n\,(1-\epsilon)^{(2n+2)/3}}{3\,\epsilon^{2n+1}d^{n+1}} \; . \tag{7.43}$$

Since the inertial forces predominate over the viscous forces in the turbulent flow regime, the non-Newtonian flow behaviour is negligible in this regime and a constant friction

factor, just as in the case of Newtonian flow, is assumed. The resulting pressure drop for purely viscous flow power law flow, analogously to the Ergun equation, is given by

$$\frac{\Delta p}{L} = \frac{40\,K\,12^n\,q^n\,(1-\epsilon)^{(2n+2)/3}}{3\,\epsilon^{2n+1}d^{n+1}} + 1.75\,\frac{\rho\,q^2(1-\epsilon)^{2/3}}{\epsilon^3 d}\,. \tag{7.44}$$

Table 7.3 shows the expressions for the coefficients $A_E$ and $B_E$ proposed by the various models and the dependence of the dimensionless resistance factor $\Lambda$ on the Reynolds number $Re$ is shown in Figure 7.3 for $n = 0.5$ and $\epsilon = 0.43$. The excellent correspondence of the RUC model with the semi-empirical models at low Reynolds numbers and especially with the model of Brea et al. (1976) over the entire steady laminar flow regime is very encouraging and confirms once again the adequate generalization of the RUC model to predict the rheological flow behaviour of power law fluids over the entire steady laminar flow regime.

| Model | Coefficient $A_E$ |
|---|---|
| Present RUC model | $2^{2n}(4.47)(1-\epsilon)^{2/3}\left(\frac{2n+1}{n}\right)^n \frac{\left(1-(1-\epsilon)^{1/3}\right)}{(1-(1-\epsilon)^{2/3})}$ |
| Christopher & Middleman (1965) | $\frac{25\,(1-\epsilon)^{(2n+2)/3}}{2^{1-n}\epsilon^{2n+1}}\left(\frac{3\,(3n+1)}{n}\right)^n\left(1-(1-\epsilon)^{1/3}\right)^{n+1}\left(1-(1-\epsilon)^{2/3}\right)^n$ |
| Brea et al. (1976) | $\frac{40(1-\epsilon)^{2n+2/3}}{3\epsilon^{2n+1}}24^n\left(1-(1-\epsilon)^{1/3}\right)^{n+1}\left(1-(1-\epsilon)^{2/3}\right)^n$ |
| Kemblowski & Michniewics (1979) | $\frac{6\sqrt{2}(1-\epsilon)^{(2n+2)/3}}{\epsilon^{2n+1}}\left(\frac{15(3n+1)}{\sqrt{2}n}\right)^n\left(1-(1-\epsilon)^{1/3}\right)^{n+1}\left(1-(1-\epsilon)^{2/3}\right)^n$ |
| | Coefficient $B_E$ |
| Present RUC model | $\frac{\left(1-(1-\epsilon)^{1/3}\right)(1-\epsilon)^{2/3}}{\epsilon}$ |
| Brea et al. (1976) | $\frac{1.75(1-\epsilon)^{2/3}\left(1-(1-\epsilon)^{1/3}\right)\left(1-(1-\epsilon)^{2/3}\right)^2}{\epsilon^3}$ |

Table 7.3: Proposals for the coefficients $A_E$ and $B_E$.

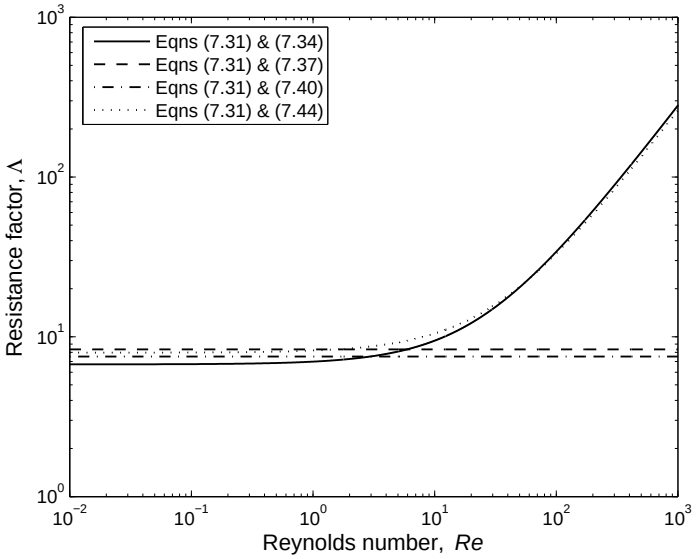


Figure 7.3: Dependence of the resistance factor $\Lambda$ on the cell Reynolds number $Re$ for $n = 0.5$ and $\epsilon = 0.43$.

## 7.2 Asymptote matching of the shear stress

The dependency of the apparent viscosity $\eta$ on the shear rate $\dot{\gamma}$ of a shear-thinning fluid may be classified into three more or less distinct regimes (Skelland (1967), Savins (1970)), as illustrated in Figure 7.4.

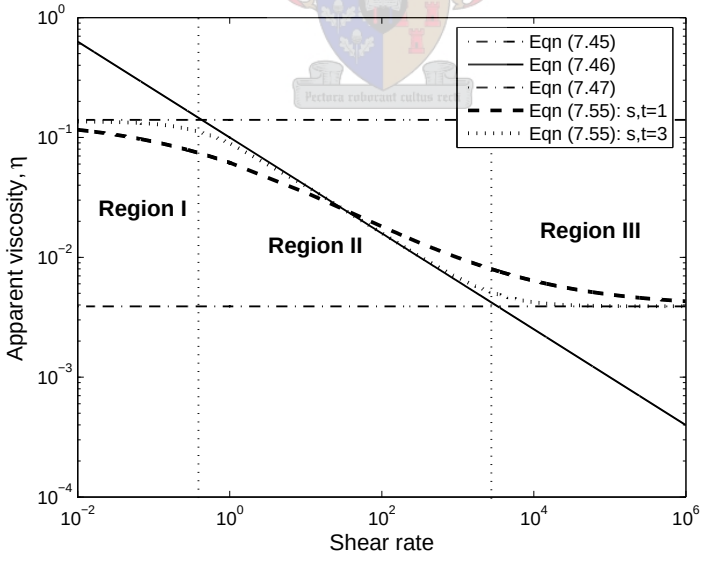


Figure 7.4: Variation of apparent viscosity $\eta$ with shear rate $\dot{\gamma}$.

At very low shear rates (Region I) the apparent viscosity is constant, corresponding to Newtonian flow behaviour, and characterized by a limiting viscosity $\eta_0$. At intermediate shear rates (Region II) the apparent viscosity decreases with increasing shear rate, resembling non-Newtonian flow behaviour and at high shear rates (Region III) a constant apparent viscosity persists once again, characterized by a limiting viscosity $\eta_\infty$, i.e.:

$$\eta_{\mathrm{I}} = \eta_0 \qquad \text{Region I,} \tag{7.45}$$

$$\eta_{\mathrm{II}} = K|\dot{\gamma}|^{n-1} \qquad \text{Region II,} \tag{7.46}$$

$$\eta_{\mathrm{III}} = \eta_\infty \qquad \text{Region III,} \tag{7.47}$$

where the apparent viscosity at intermediate shear rates (Region II) is modelled by the power law model. The parameters $\eta_0$, $K$, $\eta_\infty$ and $n$ are empirical curve fitting parameters. The values of $\eta_0$, $K$, $\eta_\infty$ and $n$ in Figure 7.4 were randomly chosen just for illustration purposes. Since equations (7.45), (7.46) and (7.47) predominate in their respective regions of applicability, a general shear-thinning purely viscous model may be introduced through application of the asymptote matching technique introduced by Churchill & Usagi (1972):

$$\eta \;=\; \left\{ \left[ \left( \eta_{\mathrm{I}}^{-s} + \eta_{\mathrm{II}}^{-s} \right)^{-1/s} \right]^t + \eta_{\mathrm{III}}^t \right\}^{1/t} , \tag{7.48}$$

where $s$ and $t$ are positive shifting parameters. Substituting the corresponding expressions for $\eta_{\mathrm{I}}$, $\eta_{\mathrm{II}}$ and $\eta_{\mathrm{III}}$, yields

$$\eta \;=\; \left\{ \left[ (\eta_0^{-s} + (K\dot{\gamma}^{n-1})^{-s})^{-1/s} \right]^t + \eta_\infty^t \right\}^{1/t} . \tag{7.49}$$

For the sake of simplicity, a value of unity is assigned to both $s$ and $t$, yielding

$$\eta \;=\; \left[ (\eta_0^{-1} + (K\dot{\gamma}^{n-1})^{-1})^{-1} \right] + \eta_\infty , \tag{7.50}$$

or equivalently,

$$\eta \;=\; \frac{\eta_0 \, K\dot{\gamma}^{n-1}}{K\dot{\gamma}^{n-1} + \eta_0} + \eta_\infty . \tag{7.51}$$

Since $n < 1$ for a shear-thinning power law fluid, it follows that

$$\eta \;=\; \frac{\eta_0 \, K}{K + \eta_0 \, \dot{\gamma}^{1-n}} + \eta_\infty . \tag{7.52}$$

Note that if $\dot{\gamma} \to \infty$, then $\eta \to \eta_\infty$, which is correct, but if $\dot{\gamma} \to 0$, then $\eta \to \eta_0 + \eta_\infty$, which is incorrect. In order to circumvent this undesired result, $\eta_\infty$ should be subtracted from the first term of equation (7.50), i.e.

$$\eta \;=\; \left[ ((\eta_0 - \eta_\infty)^{-1} + (K\dot{\gamma}^{n-1})^{-1})^{-1} \right] + \eta_\infty , \tag{7.53}$$

or equivalently,

$$\eta \;=\; \frac{(\eta_0-\eta_\infty)K}{K+(\eta_0-\eta_\infty)\,\dot\gamma^{1-n}}+\eta_\infty\;. \tag{7.54}$$

Investigation of the validity of equation (7.54) leads to the following: If $\dot\gamma \to \infty$, then $\eta \to \eta_\infty$ and if $\dot\gamma \to 0$ then $\eta \to \eta_0$, which is correct. The general asymptotically matched expression for $\eta$ is then given by

$$\eta \;=\; \left\{\left[((\eta_0-\eta_\infty)^{-s}+(K\dot\gamma^{n-1})^{-s})^{-1/s}\right]^t+\eta_\infty^t\right\}^{1/t}\;. \tag{7.55}$$

Equation (7.55) is graphically presented in Figure 7.4 for the shifting parameters $s$ and $t$ both respectively equal to 1 and 3. Despite the fact that the asymptote matching technique yields better results for the higher value of $s$ and $t$, a value of unity will be assigned to both shifting parameters, just for the sake of simplicity. A general expression for the shear stress $\tau_{yx}$ over the entire shear rate domain may be obtained from equations (7.55) and (E.2) together with $s,t=1$, leading to

$$\tau_{xy} \;=\; \left[((\eta_0-\eta_\infty)|\dot\gamma|)^{-1}+(K|\dot\gamma|^n)^{-1}\right]^{-1}+\eta_\infty|\dot\gamma|\;. \tag{7.56}$$

The wall shear rate $\dot\gamma_w$ in regions I and III may be expressed as (Appendix E.1):

$$|\dot\gamma_w| \;=\; \frac{6\,w_\parallel}{d-d_s}\,, \tag{7.57}$$

and in the power law region (region II) as:

$$|\dot\gamma_w| \;=\; \left(\frac{2n+1}{n}\right)\left(\frac{2w_\parallel}{d-d_s}\right)\;. \tag{7.58}$$

Substitution of equations (7.57), (7.58), (4.4) and (4.10) into equation (7.56) yields the following expression for the wall shear stress $\tau_{w_\parallel}$ applicable over the entire shear rate domain

$$\begin{aligned}\tau_{w_\parallel} \;=\; &\left[\left((\eta_0-\eta_\infty)\frac{6\,q}{d\,(1-(1-\epsilon)^{1/3})\,(1-(1-\epsilon)^{2/3})}\right)^{-1}\right.\\ &\left.+K^{-1}\left(\left(\frac{2n+1}{n}\right)\frac{2\,q}{d\,(1-(1-\epsilon)^{1/3})\,(1-(1-\epsilon)^{2/3})}\right)^{-n}\right]^{-1}\\ &+\eta_\infty\,\frac{6\,q}{d\,(1-(1-\epsilon)^{1/3})\,(1-(1-\epsilon)^{2/3})}\;.\end{aligned} \tag{7.59}$$

The curve fitting parameters $\eta_0$, $\eta_\infty$, $K$ and $n$ may be obtained by fitting equation (7.56) to shear viscosity data of the fluid under consideration. The streamwise pressure gradient

predicted by the RUC model for Reynolds numbers ranging over the entire steady laminar flow regime expressed in terms of the wall shear stress $\tau_{w_\parallel}$, leads to

$$\begin{aligned} -\nabla \langle p \rangle &= \left( \frac{U_f}{U_\parallel + U_t} \right) \frac{S_\parallel + \beta \xi S_\perp}{U_o} \tau_{w_\parallel} \underline{\hat{n}} + \frac{\rho w_\parallel^2 S_{\perp_U}}{U_o} \underline{\hat{n}} \\ &= \frac{4.47 \epsilon (1-\epsilon)^{2/3}}{d\left(1-(1-\epsilon)^{2/3}\right)} \tau_{w_\parallel} \underline{\hat{n}} + \frac{\rho (1-\epsilon)^{2/3}}{d\left(1-(1-\epsilon)^{2/3}\right)^2} q \underline{q} \, . \end{aligned} \tag{7.60}$$

For unidirectional discharge in the positive $x$-direction the streamwise pressure drop may be expressed as

$$-\frac{\mathrm{d}p}{\mathrm{d}x} = \frac{(1-\epsilon)^{\frac{2}{3}}}{d\left(1-(1-\epsilon)^{\frac{2}{3}}\right)} \left[ 4.47 \tau_{w_\parallel} + \frac{\rho q^2}{\epsilon \left(1-(1-\epsilon)^{\frac{2}{3}}\right)} \right] , \tag{7.61}$$

or, expressed in terms of the length $d_s$ of the solid cube, as

$$-\frac{\mathrm{d}p}{\mathrm{d}x} = \frac{(1-\epsilon)}{d_s\left(1-(1-\epsilon)^{\frac{2}{3}}\right)} \left[ 4.47 \tau_{w_\parallel} + \frac{\rho q^2}{\epsilon \left(1-(1-\epsilon)^{\frac{2}{3}}\right)} \right] . \tag{7.62}$$

The pressure drop prediction for purely viscous shear-thinning power law flow through isotropic granular porous media, applicable over the entire shear rate domain, may be obtained by substituting the expression for $\tau_{w_\parallel}$ (equation (7.59)) into either equation (7.61) or (7.62). The pressure drop prediction for purely viscous shear-thinning power law flow through granular porous media proposed by Smit & Du Plessis (2000) is given by

$$-\frac{\mathrm{d}p}{\mathrm{d}x} = \frac{(1-\epsilon)^{2/3}}{d\,\epsilon} \left[ 6.8 \tau_{w_\parallel} + \frac{\rho q^2}{(1-(1-\epsilon)^{2/3})^2} \right] , \tag{7.63}$$

where the same expression for $\tau_{w_\parallel}$ applies as given by equation (7.59). Chakrabarti et al. (1991) investigated the rheology of aqueous hydroxypropylguar (HPG) solutions in packed beds consisting of more or less uniformly sized spherical particles experimentally. The empirical data was modelled through application of the capillary tube representation of a packed bed. HPG solutions were used because it is a very stable commercial polymer. Concentrations ranging from 100 ppm to 5000 ppm were used in the experiments. The dependency of the apparent viscosity $\eta$ on the shear rate ($0.3s^{-1} < \dot{\gamma} < 1000s^{-1}$) for the various HPG concentrations is graphically presented in Figure 7.5. The transition from almost Newtonian flow behaviour at low HPG concentrations to non-Newtonian shear thinning behaviour at higher concentrations is clearly illustrated. The values of the curve fitting parameters $\eta_0$, $K$, $\eta_\infty$ and $n$ were obtained by fitting equation (7.55) with $s, t = 1$ to the experimental apparent viscosity data of the fluid. These values, together with the characteristic fluid-, particle- and bed parameters measured at 25$^o$C, are presented in Table 7.4.

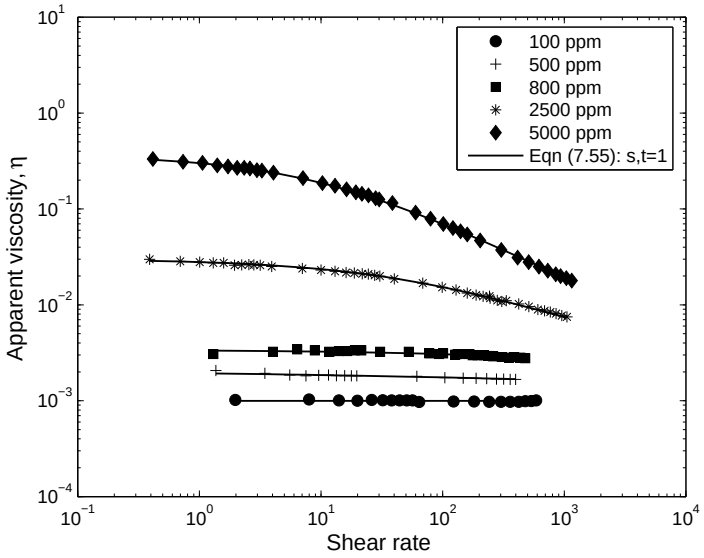


Figure 7.5: Variation of the apparent viscosity $\eta$ with the shear rate $\dot{\gamma}$ for different HPG concentrations.

| Test fluid | Packing material | $d_s$ (mm) | $\epsilon$ | $\rho_s$ (kg m$^{-3}$) | |
|---|---|---|---|---|---|
| HPG | Steel spheres | 0.794 | 0.375 | 998 | |
| | | | Concentration | | |
| Parameter | 100 ppm | 500 ppm | 800 ppm | 2500 ppm | 5000 ppm |
| $\eta_0$ (Pa.s) | 0.001 | 0.0021 | 0.0034 | 0.03 | 0.363 |
| $K$ (Pa.s) | 0.0075 | 0.0075 | 0.1 | 0.35 | 1.74 |
| $\eta_\infty$ (Pa.s) | 0.00089 | 0.00089 | 0.00089 | 0.002 | 0.002 |
| $n$ | 0.98 | 0.8 | 0.6 | 0.43 | 0.34 |
| $\eta_s$ (Pa.s) | 0.0008897 | | | | |

Table 7.4: Characteristic fluid-, particle- and bed parameters (Chakrabarti et al. (1991)).

The friction factor $f$ used for modelling the capillary tube flow is given by

$$f = \frac{6\epsilon^2 R_h}{\rho q^2}\left(\frac{\Delta p}{L}\right) , \tag{7.64}$$

where $\Delta p$ is the pressure drop measured over a bed height $L$. $R_h$ is the hydraulic radius

expressed as

$$R_h = \frac{\epsilon d_p}{6(1-\epsilon)} \left\{ 1 + \frac{2}{3} \frac{d_p}{(1-\epsilon)D} \right\}^{-1} , \tag{7.65}$$

with $d_p$ the spherical particle diameter and $D$ the inner diameter of the measuring cell. The solvent Reynolds number $Re_s^{'}$ is given by

$$Re_s^{'} = \frac{6 R_h \, \rho_s \, q}{\epsilon \, \eta_s} , \tag{7.66}$$

where $\eta_s$ denotes the viscosity of the solvent (water) with density $\rho_s$. The experimental data points of the $fRe_s^{'}$ versus $Re_s^{'}$ plot presented in Chakrabarti et al. (1991) were digitized by Smit (1997). The values of the superficial velocity were obtained by solving for $q$ from equation (7.66). The experimental pressure drop values were then calculated from equation (7.64). The predicted analytical pressure drop values are solved from equations (7.59) and (7.61) by using the same experimentally determined $q$-values and the same parameter values as given in Table 7.4. The predicted analytical pressure drop was evaluated by comparing it to the published experimental data of Chakrabarti et al. (1991), as shown in Figure 7.6.

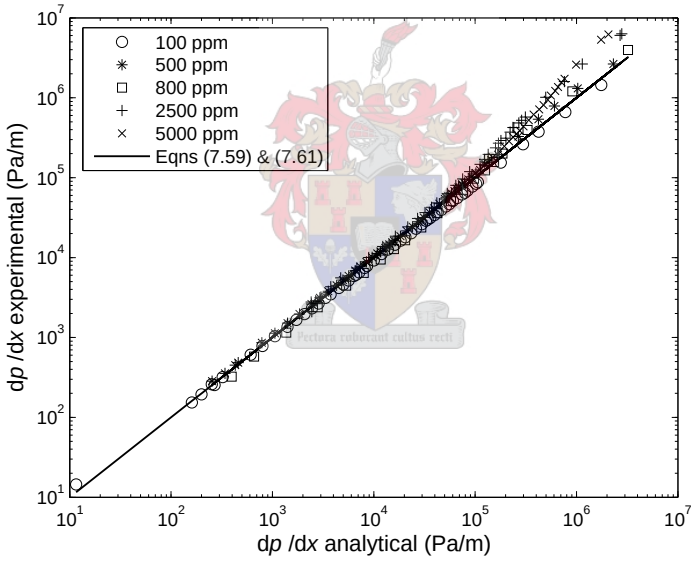


Figure 7.6: Comparison between the predicted pressure drop and the experimental pressure drop data of Chakrabarti et al. (1991).

From Figure 7.6 it is evident that the experimental data for the 100, 500 and 800 ppm solution concentrations, exhibiting purely viscous behaviour, correspond very well with the predicted pressure gradient, whereas data for the 800, 2500 and 5000 ppm concentrations, corresponding to non-Newtonian flow behaviour, deviate from the analytical pressure drop prediction. Smit & Du Plessis (2000) proposed the following friction factor $f$ for

flow through granular porous media, expressed in terms of the linear dimension $d$ of the RUC model (Appendix E.2),

$$f \;=\; -\frac{\mathrm{d}p}{\mathrm{d}x}\,\frac{d\left(1-(1-\epsilon)^{2/3}\right)^{2}\left(1-(1-\epsilon)^{1/3}\right)}{\rho_s\, q^2}\;, \tag{7.67}$$

together with a solvent Reynolds number $Re_s$, defined as

$$Re_s \;=\; \frac{2\,\rho_s\, q\, d}{\eta_s\,(1+(1-\epsilon)^{1/3})}\;. \tag{7.68}$$

Figure 7.7 compares the dimensionless resistance factor $\Lambda(= fRe_s)$, as proposed by the present RUC model with the RUC model of Smit & Du Plessis (2000) and the published experimental data of Chakrabarti et al. (1991). The experimental $\Lambda$-values were computed from equations (7.67) and (7.68) by using the experimentally determined $q$-values and the pressure drop values obtained from equation (7.64). The predicted analytical $\Lambda$-values were computed from equations (7.67) and (7.68) by using the pressure drop values obtained from equations (7.61) and (7.59). The pressure drop values used for determining the $\Lambda$-values proposed by the model of Smit & Du Plessis (2000) were obtained from equations (7.63) and (7.59).

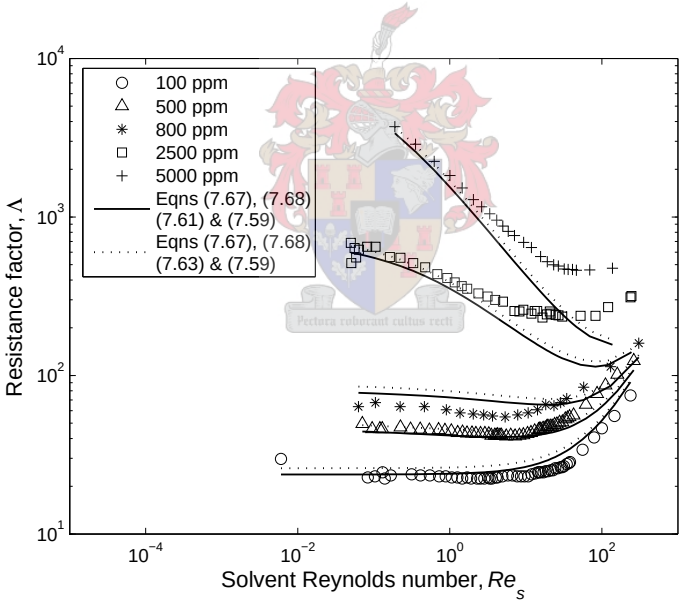


Figure 7.7: Dependence of the resistance factor $\Lambda$ on $Re_s$ as predicted by the RUC models and the experimental data of Chakrabarti et al. (1991) for different HPG concentrations.

Both Figures 7.6 and 7.7 show a satisfactory agreement between the predicted values and the experimental data for all the HPG concentrations in the low Reynolds number flow regime and thus confirm the choice of both the shifting parameters $s$ and $t$ equal to unity as acceptable. Both figures, however, show an increase in flow resistance for the higher

concentrations (2500 and 5000 ppm) in the inertial flow regime. Although Figure 7.7 graphically shows a minor difference between the present RUC model and the existing RUC model of Smit & Du Plessis (2000), the improvement of the present model on the existing one, on the basis of fundamental physical reasoning, is rather significant. Figure 7.8 shows the deviation of the present analytical $\Lambda$-values, denoted by $\Lambda_{RUC}$, from the experimental values, denoted by $\Lambda_{exp}$, in terms of the percentage error, defined as

$$\text{Percentage error} \;=\; 100\,\frac{\Lambda_{exp} - \Lambda_{RUC}}{\Lambda_{exp}}\;. \tag{7.69}$$

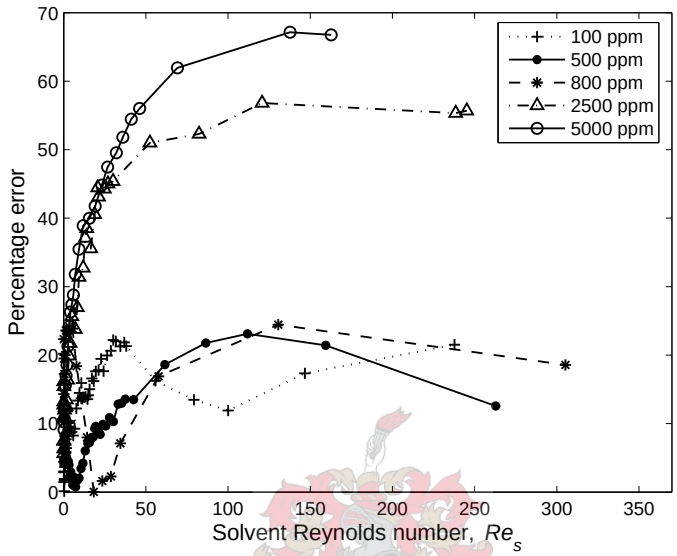


Figure 7.8: Percentage error as a function of the solvent Reynolds number $Re_s$

For $0 < Re_s < 4$ an acceptable percentage error of less than 25% is observed. As the solvent Reynolds number increases beyond this range, the percentage error increases with increasing HPG concentration. Figure 7.8 shows that for the 2500 and 5000 ppm concentrations the deviation of the predictive analytical model from the experimental data is more than 50% for $Re_s > 50$. Since the deviations are quite significant, the cause to these secondary effects need to be addressed. For the flow of polymeric liquids between parallel plates the normal stresses ($\tau_{xx}, \tau_{yy}$ and $\tau_{zz}$) are in general non-zero and unequal (Bird et al. (2002)). The generalized non-Newtonian power law model does not include the influence of normal stresses on the pressure gradient. The deviation of both the predictive analytical RUC models from the experimental data in Figures 7.6 and 7.7 may be attributed to the normal stress effects, which cause an increase in flow resistance. In order to account for the influence of the normal stresses on the pressure gradient, the general purely viscous shear-thinning model described by equations (7.61) or (7.62) needs to be extended to include the first normal stress difference into the proposed model (Smit & Du Plessis (2000)). Although the non-Newtonian fluids are classified into distinctive categories, these fluids usually exhibit a combination of characteristics of the fluids within the respective categories. It has been reported extensively in the literature that polymer

solutions, such as those used in the experiments analyzed here, exhibit a lower degree of shear-thinning in porous media flows than in steady simple shear experiments. This effect could be attributed e.g. to a size exclusion layer on the solid surface (Sorbie & Huang (1991)) or to visco-elasticity (Tatham et al. (1995)), the latter having effect in the higher range of Reynolds numbers. Christopher & Middleman (1965) also attribute the lower degree of shear-thinning to viscoelastic effects resulting from continual acceleration and deceleration of fluid flow through the irregular interstices between particles within a packed bed. Modelling efforts to include these effects warrant a careful investigation of normal stresses and the inclusion thereof in the volume averaging procedure. This clearly falls beyond the scope of this work and further research is needed to generalize the model to take proper account of these effects.

# Chapter 8

# Model Applications

## 8.1 Fluidized Beds

A fluidized bed consists of a vertical granular packed column through which gas or liquid is forced upwards through the bed at specified fluid velocities. A pressure drop results across the packed bed which varies linearly with the superficial fluid velocity and may accordingly be described by the Ergun equation (Gidaspow (1994)). When the pressure drop is sufficient to support the nett weight of particles in the bed the so-called condition of minimum fluidization is reached which is characterized by a minimum fluidization velocity and a minimum fluidization porosity. A further increase in the flow rate causes the particles to move along with the fluid resulting in a constant pressure drop across the fluidized bed. In the case of gas flow, bubble formation is observed at flow rates above the minimum fluidization state. The minimum fluidization velocity $q_{mf}$ may theoretically be determined from the pressure drop across the packed bed which is sufficient to support the nett weight per unit area of particles in the bed, i.e.

$$\frac{\Delta p}{L} \;=\; (\rho_s - \rho)\,\epsilon_s\,g\;, \tag{8.1}$$

where $\Delta p/L$ may be replaced with any model prediction for the pressure drop $\Delta p$ across a granular packed bed of length $L$. According to Mishra et al. (1975) and Yu et al. (1968) the pressure drop in the fluidized state does not increase by more than 5% of its value at minimum fluidization. The minimum fluidization velocity may therefore be determined empirically from the intersection of the pressure drop versus the superficial velocity curve for the packed bed region and the constant pressure drop which equals the weight of the bed (Gidaspow (1994), Brea et al. (1976)), as shown in Figure 8.1. Since the minimum fluidization state may also be regarded as the onset of the fluidization state, it was established by many authors in the literature (Gidaspow (1994), Yu et al. (1968), Mishra et al. (1975), Happel & Brenner (1965)) that the Ergun equation may be extended to apply within the fluidized state where both the solid and fluid phase have non-zero velocities. This may be accomplished by adapting the superficial fluid velocity to account

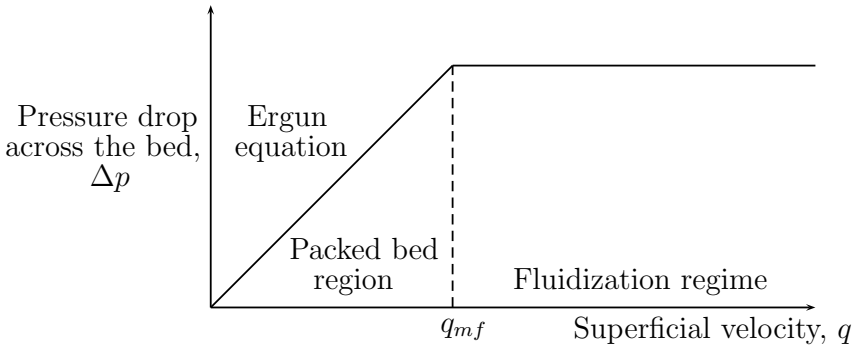


Figure 8.1: Illustration of the empirical determination of the minimum fluidization velocity $q_{mf}$, as presented in Gidaspow (1994).

for the relative fluid-particle velocity (Gidaspow (1994)), i.e.

$$q \;=\; \epsilon\,(u_f - u_s)\;, \tag{8.2}$$

where $u_f$ and $u_s$ respectively denotes the magnitude of the velocity of the fluid and solid phase. However, at minimum fluidization the velocity of the solid phase is taken to be the zero velocity of the solids within the packed bed. It thus follows that at minimum fluidization the minimum fluidization velocity reduces to $q_{mf} = \epsilon_{mf} u_f$ where $u_f$ is the magnitude of the average fluid velocity at minimum fluidization within the packed bed.

Halvorsen & Mathiesen (2002) investigated bubble formation in a particulate fluidized bed both experimentally and numerically. A computational fluid dynamics (CFD) model, named FLOTRACS-MP-3D, was developed by them to simulate bubble behaviour in a lab-scale fluidized bed of minimal width. The experimental setup consists therefore of a two-dimensional bed with a central jet and uniformly sized spherical glass particles as the packing material. Compressed air is introduced at a constant rate through an air distributor in order for the packed bed to maintain the condition of minimum fluidization. The bed is fluidized by injecting compressed air through the central jet. The bubble sizes and bubble velocities were measured with a digital video camera. The gas and solid phases are considered to be incompressible and the conservation equations for mass and momentum were solved individually for the both phases. A no-slip boundary condition is assumed for the gas phase and a bubble is assumed to be a region where $\epsilon_g > 0.80$. The momentum equation contains terms resembling pressure forces, viscous forces, mass forces (i.e. gravitation) and drag forces. The total drag between the two phases in the fluidized bed consists of both gas-particle drag and particle-particle drag. A granular temperature equation was introduced for mathematical modelling of the collisions between the solid particles. The numerical calculation domain consists of a uniform grid which is described by a two-dimensional Cartesian coordinate system. The governing equations are solved by a finite volume method in which the integration is performed in space and time using a first order upwind scheme. In a fluidized bed the friction between the particles are small so that the gravitational and drag forces are the most predominating terms in the solid phase momentum equation. Halvorsen et al. (2006) studied the influence of

different drag models, including the RUC model presented in this work, by application of the numerical simulation model of Halvorsen & Mathiesen (2002). It was found that the use of different drag models have a significant effect on the predicted bed expansion and the solid concentration in the dense phase regions of the bed. The drag models that were evaluated by Halvorsen et al. (2006) are the one proposed by Gidaspow (1994) in which the Ergun equation is combined with the equations of Rowe (1961) and Wen & Yu (1966), the drag model of Gibilaro et al. (1985), the empirical drag model proposed by Macdonald et al. (1979) and the RUC model presented in this work. Each of these drag models was used as part of a full time-dependent momentum transport equation, but during the computations a quasi-stationary and quasi-uniform $\underline{q}$-field was assumed. In the absence of acceleration, external wall friction and gravity, the gas momentum balance equation for describing the flow behaviour within a fluidized bed, reduces to (Gibilaro et al. (1985))

$$-\frac{\mathrm{d}p}{\mathrm{d}x} \;=\; \Phi_{sg}\frac{q}{\epsilon_g^2}\,, \tag{8.3}$$

where $q$ is the magnitude of the superficial gas velocity, defined as

$$q \;=\; \epsilon_g\,(u_g - u_s)\;. \tag{8.4}$$

Here $\epsilon_g$ is the porosity of the gas phase and $\Phi_{sg}$ denotes the total gas/particle drag coefficient. The model most commonly used for describing the flow behaviour in a fluidized bed is the Ergun equation, which for the current application, yields fairly accurate results for $\epsilon_g < 0.8$ (Yu et al. (1968), Mishra et al. (1975), Happel & Brenner (1965)). If the pressure drop as predicted by the Ergun equation for dense flow conditions is substituted into equation (8.3) then the following expression is obtained for the total gas/particle drag coefficient

$$\Phi_{sg} \;=\; 150\,\frac{(1-\epsilon_g)^2\mu_g}{\epsilon_g\,D_h^2} + 1.75\,\frac{\rho_g\,|u_g - u_s|\,(1-\epsilon)}{D_h} \qquad \text{for} \qquad \epsilon_g \leq 0.8\,, \tag{8.5}$$

where $D_h = \phi_s D_p$ (Appendix D.4). In a fluidized bed the porosity continuously changes with the superficial fluid velocity, yielding a fairly wide range of porosity values ($0.4 < \epsilon < 0.8$). The drag model to be used within the numerical simulation should therefore be applicable over a wide range of porosity values. In order to obtain a drag model that is applicable for both dilute and dense flow conditions, equation (8.5) is combined with the total gas/particle drag coefficient proposed by Wen & Yu (1966), i.e.

$$\Phi_{sg} \;=\; \frac{3}{4}C_D\frac{\rho_g\epsilon_s\epsilon_g}{D_h}|u_g - u_s|\epsilon_g^{-2.65} \qquad \text{for} \qquad \epsilon_g > 0.8\,, \tag{8.6}$$

where the drag coefficient $C_D$ is related to the Reynolds number by Rowe (1961) as follows:

$$\begin{aligned} C_D &= \frac{24}{Re_s}(1 + 0.15Re_s^{0.687}) && \text{for} \quad Re_s < 1000\,, \\ C_D &= 0.44 && \text{for} \quad Re_s \geq 1000\,, \end{aligned} \tag{8.7}$$

and the Reynolds number $Re_s$ is defined as

$$Re_s \;=\; \frac{D_h\,\rho_g\,|u_g - u_s|\,\epsilon_g}{\mu_g}\;. \tag{8.8}$$

Application of the asymptote matching technique of Churchill & Usagi (1972) yields the following expression, which is applicable over the entire porosity range,

$$\Phi_{sg} \;=\; 150\,\frac{(1-\epsilon_g)^2\mu_g}{\epsilon_g\,D_h^2} + 1.75\,\frac{\rho_g\,|u_g - u_s|\,(1-\epsilon)}{D_h} \;+\; \frac{3}{4}C_D\frac{\rho_g\epsilon_s\epsilon_g}{D_h}|u_g - u_s|\epsilon_g^{-2.65}\;. \tag{8.9}$$

The total gas/particle drag coefficient proposed by Gibilaro et al. (1985) covers the entire porosity range and is given by

$$\Phi_{sg} \;=\; \frac{3}{4}\,C_D\,\frac{\epsilon_s\,\epsilon_g}{D_h}\,\rho_g\,|u_g - u_s|\;, \tag{8.10}$$

where the drag coefficient $C_D$ is expressed as

$$C_D \;=\; \frac{4}{3}\left(\frac{17.3}{Re_s} + 0.336\right)\epsilon_g^{-2.80}\;. \tag{8.11}$$

The empirical verification of Macdonald et al. (1979), in combination with the models of Rowe (1961) and Wen & Yu (1966), yields

$$\Phi_{sg} \;=\; 180\,\frac{(1-\epsilon)^2\mu_g}{\epsilon_g\,D_h^2} + 1.8\,\frac{\rho_g\,|u_g - u_s|\,(1-\epsilon)}{D_h} \;+\; \frac{3}{4}C_D\frac{\rho_g\epsilon_s\epsilon_g}{D_h}|u_g - u_s|\epsilon_g^{-2.65}\;. \tag{8.12}$$

The present RUC model (equation (6.2)) yields the following expression for the total gas/particle drag coefficient:

$$\Phi_{sg} \;=\; \frac{26.8\,\mu_g\,\epsilon_g^2\,(1-\epsilon_g)^{4/3}}{d_s^2\,(1-(1-\epsilon_g)^{1/3})\,(1-(1-\epsilon_g)^{2/3})^2} \;+\; \frac{\epsilon_g\,(1-\epsilon_g)\,\rho_g\,q}{d_s\,(1-(1-\epsilon_g)^{2/3})}\;. \tag{8.13}$$

### 8.1.1 Comparison of different drag models

The relation between the total gas/particle drag coefficient $\Phi_{sg}$ and the shear factor $f$ of the RUC model, is given by

$$f \;=\; \frac{\Phi_{sg}}{\mu_g}\;. \tag{8.14}$$

Expressing the Ergun/Rowe/Wen and Yu model (equation (8.9)) in terms of the dimensionless overall shear factor $F = fd_s^2$ of the RUC model, yields

$$F \;=\; 150\,\frac{(1-\epsilon_g)^2}{\epsilon_g} \;+\; 1.75\,\frac{(1-\epsilon_g)}{\epsilon_g}\,Re_s \;+\; 18\,\frac{(1-\epsilon_g)}{\epsilon_g^{2.65}} \;+\; 2.7\,\frac{(1-\epsilon_g)}{\epsilon_g^{2.65}}\,Re_s^{0.687}\;, \tag{8.15}$$

which applies for $Re_s < 1000$. Similarly, the model of Gibilaro et al. (1985) (equations (8.10) and (8.11)) yields

$$F \;=\; 17.3\,\frac{(1-\epsilon_g)}{\epsilon_g^{2.8}} \;+\; 0.336\,\frac{(1-\epsilon_g)}{\epsilon_g^{2.8}}\,Re_s\;, \tag{8.16}$$

and the Macdonald/Rowe/Wen and Yu model (equation (8.12)) leads to

$$F \;=\; 180\,\frac{(1-\epsilon_g)^2}{\epsilon_g} \;+\; 1.8\,\frac{(1-\epsilon_g)}{\epsilon_g}\,Re_s \;+\; 18\,\frac{(1-\epsilon_g)}{\epsilon_g^{2.65}} \;+\; 2.7\,\frac{(1-\epsilon_g)}{\epsilon_g^{2.65}}\,Re_s^{0.687}\;, \tag{8.17}$$

The RUC model for Newtonian flow presented in this work, expressed in terms of the gas phase porosity $\epsilon_g$, is given by

$$F \;=\; \frac{26.8\,(1-\epsilon_g)^{4/3}}{\left(1-(1-\epsilon_g)^{1/3}\right)\left(1-(1-\epsilon_g)^{2/3}\right)^2} \;+\; \frac{(1-\epsilon_g)}{\epsilon_g\left(1-(1-\epsilon_g)^{2/3}\right)^2}\,Re_s\;. \tag{8.18}$$

Figure 8.2 shows a graphical comparison of the dependence of the overall shear factor $F$ on the Reynolds number $Re_s$ at the porosity of bubble identification, that is $\epsilon = 0.8$.

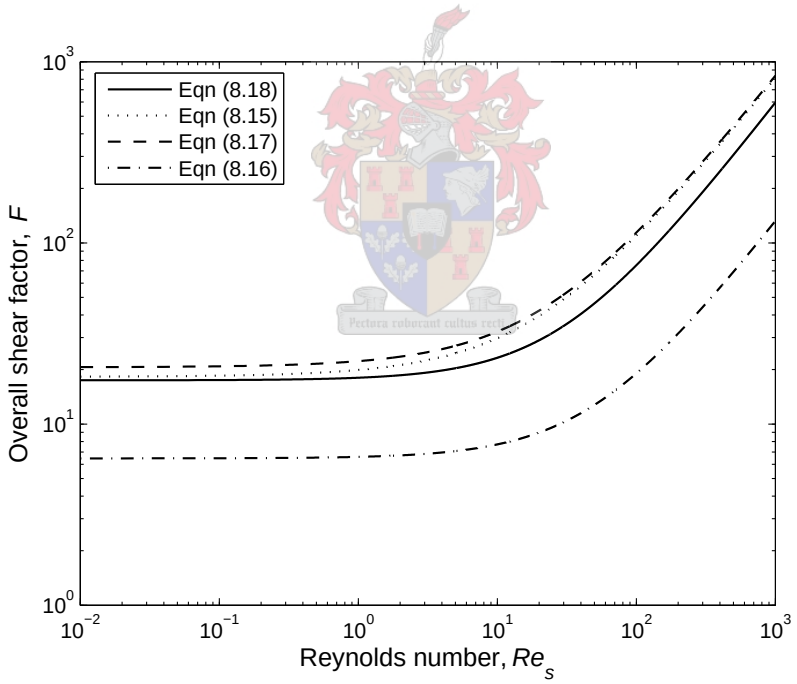


Figure 8.2: Comparison of various drag models for $\epsilon_g = 0.8$.

For predicting flow behaviour in fluidized beds, Figure 8.2 shows that the RUC model corresponds better with the the Ergun/Rowe/Wen and Yu model than with the Macdonald/Rowe/Wen and Yu model. However, the excellent agreement with the Ergun/Rowe/Wen

and Yu model verifies that the RUC model is also successfully applicable as a drag model in modelling the flow behaviour in fluidized beds. The frictional effects predicted by the model of Gibilaro et al. (1985) prove to be significantly lower than the predictions of the other models. According to the study of Halvorsen et al. (2006), the computational results obtained by the RUC model, the Ergun/Rowe/Wen and Yu model and the empirical verification of Macdonald et al. (1979) provided very good agreement with the experimental results regarding bubble velocity and shape. The results obtained by the model of Gibilaro et al. (1985) were less satisfactory. These findings, however, agree with the present results. From equations (8.1) and (8.3) it follows that the magnitude of the minimum fluidization velocity $q_{mf}$ may be obtained by solving for $q$ from

$$(1-\epsilon_g)(\rho_s-\rho_g)g \;=\; \frac{\Phi_{sg}\,q}{\epsilon_g^2}\;, \tag{8.19}$$

yielding

$$q_{mf} \;=\; \frac{\epsilon_{mf}^2(1-\epsilon_{mf})(\rho_s-\rho_g)\,g}{\Phi_{sg}}\;, \tag{8.20}$$

where $\epsilon_g = \epsilon_{mf}$ at minimum fluidization. The Ergun/Rowe/Wen and Yu model yields the following expression for the minimum fluidization velocity

$$q_{mf} \;=\; \frac{D_h^2\,(\rho_s-\rho_g)\,g\,\epsilon_{mf}^{4.65}}{\mu_g\left[18+150\,\epsilon_{mf}^{1.65}(1-\epsilon_{mf})\right]}\;. \tag{8.21}$$

According to the model of Gibilaro et al. (1985)

$$q_{mf} \;=\; \frac{D_h^2\,(\rho_s-\rho_g)\,g\,\epsilon_{mf}^{4.80}}{17.3\,\mu_g}\;. \tag{8.22}$$

The RUC model yields,

$$q_{mf} \;=\; \frac{d_s^2\,(\rho_s-\rho_g)\,g}{26.8\,\mu_g}\,\frac{\left(1-(1-\epsilon_{mf})^{1/3}\right)\left(1-(1-\epsilon_{mf})^{2/3}\right)^2}{(1-\epsilon_{mf})^{1/3}} \tag{8.23}$$

and Yu et al. (1968) propose that for a bed of uniformly sized spherical particles,

$$q_{mf} \;=\; \frac{D_h^2\,(\rho_s-\rho_g)\,g\,\epsilon_{mf}^3}{150\,\mu_g\,(1-\epsilon_{mf})}\;. \tag{8.24}$$

The various expressions for $q_{mf}$ are evaluated for air as the gas phase. The parameter values for air are shown in Table 8.1.

| Test fluid | Packing material | Mean particle diameter, $d_p$ ($\mu$m) | $\rho_s$ (kg.m$^{-3}$) | $\mu_g$ (N.s.m$^{-2}$) | $\rho_g$ (kg.m$^{-3}$) |
|---|---|---|---|---|---|
| Air | Uniform spheres | 550 | 2485 | $181 \times 10^{-7}$ | 1.20 |

Table 8.1: Parameters of the packing material and air at 1 atm and 20$^o$C.

The minimum fluidization porosity $\epsilon_{mf}$ may be approximated by a bed of uniformly sized spherical particles packed in a cubic mode $\epsilon_{mf} \approx 0.476$ which corresponds to the porosity of a loosely packed bed (Gidaspow (1994)). Brea et al. (1976) determined empirically that for a loosely packed fixed bed $\epsilon_{mf} = 0.42$ and Happel & Brenner (1965) proposed a value of $\epsilon_{mf} \approx 0.47$. The values for $q_{mf}$ evaluated at $\epsilon = 0.42$ and $\epsilon = 0.47$ are listed in Table 8.2.

| | $q_{mf}$ (m/s) | |
|---|---|---|
| Model | $\epsilon_{mf} = 0.42$ | $\epsilon_{mf} = 0.47$ |
| RUC | 0.28 | 0.43 |
| Ergun/Rowe/Wen and Yu | 0.19 | 0.30 |
| Gibilaro et al. (1985) | 0.37 | 0.63 |
| Yu et al. (1968) | 0.35 | 0.53 |
| Average: | 0.30 | 0.47 |

Table 8.2: Comparison of the magnitude of the minimum fluidization velocity $q_{mf}$.

No comment can be made regarding which model provides the correct predicted value for $q_{mf}$. The average $q_{mf}$-value for $\epsilon = 0.42$ is 0.30 and for $\epsilon = 0.47$ an average value of 0.47 is obtained. The fact that the RUC model yields in both cases the closest predicted value for $q_{mf}$ is encouraging and provides confidence in the versatility of the model.

## 8.2 Sandstones

Numerous experimental measurements for determining the permeability of sandstones have been performed on Fontainebleau sandstone (i.e. Adler et al. (1990), Bourbie & Zinszner (1985) and Doyen (1988)) due to its simple granular microstructure and its large porosity variation. Fontainebleau sandstone is composed merely of fine impermeable quartz grains cemented by silica (Bourbie & Zinszner (1985)). The material was originally non-consolidated sand after which various geological processes, such as the accretion of the sand particles took place, which lead to a decrease in porosity (Adler et al. (1990)). The constant composition and grain size of Fontainebleau sandstone as well as the well-sortedness of the grains make the material remarkably homogeneous. Another important feature is that the geometric structure is conserved with variation in porosity. Owing to the granular nature of sandstone Du Plessis & Roos (1994) have utilized the existing granular RUC model, i.e.

$$k = \frac{d_s^2\,\epsilon\left(1-(1-\epsilon)^{1/3}\right)\left(1-(1-\epsilon)^{2/3}\right)}{41\,(1-\epsilon)^{4/3}}\,, \tag{8.25}$$

to predict the permeability through various sandstones, including Fontainebleau sandstone. The permeability of Fontainebleau sandstone may therefore also be predicted by application of the granular RUC model presented in this work, given by

$$k = \frac{d_s^2\left(1-(1-\epsilon)^{1/3}\right)\left(1-(1-\epsilon)^{2/3}\right)^2}{26.8\,(1-\epsilon)^{4/3}}\,. \tag{8.26}$$

In both RUC models it is assumed that each sandstone sample has a uniform grain size. The variation in porosity and diameter $D$ of different samples of Fontainebleau sandstone is respectively given by Doyen (1988) as $0.05 < \epsilon < 0.22$ and $150 < D < 300\,\mu$m. Bourbie & Zinszner (1985) give an average diameter value of $d_p \approx 250\,\mu$m for Fontainebleau sandstone. The experimental permeability values provided by Adler et al. (1990), Bourbie & Zinszner (1985) and Doyen (1988) are shown in Figure 8.3 together with the two curves representing the permeability predictions of equations (8.25) and (8.26) corresponding to the limiting grain diameter values of 150 and 325 $\mu$m. The latter diameter value is taken as the average of 300 and 350 $\mu$m.

The fluctuations in the permeability data at a particular porosity value by almost a factor of 10 is a known phenomenon of sandstones (Adler et al. (1990)). The curved lines representing the permeability prediction of both the existing and present RUC models capture the experimental data of Bourbie & Zinszner (1985) within an envelope for porosities greater than 0.08. The deviations from all the experimental data at porosity values below 0.1 may be attributed to the occurrence of so-called blocked throats which were not accounted for in the RUC model (Du Plessis & Roos (1994)). Blocked throats result when the porosity becomes so low that regions within the interstitial pore sections randomly become clogged. Stagnant zones appear and at a certain porosity, called the percolation threshold porosity, no more seepage takes place leading to an impermeable

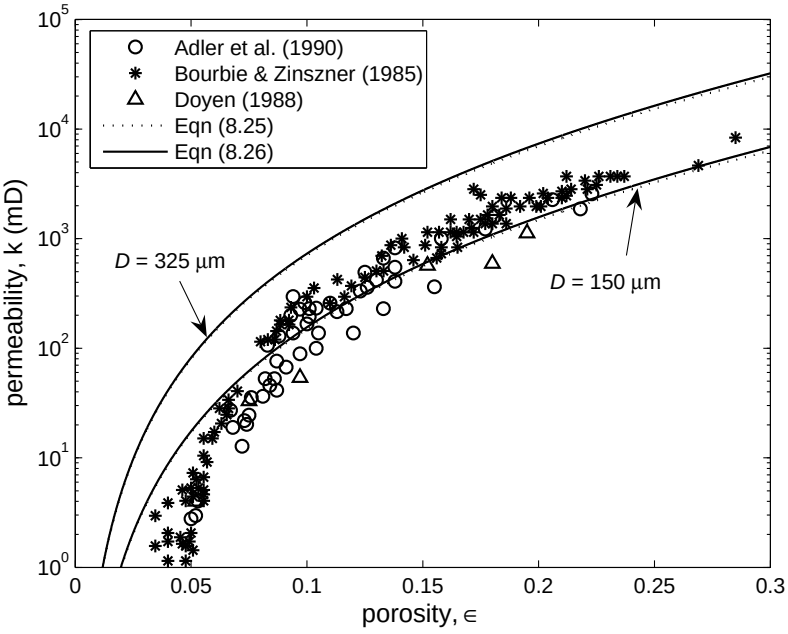


Figure 8.3: Permeability prediction of Fontainebleau sandstone.

porous medium. The percolation threshold porosity $\epsilon_c$ is a characteristic property of the particular granular structure and the particular clogging mechanism and need to be determined experimentally for the specific sandstone under consideration. In order to adjust the present RUC model to physically account for the phenomenon of blocked throats, a general porosity, called the backbone porosity $\epsilon_B$, needs to be introduced subject to the following two asymptotic limiting conditions (Du Plessis (1999)): At the percolation threshold the backbone porosity should tend to zero, i.e.

$$\epsilon_B \to 0 \qquad \text{when} \qquad \epsilon \to \epsilon_c \ , \tag{8.27}$$

and secondly, at porosities well above the threshold, pore blockage is non-existent so that the backbone porosity should take on the same values as the porosity, i.e.

$$\epsilon_B \to \epsilon \qquad \text{when} \qquad \epsilon \to 1 \ . \tag{8.28}$$

A general expression for the backbone porosity satisfying both limiting conditions may once again be obtained through application of the asymptote matching technique of Churchill & Usagi (1972), yielding

$$\epsilon_B \ = \ (\epsilon^s - \epsilon_c^s)^{1/s} \ . \tag{8.29}$$

Du Plessis (1999) found that the value of the shifting parameter $s$ which led to the best correspondence with the experimental data of Adler et al. (1990) and Bourbie & Zinszner (1985) over the entire porosity range is $s = 3/2$, leading to

$$\epsilon_B \ = \ (\epsilon^{3/2} - \epsilon_c^{3/2})^{2/3} \ . \tag{8.30}$$

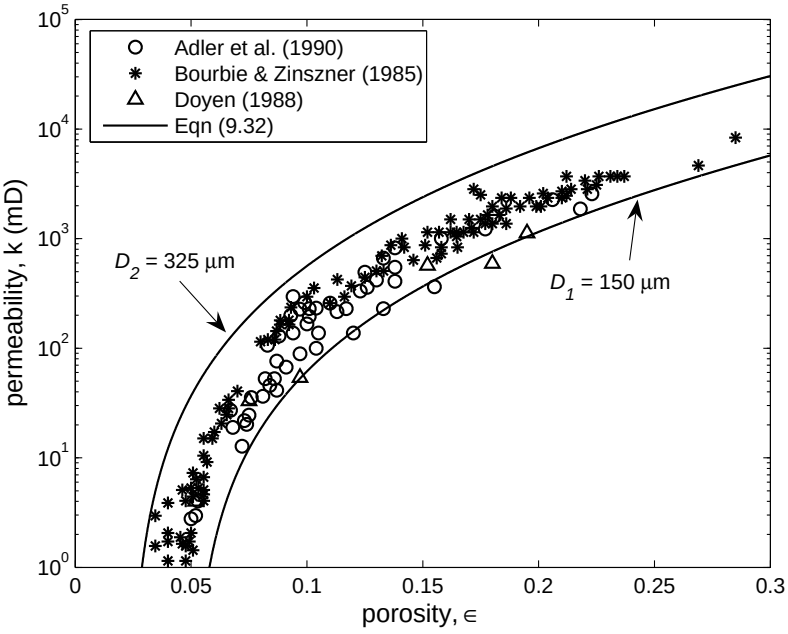


Figure 8.4: Modified permeability prediction of Fontainebleau sandstone.

Substituting $\epsilon_B$ into equation (8.26) yields the following unified expression for predicting the permeability of Fontainebleau sandstones, over the entire porosity range applicable to this porous material, in terms of only three parameters, namely, the porosity, grain size and threshold porosity:

$$k \;=\; \frac{D^2\left(1-(1-\epsilon_B)^{1/3}\right)\left(1-(1-\epsilon_B)^{2/3}\right)^2}{26.8\,(1-\epsilon_B)^{4/3}}\;. \tag{8.31}$$

Let $D_i$, with $i = 1, 2$, denote the limiting diameter values between which all the possible grain sizes of different samples of Fontainebleau sandstone lie. Also let $\epsilon_{c_i}$ denote the threshold porosity of the grain size with limiting diameter $D_i$. A reasonable assumption to make is that the threshold porosity does not depend on the grain size, but on the pore width (Du Plessis (1999)), of which the latter may be expressed in RUC notation as,

$$d - d_s \;=\; \left[(1-\epsilon)^{-1/3}-1\right] D\;. \tag{8.32}$$

For samples of known $D_i$-values it is possible to obtain an expression for the threshold porosity $\epsilon_{c_i}$, if either the value of $\epsilon_{c_1}$ or $\epsilon_{c_2}$ is known and subject to the assumption that the samples have an equivalent uniform pore width in which the same clogging processes take place. For a sample of known limiting diameter $D_1$ and a known threshold porosity $\epsilon_{c_1}$, the threshold porosity $\epsilon_{c_2}$ of a sample with known limiting diameter $D_2$ may be obtained by application of equation (8.32), i.e.

$$\left[(1-\epsilon_{c_1})^{-1/3}-1\right] D_1 \;=\; \left[(1-\epsilon_{c_2})^{-1/3}-1\right] D_2\;. \tag{8.33}$$

Solving for $\epsilon_{c_2}$ yields

$$\epsilon_{c_2} \;=\; 1 - \left[\frac{D_2}{D_1\left[(1-\epsilon_{c_1})^{-1/3} - 1\right] + D_2}\right]^3 \quad . \tag{8.34}$$

Choosing the limiting diameter values of Fontainebleau sandstone to be $D_1 = 150\,\mu$m and $D_2 = 325\,\mu$m and a threshold porosity of $\epsilon_{c_1} = 0.05$, as proposed by Doyen (1988), yields $\epsilon_{c_2} = 0.0235$. The curves representing the modified RUC model (equation (8.31)) for the parameter values given above are shown in Figure 8.4. It is evident that the adaptation to the granular RUC model to incorporate the effect of blocked throats at very low porosities provides an accurate prediction for the permeability of Fontainebleau sandstone of samples of different grain diameters. The resulting envelope produced by the two limiting grain diameter values for this particular sandstone provides a satisfactory enclosure of the experimental data.

# Chapter 9

# Conclusions and Recommendations

The present study involved the analytical closure modelling of the fluid-solid interaction within a granular porous medium with a simple pore-scale model to obtain a unified deterministic expression for the pressure gradient prediction through application of the asymptote matching technique. The real complex geometry of the isotropic granular porous microstructure was approximated with cubic geometry. The RUC model is derived for the flow of an incompressible Newtonian fluid through granular porous media over a wide range of porosities and Reynolds numbers within the entire steady laminar flow regime. The only changeable parameters in the predictive expression for the pressure gradient for Newtonian flow over the entire steady laminar flow regime is the porosity, the microscopic length scale and the constant fluid properties. Due to the difficulty in formulating the tortuosity mathematically, an explicit introduction of the tortuosity concept into the analytical model was avoided on purpose.

The asymptote matching technique proves to be a very useful technique to obtain a unified expression over a wide range of parameter values under consideration, since it provides a gradual transition between two asymptotic limits. The technique is especially advantageous in the matching of the two asymptotic limits of the steady laminar flow regime since the transition regime where boundary layers are developed need not be modelled analytically, although its contribution is accounted for implicitly in the resulting expression. Assigning a value of unity to the shifting parameters for the purpose of simplicity proves to be acceptable, albeit the predictive capabilities may be improved with higher values of the shifting parameter. It was found that the asymptote matching of the low to moderate porosity RUC model in the limit of low Reynolds number flow with a high porosity model is unnecessary when the matching technique is performed over the two limits of the steady laminar flow regime.

Based on the excellent correspondence of the RUC model with the Ergun equation, the analytical model may be regarded as a theoretical derivation of the semi-empirical equation. The major advantage of the RUC model over the Ergun equation is that the assumptions are based purely on physical principles without the need for the introduction of redundant coefficients for empirical correlation. The RUC model also provides a more realistic

representation of a granular packed bed through inter-connectedness of the pore-space. The introduction of a shape factor to account for the non-sphericity of the RUC model seems unnecessary since the cubic approximation of the granular micro-structure proves to be adequate. Besides, the sphericity factor introduced into the Ergun equation yields a value of 0.803 for cubes, which is close to the value of 1.0 for spheres (Yu et al. (1968)).

Although the difference between the present and existing RUC models seems graphically to be minor, the analytical derivation of the proposed RUC model is from a physical point of view more justifiable than the existing RUC model, since it lends sound mathematical support to the assumptions being made in the model.

The RUC model disposes of the ability to be generalized to broaden its range of applicability which is a major advantage over most of the predictive models in the literature. The RUC model for Newtonian flow has been generalized successfully to account for the rheological flow behaviour of purely viscous power law flow through isotropic granular porous media over a wide range of shear rates. The modification was accomplished by introducing the dependence of the apparent viscosity on the shear rate through the wall shear stress. The only additional parameters included in the expression for the pressure gradient prediction are the two power law parameters and the expression may easily be reduced to the expression for Newtonian flow. The failure of the generalized RUC model to predict the non-Newtonian flow behaviour of high concentration polymer solutions is attributed to the additional normal stresses which tend to increase the pressure gradient for flow through porous media. These normal stresses were not accounted for in the power law model. The RUC model was also adapted to predict the flow behaviour in a fluidized bed by adjusting the superficial velocity to account for the relative fluid-particle velocity within the bed. The adapted model was used as a drag model in an existing numerical simulation program and the end result was a very successful prediction of bubble formation within the bed. The RUC model for Newtonian flow was furthermore adapted to predict fluid flow through Fontainebleau sandstone by accounting for the effect of blocked throats. The only additional parameter value required was the threshold porosity.



The generalized RUC model may easily be adjusted to predict other types of non-Newtonian flow behaviour through modification of the expression for the wall shear stress. The accuracy of the RUC model may be improved by choosing a shifting parameter greater than unity, but a trade-off exists between accuracy and simplicity. The predictive capability of the proposed RUC model was verified against a large number of available experimental data from the literature and the accuracy of the model proves to be acceptable for most engineering designs.

Dagan (1989) stated the following concerning the essential requirements for rendering models to be useful:

> *They should capture the main mechanisms involved in the phenomena of interest, they should be simple, they should resemble, even though schematically, actual media and they should lead to the right order of magnitude of the coefficients of interest.*

Since the proposed RUC model satisfies all these requirements, it may be concluded that the RUC model is a useful and versatile model in predicting laminar flow through isotropic granular porous media.

# Appendix A

# Volume averaging of transport equations

## A.1 Volume averaging theory

Macroscopic volume averaged quantities may be obtained through the introduction of phase average operators (e.g. Bachmat & Bear (1986) and Whitaker (1969)). The phase average $\langle\phi\rangle$ of any finite, continuous and differentiable tensorial quantity $\phi$ within $\mathcal{U}_f$ is defined as

$$\langle\phi\rangle \equiv \frac{1}{\mathcal{U}_0} \iiint_{\mathcal{U}_f} \phi \, d\mathcal{U} \, . \tag{A.1}$$

Similarly, the intrinsic phase average $\langle\phi\rangle_f$ is defined as

$$\langle\phi\rangle_f \equiv \frac{1}{\mathcal{U}_f} \iiint_{\mathcal{U}_f} \phi \, d\mathcal{U} \, . \tag{A.2}$$

From these definitions the following identities are obtained:

$$\langle\phi\rangle = \epsilon \langle\phi\rangle_f \, , \tag{A.3}$$

$$\langle\alpha\,\phi\rangle = \alpha \langle\phi\rangle \, , \quad \alpha = \text{constant} \, , \tag{A.4}$$

$$\langle\phi_1 + \phi_2\rangle = \langle\phi_1\rangle + \langle\phi_2\rangle \, , \tag{A.5}$$

$$\langle\phi_1\,\phi_2\rangle = \langle\phi_1\rangle\langle\phi_2\rangle/\epsilon + \langle\{\phi_1\}\{\phi_2\}\rangle \, . \tag{A.6}$$

By application of the preceding identities the average of a gradient (or divergence) may be expressed as the gradient of an average (or divergence) (e.g. Slattery (1969) and Whitaker

(1969)), i.e.

$$\langle \nabla \phi \rangle \;=\; \nabla \langle \phi \rangle \;+\; \frac{1}{\mathcal{U}_0} \iint\limits_{\mathcal{S}_{fs}} \underline{n}\, \phi \, d\mathcal{S} \;, \tag{A.7}$$

or

$$\left\langle \nabla \cdot \underline{\phi} \right\rangle \;=\; \nabla \cdot \left\langle \underline{\phi} \right\rangle \;+\; \frac{1}{\mathcal{U}_0} \iint\limits_{\mathcal{S}_{fs}} \underline{n} \cdot \underline{\phi} \, d\mathcal{S} \;. \tag{A.8}$$

Here $\underline{n}$ is the inwardly (with respect to the solid) directed unit vector normal to the fluid-solid interface. From equation (A.7) it follows that

$$\nabla \epsilon \;=\; -\frac{1}{\mathcal{U}_0} \iint\limits_{\mathcal{S}_{fs}} \underline{n} \, d\mathcal{S} \;. \tag{A.9}$$

The phase average of a time derivative may be expressed as

$$\left\langle \frac{\partial \phi}{\partial t} \right\rangle \;=\; \frac{\partial \langle \phi \rangle}{\partial t} \;-\; \frac{1}{\mathcal{U}_0} \iint\limits_{\mathcal{S}_{fs}} \underline{n} \cdot \underline{v}\, \phi \, d\mathcal{S} \;. \tag{A.10}$$

## A.2 Volume averaging of the continuity equation

From equation (A.8) it follows that the phase average of the continuity equation for an incompressible fluid may be expressed as

$$\langle \, \nabla \cdot \underline{v} \, \rangle \;=\; \nabla \cdot \langle \underline{v} \rangle \;+\; \frac{1}{\mathcal{U}_0} \iint\limits_{\mathcal{S}_{fs}} \underline{n} \cdot \underline{v} \, d\mathcal{S} \;=\; \langle 0 \rangle \;, \tag{A.11}$$

yielding the following expression for the volume averaged continuity equation for an incompressible fluid

$$\nabla \cdot \underline{q} \;=\; 0 \;, \tag{A.12}$$

due to the vectorial cancellation of the surface integral in equation (A.11).

## A.3 Volume averaging of the Navier-Stokes equation

Volume averaging of the Navier-Stokes equation for an incompressible fluid in which the gravitation term is included in the pressure as a pressure head, leads to

$$\left\langle \rho \frac{\partial \underline{v}}{\partial t} \right\rangle + \langle \nabla \cdot (\rho \underline{v}\, \underline{v}) \rangle + \langle \nabla p \rangle - \left\langle \nabla \cdot \underline{\underline{\tau}} \right\rangle = \langle \underline{0} \rangle \ . \tag{A.13}$$

Application of the averaging identities to each term on the left hand side of equation (A.13) respectively yields

$$\left\langle \rho \frac{\partial \underline{v}}{\partial t} \right\rangle = \rho \left\langle \frac{\partial \underline{v}}{\partial t} \right\rangle = \rho \frac{\partial \underline{q}}{\partial t} - \frac{\rho}{\mathcal{U}_0} \iint\limits_{\mathcal{S}_{fs}} \underline{n} \cdot \underline{v}\, \underline{v}\, d\mathcal{S} \ , \tag{A.14}$$

$$\langle \nabla \cdot (\rho \underline{v}\, \underline{v}) \rangle = \rho \nabla \cdot \left( \underline{q}\, \underline{q} / \epsilon \right) + \rho \nabla \cdot \langle \{\underline{v}\} \{\underline{v}\} \rangle + \frac{\rho}{\mathcal{U}_0} \iint\limits_{\mathcal{S}_{fs}} \underline{n} \cdot \underline{v}\, \underline{v}\, d\mathcal{S} \ , \tag{A.15}$$

$$\langle \nabla p \rangle = \nabla \langle p \rangle + \frac{1}{\mathcal{U}_0} \iint\limits_{\mathcal{S}_{fs}} \underline{n} \{p\} \, d\mathcal{S} \ , \tag{A.16}$$

$$\left\langle \nabla \cdot \underline{\underline{\tau}} \right\rangle = \nabla \cdot \left\langle \underline{\underline{\tau}} \right\rangle + \frac{1}{\mathcal{U}_0} \iint\limits_{\mathcal{S}_{fs}} \underline{n} \cdot \underline{\underline{\tau}} \, d\mathcal{S} \ . \tag{A.17}$$

Substituting equations (A.14) to (A.17) into equation (A.13) yields the following expression for the volume averaged Navier-Stokes equation for an incompressible fluid

$$-\nabla \langle p \rangle = \rho \frac{\partial \underline{q}}{\partial t} + \rho \nabla \cdot \left( \underline{q}\, \underline{q} / \epsilon \right) + \rho \nabla \cdot \langle \{\underline{v}\} \{\underline{v}\} \rangle - \nabla \cdot \left\langle \underline{\underline{\tau}} \right\rangle + \frac{1}{\mathcal{U}_0} \iint\limits_{\mathcal{S}_{fs}} \left( \underline{n} \{p\} - \underline{n} \cdot \underline{\underline{\tau}} \right) d\mathcal{S} \ . \tag{A.18}$$

By application of equations (A.3) and (A.5) the momentum dispersion term $\rho \nabla \cdot \langle \{\underline{v}\} \{\underline{v}\} \rangle$ may be expressed in terms of the superficial velocity $\underline{q}$ as follows

$$\begin{aligned}
\rho \nabla \cdot \langle \{\underline{v}\} \{\underline{v}\} \rangle &= \rho \nabla \cdot \left\langle \left( \langle \underline{v} \rangle - \langle \underline{v} \rangle_f \right) \left( \langle \underline{v} \rangle - \langle \underline{v} \rangle_f \right) \right\rangle \\
&= \rho \nabla \cdot \left\langle \langle \underline{v} \rangle \langle \underline{v} \rangle - \langle \underline{v} \rangle \langle \underline{v} \rangle_f - \langle \underline{v} \rangle_f \langle \underline{v} \rangle + \langle \underline{v} \rangle_f \langle \underline{v} \rangle_f \right\rangle \\
&= \rho \nabla \cdot \left\langle \langle \underline{v} \rangle \langle \underline{v} \rangle - 2 \frac{\langle \underline{v} \rangle \langle \underline{v} \rangle}{\epsilon} + \frac{1}{\epsilon^2} \langle \underline{v} \rangle \langle \underline{v} \rangle \right\rangle \\
&= \rho \nabla \cdot \langle \langle \underline{v} \rangle \langle \underline{v} \rangle \rangle - \frac{2}{\epsilon} \rho \nabla \cdot \langle \langle \underline{v} \rangle \langle \underline{v} \rangle \rangle + \frac{1}{\epsilon^2} \rho \nabla \cdot \langle \langle \underline{v} \rangle \langle \underline{v} \rangle \rangle \\
&= \rho \nabla \cdot \left\langle \underline{q}\, \underline{q} \right\rangle - \frac{2}{\epsilon} \rho \nabla \cdot \left\langle \underline{q}\, \underline{q} \right\rangle + \frac{1}{\epsilon^2} \rho \nabla \cdot \left\langle \underline{q}\, \underline{q} \right\rangle \ .
\end{aligned} \tag{A.19}$$

# Appendix B

# Discussion of the closure modelling procedure presented by Lloyd et al. (2004)

Lloyd et al. (2004) stated that the shear stress integral evaluated over the transverse surfaces is zero, i.e.

$$\frac{1}{U_o}\iint_{S_\perp} \underline{n}\cdot\underline{\underline{\tau}}\,dS \;=\; \underline{0}\,, \tag{B.1}$$

and at the same time mentioned that these shear stresses on the transverse surfaces create interstitial transverse pressure drops, which is indeed the case, but the explanation given for the contribution of the pressure term in the surface integral of equation (4.1) to the streamwise pressure gradient in the low Reynolds number limit is incorrect. The analytical closure modelling procedure followed involved the splitting of the pressure in the surface integral evaluated over the transverse and stagnant surfaces, i.e.

$$\frac{1}{U_o}\iint_{S_\perp + S_g} \underline{n}\,p\,dS\,, \tag{B.2}$$

into a channel wall average pressure $\overline{p_w}$ and a wall pressure deviation $\widetilde{p_w}$. It is assumed that the pressure deviations are caused by shear stresses at the transverse surfaces and that the transverse pressure deviation integral is of similar magnitude as the transverse shear integral, i.e.

$$\frac{1}{U_o}\iint_{S_\perp} \underline{n}\,\widetilde{p_w}\,dS \;=\; \widehat{\underline{n}}\,\frac{1}{U_o}\iint_{S_\perp} \underline{n}\cdot\underline{\underline{\tau}}\cdot\widetilde{\underline{n}}\,dS\,. \tag{B.3}$$

The pressure deviation integral is then incorporated by integrating the wall shear stresses over the total fluid-solid interfaces $S_{fs}$. The modelling procedure mentioned above pro-

duces the same result as obtained in this work, but the following remarks should be made: The transverse shear stress integral is not zero, that is, equation (B.1) is incorrect. For a certain range of possible RUC locations in the streamwise direction the transverse shear stresses cancel vectorially, due to the quasi-periodic structure of the RUC model, but there do exist a range of RUC locations in the streamwise direction, in which the transverse shear stresses do contribute significantly to the streamwise pressure gradient. Another drawback in the closure modelling procedure of Lloyd et al. (2004) is that the pressure deviation integral evaluated over $S_g$ and $S_\perp$ are both claimed to be zero. Hence the assumption that the transverse pressure deviation integral is of similar magnitude as the transverse shear integral is invalid. The present closure modelling procedure involves a rectification of the closure modelling procedure followed by Lloyd et al. (2004).

# Appendix C

# Evaluating the displacement $\Delta s$

In order to determine the value of $\beta$ for a fully staggered array, the transverse displacement $\Delta s$ of the centroid of the fluid need to be determined. Let the coordinates of the position of the centroid before the transverse shift be denoted by $(\bar{x}, \bar{y})$, as indicated in Figure C.1.

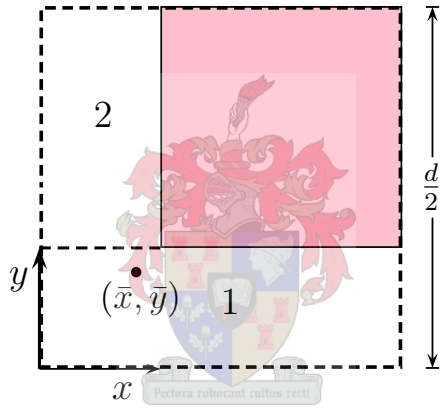


Figure C.1: A two-dimensional representation of the partitioning of the fluid domain of the RUC to determine the position of the centroid of the fluid before the transverse shift.

The coordinates of the position of the centroid before the transverse shift, may be expressed in terms of the linear dimensions $d$ and $d_s$ as follows

$$\bar{x} = \frac{\sum A_i x_i}{\sum A_i} = \frac{\frac{1}{2}d^3 - dd_s^2 + \frac{1}{2}d_s^3}{d^2 - d_s^2}\,, \tag{C.1}$$

$$\bar{y} = \frac{\sum A_i y_i}{\sum A_i} = \frac{\frac{1}{2}d^3 - dd_s^2 + \frac{1}{2}d_s^3}{d^2 - d_s^2}\,. \tag{C.2}$$

Let the coordinates of the position of the centroid after the transverse shift be denoted by $(\bar{x}\,', \bar{y}\,')$, as shown in Figure C.2.

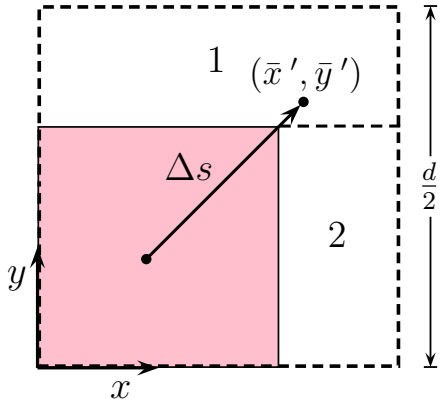


Figure C.2: A two-dimensional representation of the partitioning of the fluid domain of the RUC to determine the position of the centroid of the fluid after the transverse shift.

Similarly, the coordinates of the position of the centroid after the transverse shift, may be expressed as follows in terms of the linear dimensions $d$ and $d_s$:

$$\bar{x}\,' \;=\; \frac{\frac{1}{2}d^3 - \frac{1}{2}d_s^3}{d^2 - d_s^2}\,, \tag{C.3}$$

$$\bar{y}\,' \;=\; \frac{\frac{1}{2}d^3 - \frac{1}{2}d_s^3}{d^2 - d_s^2}\,. \tag{C.4}$$

The displacement of the centroid of the fluid in the $x$-direction, $\Delta\bar{x}$, yields

$$\Delta\bar{x} \;=\; \bar{x}\,' - \bar{x} \;=\; \frac{dd_s^2 - d_s^3}{d^2 - d_s^2} \;=\; \frac{d_s^2}{d + d_s}\,, \tag{C.5}$$

and the displacement in the $y$-direction, $\Delta\bar{y}$, leads to

$$\Delta\bar{y} \;=\; \bar{y}\,' - \bar{y} \;=\; \frac{dd_s^2 - d_s^3}{d^2 - d_s^2} \;=\; \frac{d_s^2}{d + d_s}\,. \tag{C.6}$$

The resulting expression for the transverse displacement $\Delta s$ of the centroid of the fluid is then given by

$$\Delta s \;=\; \sqrt{(\Delta\bar{x})^2 + (\Delta\bar{y})^2} \;=\; \frac{\sqrt{2}\,d_s^2}{d + d_s}\,. \tag{C.7}$$

# Appendix D

# Derivation of the Ergun equation

The Ergun equation (e.g. Bird et al. (2002)) is a well-known semi-empirical capillary tube model for predicting the pressure drop across a packed bed for Reynolds numbers ranging form the laminar to the turbulent flow regimes. The packed column is assumed to have a uniform diameter with smooth uniformly sized spherical particles as the packing material. It is assumed that the column diameter is much larger than the particle diameter so that an increase in local porosity near the column wall as well as any entrance effects may be discarded. It is furthermore assumed that the random packing of spheres is statistically uniform. The flow through the interstices of the packed bed is regarded as flow through a bundle of tortuous irregularly shaped capillaries with a uniform average cross-sectional area. The Ergun equation is a direct superposition of two asymptotic limits: a lower laminar limit described by the *Blake-Kozeny equation* and an upper limit for modelling turbulent flow described by the *Burke-Plummer equation*.

## D.1 Blake-Kozeny equation

The capillary tube flow is approximated by the following generalization of the Hagen-Poiseuille equation for laminar Newtonian flow through a long straight channel of arbitrary shape

$$u \;=\; \frac{\Delta p\, R_h^2}{k_o\, \mu\, L_e}\,, \tag{D.1}$$

where $u$ is the average channel velocity, $\Delta p$ is the pressure drop over the channel length $L_e$ and $k_o$ is a constant shape factor which depends on the shape of the cross-section of the channel. For a circular cross-section $k_o = 2$ and equation (D.1) reduces to the Hagen-Poiseuille equation (Bird et al. (2002)). Introducing the Dupuit-Forchheimer velocity relationship, i.e.

$$u \;=\; \frac{q}{\epsilon}\,, \tag{D.2}$$

in which it is assumed that the packed bed may be regarded as a bundle of straight capillary tubes placed parallel to the column axis, and the hydraulic diameter $D_h$ through the following relationship with the hydraulic radius $R_h$,

$$R_h \;=\; \frac{\epsilon D_h}{6\,(1-\epsilon)}\;, \tag{D.3}$$

into equation (D.1) yields

$$-\Delta p \;=\; 36\,k_o\,\frac{(1-\epsilon)^2}{\epsilon^3}\frac{\mu\,q\,L_e}{D_h^2}\;. \tag{D.4}$$

To account for the actual tortuous flow path of the traversing fluid an empirical correction factor of 25/12 was introduced for agreement with experimental data. The introduction of the factor of 25/12 together with $k_o = 2$ yields a coefficient of 150, i.e.

$$-\frac{\Delta p}{L} \;= 150\,\frac{(1-\epsilon)^2}{\epsilon^3}\frac{\mu\,q}{D_h^2}\;, \tag{D.5}$$

which is known as the Blake-Kozeny equation. From Darcy's law it follows that the permeability of the Blake-Kozeny equation, $k_{BK}$, may be expressed as

$$k_{BK} \;=\; \frac{D_h^2}{150}\frac{\epsilon^3}{(1-\epsilon)^2}\;. \tag{D.6}$$

The friction factor is defined as

$$f_{BK} \;=\; \frac{-\Delta p}{\rho\,q^2}\frac{D_h}{L}\frac{\epsilon^3}{(1-\epsilon)}\;, \tag{D.7}$$

and the Reynolds number is given by

$$Re_{BK} \;=\; \frac{\rho\,q\,D_h}{\mu\,(1-\epsilon)}\;, \tag{D.8}$$

which allows for the friction factor $f_{BK}$ to be expressed as

$$f_{BK} \;=\; \frac{150}{Re_{BK}} \;=\; \frac{A}{Re_{BK}}\;. \tag{D.9}$$

## D.2 Carman-Kozeny-Blake equation

Carman (1937) argued that the real average velocity in a tortuous channel of length $L_e$ is $L_e/L$ times greater than the value $q/\epsilon$ in a straight channel of length $L$ which leads to the introduction of the tortuosity factor $\chi$,

$$L_e \;=\; \chi\,L\;, \tag{D.10}$$

and the replacement of the expression for the average channel velocity (equation (D.2)) with

$$u \;=\; \frac{q}{\epsilon}\frac{L_e}{L}\;. \tag{D.11}$$

Substituting equations (D.10), (D.3) and (D.11) into equation (D.1) yields

$$-\frac{\Delta p}{L} \;=\; 36\,k_o\,\chi^2\,\frac{(1-\epsilon)^2}{\epsilon^3}\frac{\mu\,q}{D_h^2}\;, \tag{D.12}$$

where the factor

$$k_{koz} \;=\; k_o\,\chi^2 \;=\; k_o\left(\frac{L_e}{L}\right)^2\;, \tag{D.13}$$

is known as the Kozeny constant. Utilizing the expressions for $f_{BK}$ and $Re_{BK}$ leads to

$$f_{BK} \;=\; \frac{36\,k_{koz}}{Re_{BK}} \;=\; \frac{A}{Re_{BK}}\;. \tag{D.14}$$

From the available data from the literature Carman proposed an average value for the Kozeny constant of $k_{koz} = 5.0$. He determined that in a bed of spheres the average value of the slope of the traversing fluid with respect to the column axis is $45^o$, that is

$$\chi \;=\; \frac{L_e}{L} \;=\; \sqrt{2}\;, \tag{D.15}$$

which yields a value of 2.5 for the shape factor $k_o$ and produces a coefficient value of $A = 180$. The pressure drop my there-upon be expressed as

$$-\frac{\Delta p}{L} \;=\; 180\,\frac{(1-\epsilon)^2}{\epsilon^3}\frac{\mu\,q}{D_h^2}\;, \tag{D.16}$$

which is known as the Carman-Kozeny-Blake equation. Application of Darcy's law leads to

$$k_{BK} \;=\; \frac{D_h^2}{180}\frac{\epsilon^3}{(1-\epsilon)^2}\;. \tag{D.17}$$

## D.3 Burke-Plummer equation

For highly turbulent flow, according to Bird et al. (2002), the friction factor $f_{BK}$ is no longer dependent on the Reynolds number $Re_{BK}$ and is constant for a given relative roughness, i.e.

$$f_{BK} \;=\; \text{constant} \;=\; B\;. \tag{D.18}$$

From numerous experimental data a value of $B = 1.75$ was proposed, yielding

$$-\frac{\Delta p}{L} \;=\; 1.75\,\frac{(1-\epsilon)}{\epsilon^3}\frac{\rho\, q^2}{D_h}\;, \tag{D.19}$$

which is known as the Burke-Plummer equation.

## D.4 Ergun equation

Ergun (1952) superimposed the Blake-Kozeny and Burke-Plummer equations to provide an expression for the pressure drop across a packed bed for Reynolds numbers ranging from the laminar to the turbulent flow regimes ($1 < Re_{BK} < 3000$), i.e.

$$-\frac{\Delta p}{L} \;=\; 150\,\frac{(1-\epsilon)^2}{\epsilon^3}\frac{\mu\, q}{D_h^2} \;+\; 1.75\,\frac{(1-\epsilon)}{\epsilon^3}\frac{\rho\, q^2}{D_h}\;, \tag{D.20}$$

which is the well-known Ergun equation. This equation usually gives good agreement with experimental data for $\epsilon < 0.5$. For $Re_{BK} < 10$ the first term in equation (D.20) dominates and the Ergun equation reduces to the Blake-Kozeny equation. For $10 < Re_{BK} < 10^3$ a gradual transition occurs after which the flow apparently becomes fully turbulent. Thus for $Re_{BK} > 10^3$ the second term in equation (D.20) predominates and the Ergun equation reduces to the Burke-Plummer equation. Equation (D.20) may be expressed as follows in dimensionless form

$$f_{BK} \;=\; \frac{A}{Re_{BK}} \;+\; B\;. \tag{D.21}$$

A customary modification of the Ergun equation is to account for a packed bed consisting of non-spherical particles by expressing the hydraulic diameter as

$$D_h \;=\; \phi_s\, D_p\;, \tag{D.22}$$

where $D_p$ is the diameter of a sphere of identical volume and $\phi_s$ is an empirical sphericity factor, defined as (Wen & Yu (1966))

$$\phi_s \;=\; \frac{\pi^{\frac{1}{3}}\,(6V_p)^{\frac{2}{3}}}{A_p}\;, \tag{D.23}$$

with $V_p$ and $A_p$ the particle volume and surface area, respectively. For spherical particles $\phi_s = 1$ and for non-spherical particles $\phi_s < 1$.

# Appendix E

# Generalized shear stress model

The generalized shear stress model describing the flow behaviour of both purely viscous non-Newtonian and Newtonian fluids may be expressed as (Bird et al. (2002))

$$\underline{\underline{\tau}} = -\eta\left(\nabla\underline{v} + \widetilde{\nabla\underline{v}}\right) \equiv -\eta\,\underline{\underline{\dot{\gamma}}}\,, \tag{E.1}$$

where $\underline{\underline{\dot{\gamma}}}$ is referred to as the rate of strain tensor or rate of deformation tensor and $\eta$ is the apparent viscosity defined as the ratio of the shear stress $\tau_{yx}$ to the shear rate $\dot{\gamma}$, i.e.

$$\eta\left(\dot{\gamma}\right) = \left|\frac{\tau_{yx}}{\dot{\gamma}}\right|, \tag{E.2}$$

where $\dot{\gamma} = \mathrm{d}v/\mathrm{d}y$. For non-Newtonian fluids the apparent viscosity is a function of the shear rate resulting in a non-linear dependence of the shear stress on the shear rate which may be expressed as

$$\tau_{yx} = \eta\left(\dot{\gamma}\right)\left|\frac{\mathrm{d}v}{\mathrm{d}y}\right| \,. \tag{E.3}$$

A Newtonian fluid obeys Newton's law of viscosity which states that the shear stress is linearly proportional to the shear rate, i.e.

$$\tau_{yx} = \mu\left|\frac{\mathrm{d}v}{\mathrm{d}y}\right| \,, \tag{E.4}$$

where the constant of proportionality $\mu$ ($\equiv \eta$) is referred to as the dynamic viscosity of the traversing fluid. For Newtonian fluids the normal stresses $\tau_{xx}$, $\tau_{yy}$ and $\tau_{zz}$ are all zero which is not necessarily the case for non-Newtonian fluids.

## E.1 Generalized plane Poiseuille flow

The Navier-Stokes equation (equation (2.2)) for fully developed and time-independent flow, in which the body forces are included into the pressure as a pressure head, reduces to

$$\nabla p \;=\; \nabla \cdot \underline{\underline{\tau}} \,. \tag{E.5}$$

For unidirectional discharge in the positive $x$-direction of a Cartesian coordinate system, it leads to

$$-\frac{\mathrm{d}p}{\mathrm{dx}}\,\underline{\hat{n}} \;=\; -\frac{\mathrm{d}\tau_{yx}}{\mathrm{dy}}\,\underline{\hat{n}} \,. \tag{E.6}$$

The magnitude of the local shear stress may thus be expressed as

$$\tau_{yx} \;=\; y\,\frac{\mathrm{d}p}{\mathrm{dx}} \,. \tag{E.7}$$

A general expression for the magnitude of the shear stress tensor $\underline{\underline{\tau}}$ is given by the power law model, that is,

$$\tau_{yx} \;=\; K\,|\dot{\gamma}|^{n} \qquad , \qquad n \leq 1 \,, \tag{E.8}$$

where $K$ and $n$ are constants characterizing the fluid and respectively referred to as the consistency and behaviour indices and

$$\dot{\gamma} \;=\; \frac{\mathrm{d}v}{\mathrm{d}y} \,. \tag{E.9}$$

It thus follows that

$$\left|\frac{\mathrm{d}v}{\mathrm{d}y}\right|^{n} = \frac{y}{K}\frac{\mathrm{d}p}{\mathrm{dx}}. \tag{E.10}$$

Consider unidirectional flow between parallel plates a distance $2B$ apart. The plates are positioned at $y = \pm B$ with a symmetry plane at $y = 0$. Considering therefore only the top half of the flow domain, i.e. $y \geq 0$, where $\mathrm{d}v/\mathrm{d}y$ is negative, yields the following expression for the velocity gradient:

$$\frac{\mathrm{d}v}{\mathrm{d}y} \;=\; -\left[\frac{y}{K}\frac{\mathrm{d}p}{\mathrm{dx}}\right]^{1/n} \,. \tag{E.11}$$

Solving for the magnitude of the interstitial fluid velocity $v$, leads to

$$v\,(y) \;=\; -\left(\frac{1}{K}\right)^{1/n}\left(\frac{\mathrm{d}p}{\mathrm{dx}}\right)^{1/n}\left(\frac{n}{n+1}\right)y^{(n+1/n)} + c \,, \tag{E.12}$$

where $c$ is the integration constant. Assumption of a no-slip boundary condition, i.e. $v|_{y=B} = 0$, yields the following expression for the integration constant

$$c = \left(\frac{1}{K}\right)^{1/n} \left(\frac{\mathrm{d}p}{\mathrm{dx}}\right)^{1/n} \left(\frac{n}{n+1}\right) B^{(n+1/n)} , \tag{E.13}$$

which leads to

$$v(y) = \left(\frac{1}{K}\right)^{1/n} \left(\frac{\mathrm{d}p}{\mathrm{dx}}\right)^{1/n} \left(\frac{n}{n+1}\right) \left[B^{(n+1/n)} - y^{(n+1/n)}\right] . \tag{E.14}$$

The magnitude of the average streamwise channel velocity $w$ between the plates is then given by

$$\begin{aligned} w &= \frac{1}{B}\int_0^B v(y)\mathrm{d}y \\ &= \left(\frac{1}{K}\right)^{1/n} \left(\frac{\mathrm{d}p}{\mathrm{dx}}\right)^{1/n} \left(\frac{n}{2n+1}\right) B^{(n+1/n)} \\ &= \left(\frac{1}{K}\right)^{1/n} \left(B\frac{\mathrm{d}p}{\mathrm{dx}}\right)^{1/n} \left(\frac{n}{2n+1}\right) B \\ &= \left(\frac{n}{2n+1}\right) B^{1+(1/n)} \left(\frac{\mathrm{d}p}{K\mathrm{d}x}\right)^{1/n} . \end{aligned} \tag{E.15}$$

Since the shear stress on the surface of the plate at $y = B$ is given by

$$\tau_w = B\frac{\mathrm{d}p}{\mathrm{d}x} , \tag{E.16}$$

it follows that

$$w = \left(\frac{1}{K}\right)^{1/n} \tau_w^{1/n} \left(\frac{n}{2n+1}\right) B . \tag{E.17}$$

The wall shear stress for a power law fluid may thus be expressed as

$$\tau_w = K\left(\frac{2n+1}{n}\right)^n \left(\frac{w}{B}\right)^n . \tag{E.18}$$

Expressing the channel width between the parallel plates in RUC notation, yields

$$B = \frac{d-d_s}{2} . \tag{E.19}$$

The wall shear stress for purely viscous power law flow between parallel plates a distance $d - d_s$ apart may thereupon be expressed as

$$\tau_w = K\left(\frac{2n+1}{n}\right)^n \left(\frac{2w}{d-d_s}\right)^n , \tag{E.20}$$

which reduces for a Newtonian fluid ($n = 1$ and $K = \mu$) to

$$\tau_w \;=\; \frac{6\mu w}{d - d_s}\;. \tag{E.21}$$

## E.2 Reynolds number and friction factor for power law flow through granular porous media

The Reynolds number is a dimensionless entity used for comparison between different flow systems and is generally defined as (Massey (1989))

$$Re \;=\; \frac{|\text{inertial forces}|}{|\text{viscous forces}|} \;=\; \frac{|\text{mass} \times \text{acceleration}|}{|\text{shear stress} \times \text{area over which shear stress act}|}\;. \tag{E.22}$$

Since the shear stress of a power law fluid is equal to $K|\mathrm{d}v/\mathrm{d}y|^n$, it follows that the viscous force is proportional to $K(v/l)^n l^2 = K v^n l^{2-n}$, where $l$ and $v$ respectively denotes a characteristic length and velocity. The Reynolds number may there-upon be expressed as

$$Re \;\propto\; \frac{\rho\, l^2 v^2}{K v^n l^{2-n}} \;=\; \frac{\rho\, v^{2-n} l^n}{K}\;, \tag{E.23}$$

### E.2.1 Reynolds number used by Smit (1997)

The Reynolds number for power law flow in a duct with hydraulic diameter $D_h$ chosen as the characteristic length $l$ and an average tube velocity $u_m$ chosen as the characteristic velocity $v$ may be expressed as

$$Re \;=\; \frac{\rho\, u_m^{2-n} D_h^n}{K}\;. \tag{E.24}$$

For flow between parallel plates a distance $2B$ apart, the hydraulic diameter may be expressed as

$$D_h \;=\; 4R_h \;=\; 4\frac{2Bd_s}{2d_s} \;=\; 4B\;. \tag{E.25}$$

It thus follows that for power law flow between parallel plates a distance $2B$ apart with an average channel velocity $w$, the Reynolds number may be expressed as

$$Re \;=\; \frac{\rho\, w^{2-n}(4B)^n}{K}\;. \tag{E.26}$$

From equations (4.4) and (4.10) it follows that

$$2B = d - d_s = d - (1-\epsilon)^{1/3} d = (1 - (1-\epsilon)^{1/3}) d\;, \tag{E.27}$$

and

$$w = \frac{q\,d^2}{d^2 - d_s^2} \;=\; \frac{q}{(1-(1-\epsilon)^{2/3})}\;, \tag{E.28}$$

yielding the Reynolds number of equation (7.33), i.e.

$$Re \;=\; \frac{2^n \rho\, q^{2-n} d^n}{K} \frac{\left(1-(1-\epsilon)^{1/3}\right)^n}{(1-(1-\epsilon)^{2/3})^{2-n}}\;. \tag{E.29}$$

### E.2.2 Reynolds number used by Smit & Du Plessis (2000)

For Newtonian flow equation (E.24) simplifies to

$$Re \;=\; \frac{\rho\, u_m D_h}{\mu}\;. \tag{E.30}$$

For power law flow between parallel plates a distance $2B$ apart with an average channel velocity $w$, it follows from equations (E.25), (E.27) and (E.28) that the Reynolds number may be expressed as

$$Re \;=\; \frac{2\,\rho\, q\, d\,(1-(1-\epsilon)^{1/3})}{\mu\,(1-(1-\epsilon)^{2/3})}\;, \tag{E.31}$$

or, equivalent to equation (7.68),

$$Re \;=\; \frac{2\,\rho\, q\, d}{\mu\,(1+(1-\epsilon)^{1/3})}\;. \tag{E.32}$$

### E.2.3 Friction factor used by Smit (1997) and Smit & Du Plessis (2000)

The friction factor for flow in a straight tube with hydraulic radius $R_h$ and an average tube velocity $u_m$ may be expressed as (Bird et al. (2002))

$$f \;=\; -\frac{\mathrm{d}p}{\mathrm{d}x}\,\frac{R_h}{(1/2)\,\rho\, u_m^2}\;. \tag{E.33}$$

For flow between parallel plates a distance $2B$ apart with an average channel velocity $w$, it follows from equations (E.25) and (E.27) that

$$f \;=\; \frac{\mathrm{d}p}{\mathrm{d}x}\,\frac{d\,(1-(1-\epsilon)^{1/3})}{\rho\, w^2}\;. \tag{E.34}$$

Substituting for $w$ from equation (E.28), yields

$$f \;=\; \frac{\mathrm{d}p}{\mathrm{d}x}\,\frac{d\,(1-(1-\epsilon)^{1/3})(1-(1-\epsilon)^{2/3})^2}{\rho q^2}\;. \tag{E.35}$$

# Bibliography


Adler, P. M., Jacquin, C. G., & Quiblier, J. A. (1990). Flow in Simulated Porous Media. *International Journal of Multiphase Flow*, *16*(4), 691–712.

Bachmat, Y. & Bear, J. (1986). Macroscopic Modelling of Transport Phenomena in Porous Media. 1: The Continuum Approach. *Transport in Porous Media*, *1*, 213–240.

Bear, J. & Bachmat, Y. (1986). Macroscopic Modelling of Transport Phenomena in Porous Media. 2: Applications to Mass, Momentum and Energy Transport. *Transport in Porous Media*, *1*, 241–269.

Bird, R. B., Stewart, W. E., & Lightfoot, E. N. (2002). *Transport Phenomena, Second Edition*. John Wiley and Sons, Inc.

Bourbie, T. & Zinszner, B. (1985). Hydraulic and Acoustic Properties as a Function of Porosity in Fontainebleau Sandstone. *Journal of Geophysical Research*, *90*(B13), 11524–11532.

Brea, F. M., Edwards, M. F., & Wilkinson, W. L. (1976). The Flow of Non-Newtonian Slurries Through Fixed and Fluidised Beds. *Chemical Engineering Science*, *31*, 329–336.

Carman, P. C. (1937). Fluid Flow Through Granular Beds. *Transaction of the Institution of Chemical Engineers*, *15*, 150–166.

Chakrabarti, S., Seidl, B., Vorwerk, J., & Brunn, P. O. (1991). The rheology of Hydroxypropylguar (HPG) solutions and its influence on the flow through a porous medium and turbulent tube flow, respectively (Part 1). *Rheologica Acta*, *30*, 114–123.

Chester, W. (1962). On Oseen's approximation. *Journal of Fluid Mechanics*, *13*, 557–569.

Chhabra, R. P. & Srinivas, B. K. (1991). Non-Newtonian (purely viscous) fluid flow through packed beds: effect of particle shape. *Powder Technology*, *67*, 15–19.

Chorlton, F. (1967). *Textbook of Fluid Dynamics*. D. van Nostrand Company LTD.

Christopher, R. H. & Middleman, S. (1965). Power-Law Flow Through a Packed Tube. *I & EC Fundamentals*, *4*(4), 422–426.

Churchill, S. W. & Usagi, R. (1972). A General Expression for the Correlation of Rates of Transfer and Other Phenomena. *A.I.Ch.E. Journal*, *18*(6), 1121–1128.

Dagan, G. (1989). *Flow and Transport in Porous Formations*. Springer-Verlag.

Doyen, P. M. (1988). Permeability, Conductivity and Pore Geometry of Sandstone. *Journal of Geophysical Research*, *93*(B7), 7729–7740.

Du Plessis, J. P. (1992). High Reynolds Number Flow Through Granular Porous Media. *Computaional Methods in Water Resources IX, Vol. 2: Mathematical Modeling in Water Resources, Computational Mechanics Publications, Southampton*, 179–186.

Du Plessis, J. P. (1994). Analytical Quantification of Coefficients in the Ergun Equation for Fluid Friction in a Packed Bed. *Transport in Porous Media*, *16*, 189–207.

Du Plessis, J. P. (1996). Power Law Flow in Isotropic Porous Media. *Proceedings of the Seventh International Congress on Rheology, Quebec, Canada, August 1996*, 375–376.

Du Plessis, J. P. (1999). Introducing a Percolation Threshold in Pore-Scale Modelling. *Phys. Chem. Earth (A)*, *24*(7), 617–620.

Du Plessis, J. P. & Masliyah, J. H. (1988). Mathematical Modelling of Flow Through Consolidated Isotropic Porous Media. *Transport in Porous Media*, *3*, 145–161.

Du Plessis, J. P. & Masliyah, J. H. (1991). Flow Through Isotropic Granular Porous Media. *Transport in Porous Media*, *6*, 207–221.

Du Plessis, J. P. & Roos, L. I. (1994). Predicting the hydrodynamic permeability of sandstone with a pore-scale model. *Journal of Geophysical Research*, *99*(B10), 19,771–19,776.

Du Plessis, J. P. & Van der Westhuizen, J. (1993). Laminar Crossflow Through Prismatic Porous Domains. *R&D Journal*, *9*(2), 18–24.

Dullien, F. A. L. (1979). *Porous Media: Fluid Transport and Pore Structure*. Academic Press.

Dybbs, A. & Edwards, R. V. (1982). A New Look at Porous Media Fluid Mechanics - Darcy to Turbulent. *Fundamentals of Transport Phenomena in Porous Media, Proceedings of the NATO Advanced Study Institute on Mechanics of Fluids in Porous Media, Newark, Delaware, USA, Martinus Nijhoff Publishers*, 201–256.

Ergun, S. (1952). Fluid Flow Through Packed Columns. *Chemical Engineering Progress*, *48*(2), 89–94.

Forchheimer, P. H. (1901). Wasserbeweguing durch boden. *Zeit. Ver. Deutsch Ing.*, *45*, 1782–1788.

Gibilaro, L. G., Di Felice, R., Waldram, S. P., & Foscolo, P. U. (1985). Generalized Friction Factor and Drag Coefficient Correlations for Fluid-Particle Interactions. *Chemical Engineering Science*, *40*(10), 1817–1823.

Gidaspow, D. (1994). *Multiphase Flow and Fluidization*. Academic Press, Inc.

Halvorsen, B. M., du Plessis, J. P., & Woudberg, S. (2006). The Performance of Drag Models on Flow Behaviour in the CFD Simulation of a Fluidized Bed. *Proceedings of the Sixth International Conference on Advances in Fluid Mechanics, Skiathos, Greece, May 2006*, 3–12.

Halvorsen, B. M. & Mathiesen, V. (2002). CFD Modeling and Simulation of a lab-scale Fluidised Bed. *Modeling, Identification and Control*, *23*(2), 117–133.

Happel, J. (1958). Viscous Flow in Multiparticle Systems: Slow Motion of Fluids Relative to Beds of Spherical Particles. *A.I.Ch.E. Journal*, *4*(2), 197–201.

Happel, J. & Brenner, H. (1965). *Low Reynolds Number Hydrodynamics*. Prentice-Hall, Inc.

Harris, J. (1977). *Rheology and Non-Newtonian Flow*. Longman Group LTD.

Hasimoto, H. (1958). On the periodic fundamental solutions of the Stokes equations and their application to viscous flow past a cubic array of spheres. *Fluid Mechanics*, *5*, 317–328.

Kaviany, M. (1995). *Principles of Heat Transfer in Porous Media, Second Edition*. Springer-Verlag.

Kemblowski, Z. & Michniewics, M. (1979). A new look at the laminar flow of power law fluids through granular beds. *Rheology Acta*, *18*(6), 572–739.

Lloyd, C. A. (2003). *Hydrodynamic Permeability of Staggered and Non-Staggered Regular Arrays of Squares*. MScEng thesis, University of Stellenbosch, South Africa.

Lloyd, C. A., Du Plessis, J. P., & Halvorsen, B. M. (2004). On Closure Modelling of Volume Averaged Equations for Flow Through Two-Dimensional Arrays of Squares. *Proceedings of the Fifth International Conference on Advances in Fluid Mechanics, March 2004, Lisbon, Portugal*, 85–93.

Macdonald, I. F., El-Sayed, M. S., Mow, K., & Dullien, F. A. L. (1979). Flow through Porous Media - the Ergun Equation Revisited. *Industrial & Engineering Chemistry Fundamentals*, *18*(3), 199–208.

Massey, B. S. (1989). *Mechanics of Fluids, Sixth Edition*. Van Nostrand Reinhold (Int.).

Mehta, D. & Hawley, M. C. (1969). Wall Effect in Packed Columns. *I & EC Process Design and Development*, *8*(2), 280–282.

Mishra, P., Singh, D., & Mishra, I. M. (1975). Momentum Transfer to Newtonian and Non-Newtonian Fluids Flowing Through Packed and Fluidized Beds. *Chemical Engineering Science*, *30*, 397–405.

Roberson, J. A. & Crowe, C. T. (1985). *Engineering Fluid Mechanics, Third Edition*. Houghton Mifflin Company.

Rowe, P. N. (1961). Drag Forces in a Hydraulic Model of a Fluidised Bed - Part II. *Transaction of the Institution of Chemical Engineers*, *39*, 175–180.

Sabiri, N.-E. & Comiti, J. (1995). Pressure Drop in Non-Newtonian Purely Viscous Fluid Flow Through Porous Media. *Chemical Engineering Science*, *50*(7), 1193–1201.

Savins, J. G. (1970). *Flow Through Porous Media*. American Chemical Society.

Skelland, A. H. P. (1967). *Non-Newtonian Flow and Heat Transfer*. John Wiley & Sons, Inc.

Slattery, J. C. (1969). Single-Phase Flow Through Porous Media. *A.I.Ch.E. Journal*, *15*, 866–872.

Smit, G. J. F. (1997). *Mathematical Modelling of Non-Newtonian Flow Through Isotropic Porous Media*. PhD thesis, University of Stellenbosch, South Africa.

Smit, G. J. F. & Du Plessis, J. P. (1997). Pressure drop prediction of power law fluid through granular media. *Journal of Non-Newtonian Fluid Mechanics*, *72*, 319–323.

Smit, G. J. F. & Du Plessis, J. P. (2000). Modelling of non-Newtonian flow through isotropic porous media. *Math. Engng. Ind.*, *8*(1), 19–40.

Sorbie, K. S. & Huang, Y. (1991). Rheological and Transport Effects in the Flow of Low Concentration Xanthan Solution Through Porous Media. *Journal of Colloid and Interface Sciences*, *145*, 74–89.

Tatham, J. P., Carrington, S., Odell, J. A., Gamboa, A. C., Muller, A. J., & Sáez, A. E. (1995). Extensional behavior of hydroxypropyl guar solutions: Optical rheometry in opposed jets and flow through porous media. *Journal of Rheology*, *39*(5), 961–986.

Wen, C. Y. & Yu, Y. H. (1966). Mechanics of Fluidization. *Chemical Engineering Progress*, *62*(62), 100–111.

Whitaker, S. (1969). Advances in Theory of Fluid Motion in Porous Media. *Industrial Engineering Chemistry*, *61*, 14–28.

Whitaker, S. (1999). *The Method of Volume Averaging*. Kluwer Academic Publishers.

Woudberg, S., Du Plessis, J. P., & Smit, G. J. F. (2006). Non-Newtonian purely viscous flow through isotropic granular porous media. *Chemical Engineering Science*, *61*, 4299–4308.

Yu, Y. H., Wen, C. Y., & Bailie, R. C. (1968). Power-Law Fluids Flow Through Multi-particle System. *The Canadian Journal of Chemical Engineering*, *46*, 149–154.